This material is based upon work supported by the United States Air Force under Air Force Contract No. FA8702-15-D-0001. Any opinions, findings, conclusions or recommendations expressed in this material are those of the author(s) and do not necessarily reflect the views of the United States Air Force.

MASSACHUSETTS INSTITUTE OF TECHNOLOGY
LINCOLN LABORATORY

7 December 2018

TO: MIT Course 6.630 (Electromagnetics) Fall 2018 Students

FROM: H. C. Lambert

SUBJECT: Electromagnetic Wave Propagation through the Turbulent Atmosphere

This monograph contains supplementary notes to an invited lecture that the author delivered to the students of MIT Course 6.630 (Electromagnetics) on 7 December 2018.

1 Introduction

Random fluctuations in the air density distort electromagnetic waves propagating through the atmosphere. The effect is more severe at higher frequencies or shorter wavelengths (millimeter, infrared, optical, and shorter wavelengths), but microwave signals propagating through the atmosphere can also be distorted under strong turbulent conditions. The twinkling of stars, a phenomenon familiar to any casual observer of the night sky, is caused by this effect. Another familiar phenomenon caused by turbulence is the dancing of mirages observed above hot road surfaces. These phenomena are collectively referred to as "atmospheric seeing." This monograph covers the basic physics describing the propagation effects caused by such phenomena.

Propagation effects caused by atmospheric turbulence include, among others, the broadening of beams, the random wandering of observed images, and the random fluctuation of signal intensities (referred to as "scintillation"). Smooth plane wavefronts—for example, those received from stars—are "corrugated" due to phase delays caused by air density fluctuations as they propagate through the atmosphere. The random phase delays, in turn, result in a complex diffraction pattern observed at a receiving station due to random constructive and destructive interference. Atmospheric seeing is a nuisance in many applications involving the propagation of high-frequency electromagnetic waves (e.g., in infrared or optical astronomy, laser communications, infrared or optical tacking of space objects, etc.), and its effects must be mitigated.

Adaptive optics (AO), a technique for mitigating or nearly eliminating atmospheric propagation effects, is playing an increasingly prominent role in astronomy and other application areas (see Figure 1). AO systems rely on a flexible secondary mirror—made from a flexible surface (or an array of smooth surfaces) supported by actuators—that can be deformed to compensate for the atmospheric distortion of the received wavefronts before they reach the primary mirror of an infrared or optical telescope. AO systems also rely on a "guide star," either real or virtual, near the line of sight of the object of interest to serve as a point of reference. In the absence of a real guide star, a laser beam is used to generate an artificial light source, or a virtual "star," by exciting the sodium atoms in the upper layers of the atmosphere (in the range of 80 km to 105 km altitude) and hence causing them to glow and appear as a star. The design and development of AO systems rely on a solid understanding of the physics of electromagnetic wave propagation through turbulent media. High-level design analyses require a knowledge of how the parameters characterizing the statistical behavior of propagation effects vary as functions of system parameters such as frequency, distance, and channel parameters. Detailed design decisions also often rely on high-fidelity simulation results, the

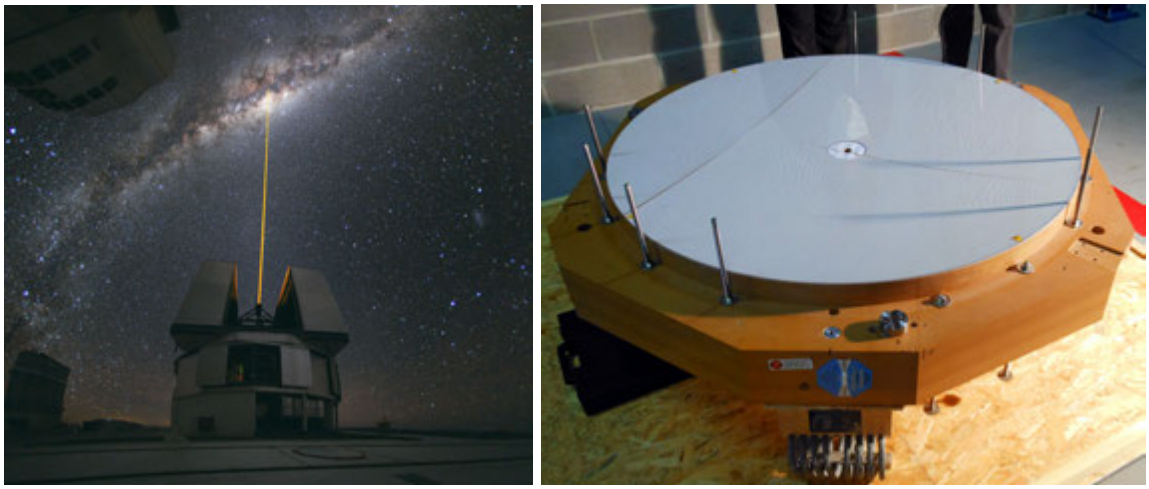

Figure 1: The adaptive optics system at the Paranal Observatory in Chile operated by the European Southern Observatory. Left: laser beam creating a virtual guide star near the desired line of sight. Right: secondary mirror smoothing the distorted wavefronts received from the desired source. Source: European Southern Observatory website (`https://www.eso.org/public/images`). The photographs are licensed under the Creative Commons Attribution 4.0 International License.

implementation of which, in turn, rely on a thorough understanding of the propagation equations—and their limitations.

The subject begins in Section 2 with a discussion of the power spectral density of the fluctuations in the air's index of refraction. The index of refraction is the fundamental physical parameter that couples the propagation of electromagnetic waves with the random behavior of the turbulent medium. In Section 3, the parabolic wave equation—a stochastic partial differential equation governing the propagation of waves in turbulent media—is derived from the Maxwell equations. In Section 4, two formal solutions of the parabolic wave equation corresponding to two limiting scenarios are derived: one corresponding to the case when the turbulent medium is concentrated in a thin layer or screen perpendicular to the direction of propagation, and one corresponding to the case when the turbulent medium is extended all the way to the observation plane. In Sections 5 and 6, expressions are derived for the second and fourth statistical moments of the scattered wave field, respectively, for the case when the turbulent medium is concentrated in a thin screen. System parameters characterizing the statistical properties of the scattered wave field obtained from the second and fourth statistical moments are discussed in Section 7. The numerical simulation of electromagnetic waves propagating through turbulent media is covered in Section 8. A summary of the topics covered in this monograph is provided in Section 9. The derivations covered in much of the discussion below rely on Fourier transform techniques. Important Fourier transform pairs relevant to these derivations are summarized in Appendix A.

Although the discussion in this monograph is limited to electromagnetic waves propagating through the turbulent atmosphere, the derived propagation equations apply equally well to problems involving lower-frequency radio waves propagating through the turbulent plasmas of the Earth's ionosphere, or acoustic waves propagating through turbulent oceans. Furthermore, while the topics discussed in this monograph are motivated mainly by practical engineering applications, such as improving the reliability of laser communi-

cations or improving the accuracy of tracking and imaging of space objects with infrared or optical sensors, the propagation equations derived here can also be used to solve the inverse problem of inferring the characteristics of the turbulent medium from the observed distortion of electromagnetic waves. For example, in the case of the interstellar medium, the observed distortions of radio waves emitted by pulsars provide clues to the galactic electron density variations. In other words, while one scientist might regard the propagation effects caused by turbulence as a source of noise, another might view them as the signal.

2 The Turbulent Atmosphere

The index of refraction, n, of the air is the fundamental physical parameter affecting the propagation of electromagnetic waves through the Earth's atmosphere. The index of refraction is a function of air pressure, p; temperature, T; and humidity, e. Its dependence on these variables is often expressed as

$$n(\mathbf{r},t) = 1 + \frac{77.6}{T(\mathbf{r},t)}\left[p(\mathbf{r},t) + \frac{4810\,e(\mathbf{r},t)}{T(\mathbf{r},t)}\right] \times 10^{-6}, \tag{1}$$

where p is in millibars; T is in Kelvins; and e, expressed as the water vapor partial pressure, is also in millibars. Since p, T, and e vary with position, $\mathbf{r}$, and time, t, the index of refraction, n, also varies with $\mathbf{r}$ and t. Due to the factor of 10^{-6} in the second term on the right-hand side of Equation (1), the index of refraction of the Earth's atmosphere is clearly very nearly equal to one. For example, at standard temperature and pressure (defined at a temperature of 273.15 K and an absolute pressure of 10^5 Pa), the air's index of refraction is specified to be 1.00029, a value commonly used in many basic calculations.

The spatial and temporal variations of air pressure, temperature, and humidity are prescribed by the atmospheric air flow, quantified by the velocity field, $\mathbf{v}(\mathbf{r},t)$. Hence, the spatial and temporal variations of the air's index of refraction are also prescribed by the air velocity field, $\mathbf{v}(\mathbf{r},t)$. The dynamic behavior of air flow, in turn, is described by the equations of hydrodynamics, which consist of the Navier–Stokes and continuity equations. The Reynolds number is a dimensionless parameter that is used to determine whether air flow is laminar (i.e., smooth) or turbulent (i.e., random). It is defined as

$$\mathrm{Re} = \frac{v\ell}{\nu}, \tag{2}$$

where v denotes the characteristic or typical speed of the air; ℓ is the typical length scale associated with the air flow; and ν here denotes the kinematic viscosity of the air[1]. Laminar flow is characterized by small Reynolds numbers ($\mathrm{Re} < 2300$), while turbulent flow is characterized by large Reynolds numbers ($\mathrm{Re} > 4000$). Reynolds numbers in the range $2300 < \mathrm{Re} < 4000$, in turn, characterize air flows that are transitioning from laminar to turbulent flow. The velocity field is a deterministic function of position and time when flow is laminar. It becomes a random function of position and time when flow is turbulent. The atmospheric turbulence conditions relevant to the subject of this monograph correspond to very large Reynolds numbers, lying in the range of 10^6 to 10^7.

At the onset of turbulence, as air velocity increases (due to, say, increasing temperature gradients), large eddies are formed. The large eddies, in turn, break into smaller eddies, giving rise to a turbulent flow pattern. An example of such a flow pattern is shown in Figure 2, which illustrates how the air transitions from laminar to turbulent flow above a burning candle. As the eddies break into smaller pieces, kinetic

[1]The symbol ν is used in Section 3 to denote the frequency of a propagating electromagnetic wave.

energy is transferred from larger eddies to the smaller eddies without any loss. In 1941, using dimensional analysis arguments, the Russian mathematician, Andrey Nikolaevich Kolmogorov, showed that the three-dimensional spatial power spectral density, P_{KE}, of the kinetic energy transfer has a power law form (see for example [1]):

$$P_{\text{KE}}(q) \propto q^{-11/3}, \tag{3}$$

where $q = \|\mathbf{q}\| = \sqrt{q_x^2 + q_y^2 + q_z^2}$ denotes the magnitude of the three-dimensional wave number (spatial frequency).

Figure 2: Transition from laminar to turbulent flow above a burning candle. Source: Wikipedia. The Schlieren photograph, created by Dr. Gary Settles of Floviz, Inc. (`http://www.flovizinc.com`), is licensed under the Creative Attribution-ShareAlike 3.0 Unported License.

Since the spatial variations in the air's index of refraction are prescribed by the random behavior of the velocity field, $\mathbf{v}(\mathbf{r}, t)$, the power spectral density of the random fluctuations in the index of refraction also have a power law form. Writing the index of refraction as the sum of an average term, $\langle n \rangle$, and a fluctuating term, δn,

$$n(\mathbf{r}, t) = \langle n \rangle + \delta n(\mathbf{r}, t) = \langle n \rangle \left[1 + n_1(\mathbf{r}, t)\right], \tag{4}$$

where

$$n_1(\mathbf{r}, t) = \frac{\delta n(\mathbf{r}, t)}{\langle n \rangle} \tag{5}$$

denotes the relative (to the mean) fluctuations of the index of refraction, the three-dimensional spatial power spectral density of n_1 is given by [2]

$$P_n(q) = 0.033 C_n^2 q^{-11/3}. \tag{6}$$

Here, C_n^2 is referred to as the *turbulence structure constant* and determines the strength of turbulence. Since P_n has dimension one divided by wavenumber (or length), C_n^2 has dimension length$^{-2/3}$. Typical values of C_n^2 are in the range of 10^{-18} m$^{-2/3}$ to 10^{-16} m$^{-2/3}$ (see for example [3]).

Equations (3) and (6) are valid over a very wide range of wavenumbers (or spatial scales), a range referred to as the *energy* or *dynamic range* of turbulence. However, the transfer of kinetic energy from large-scale eddies to small-scale eddies eventually leads to energy dissipation. The Reynolds number determines at what scale energy dissipation occurs. Larger Reynolds numbers lead to wider dynamic ranges, and hence to energy dissipation occurring at smaller spatial scales. To include the effect of energy dissipation, the power spectral density of the index of refraction fluctuations can be written as [2]

$$P_n(q) = 0.033 C_n^2 q^{-11/3} \exp\left(-\frac{q^2}{\kappa_i^2}\right), \tag{7}$$

where

$$\kappa_i = \frac{2\pi}{\ell_i}, \tag{8}$$

and ℓ_i is referred to as the *inner scale* of turbulence. The exponential term in Equation (7) halts the eddy fragmentation process and the lossless transfer of kinetic energy from larger to smaller eddies. Energy dissipation occurs at the inner scale, ℓ_i. Typical values of the inner scale range from a few millimeters to tens of centimeters (see for example [4]).

Similarly, the lowest possible wavenumber (largest spatial scale) in the dynamic range of turbulence is determined by the size of the largest turbulent eddy. At low wavenumbers, the power spectral density of the index of refraction fluctuations can, in turn, be written as [2]

$$P_n(q) = \frac{0.033 C_n^2}{\left(q^2 + \kappa_o^2\right)^{11/6}}, \tag{9}$$

where

$$\kappa_o = \frac{2\pi}{\ell_o}, \tag{10}$$

and ℓ_o is referred to as the *outer scale* of turbulence. The outer scale corresponds to the typical size of the largest eddy. Typical values of the outer scale are on the order of hundreds of meters (see for example [4]).

Equations (6), (7), and (9) can be combined and generalized into a single equation:

$$P_n(q) = \frac{f(\beta) C_n^2}{\left(q^2 + \kappa_o^2\right)^{\beta/2}} \exp\left(-\frac{q^2}{\kappa_i^2}\right), \quad 2 < \beta < 4 \tag{11}$$

where

$$f(\beta) = \frac{\Gamma(\beta - 1)}{4\pi^2} \sin\left(\frac{\pi}{2}(\beta - 3)\right). \tag{12}$$

Here, β (lying in the range $2 < \beta < 4$) is referred to as the *spectral index*. For the Kolmogorov power spectral density, $\beta = 11/3$. It follows that

$$f(11/3) = 0.033. \tag{13}$$

The value of the power spectral density at $q = 0$,

$$P_n(0) = f(\beta) C_n^2 \kappa_o^{-\beta}, \tag{14}$$

can be regarded as characterizing the *level of turbulence*. Plots of the index of refraction power spectral density for the general and the asymptotic simple power law cases, equations (11) and (6), respectively, with $\beta = 11/3$ (Kolmogorov spectral index) are shown in Figure 3. The power spectral density of the air's index of refraction fluctuations plays a central role in quantifying propagation effects induced by the turbulent atmosphere.

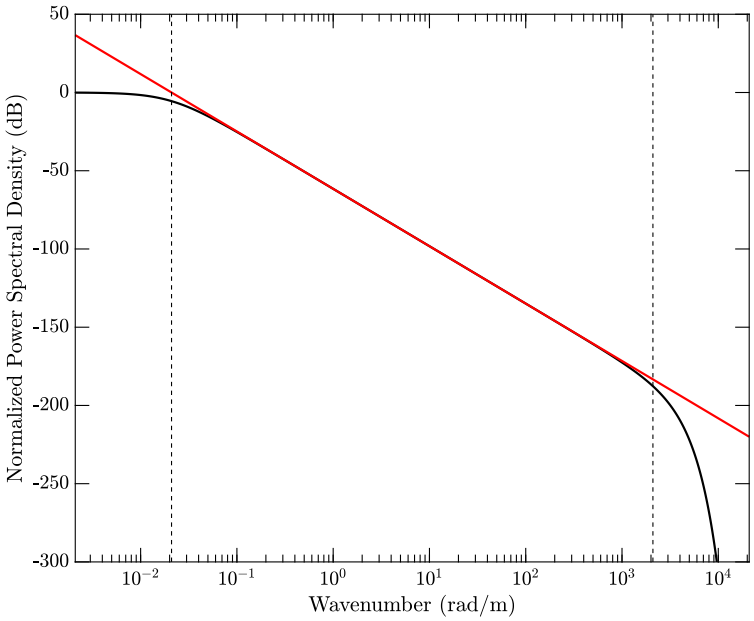

Figure 3: Normalized power spectral densities, $P_n(q)/P_n(0)$, of the fluctuations in the air's index of refraction. The black line corresponds to the general model (11) in text, while the red line corresponds to the asymptotic power law model (6) in text. The spectral index, β, is 11/3, corresponding to the Kolmogorov power spectral density. The outer scale (corresponding to the left vertical dashed line) is 300 m, while the inner scale (corresponding to the right vertical dashed line) is 3 mm.

3 The Parabolic Wave Equation

The propagation of electromagnetic waves through a turbulent medium (such as the Earth's atmosphere) is governed by a parabolic wave equation. The parabolic wave equation is a stochastic partial differential equation that provides the spatial distribution of a scalar wave field scattered by the turbulent medium. The scalar wave field can represent any component of an electromagnetic wave. Since the parabolic wave equation is a scalar equation, it can also be applied to problems involving propagation of acoustic waves through the turbulent ocean. There are other natural phenomena that can be described by parabolic wave equations. For example, the time-dependent Schrödinger equation is also a parabolic wave equation.

In this section, the parabolic wave equation is derived from the Maxwell equations. The derivation is based on dimensional analysis arguments that rely on a number of assumptions concerning the relative scaling of parameters describing the average temporal and spatial characteristics of the propagating electromagnetic wave and the random medium. The assumptions are introduced when they are needed while

marching through the steps of the derivation. They are then listed at the end of the section for future reference. All assumptions have been verified by measurements and can be applied reliably. At a high level, the interaction of the components of the propagating electromagnetic wave and the turbulent medium is such that the wave components are scattered mainly in the forward direction at small angles; that is, there is essentially no backscattering or reflection of the waves. This fact results in the reduction of the second partial derivative with respect to the coordinate in the direction of propagation that appears in the more general forms of the wave equation to a first partial derivative.

The derivation begins by assuming that only those regions of space that are far away from any sources of radiation are of interest. In other words, the source-free form of the Maxwell equations with charge density and current density set equal to zero will be the point of departure for deriving the parabolic wave equation:

$$\nabla \times \mathbf{E}(\mathbf{r}, t) = -\frac{\partial}{\partial t}\mathbf{B}(\mathbf{r}, t), \tag{15}$$

$$\nabla \times \mathbf{H}(\mathbf{r}, t) = \frac{\partial}{\partial t}\mathbf{D}(\mathbf{r}, t), \tag{16}$$

$$\nabla \cdot \mathbf{D}(\mathbf{r}, t) = 0, \tag{17}$$

$$\nabla \cdot \mathbf{B}(\mathbf{r}, t) = 0. \tag{18}$$

For the problem of electromagnetic waves propagating through the turbulent atmosphere, the **D** and **B** fields are related to the **E** and **H** fields via the following constitutive relations:

$$\mathbf{D}(\mathbf{r}, t) = \varepsilon(\mathbf{r}, t)\mathbf{E}(\mathbf{r}, t), \tag{19}$$

$$\mathbf{B}(\mathbf{r}, t) = \mu_0\mathbf{H}(\mathbf{r}, t). \tag{20}$$

The magnetic permeability of the atmosphere, μ, is simply equal to the free-space magnetic permeability, μ_0, since the atmosphere is not magnetized. The electric permittivity, ε, of the atmosphere, however, is in general inhomogeneous (i.e., a function of position, $\mathbf{r}$) and nonstationary (i.e., a function of time, t). In fact, ε is a stochastic function of position and time, and through the above constitutive relations and the Maxwell equations, it causes the electric and magnetic fields to become stochastic functions of position and time as well. One must therefore resort to statistical techniques to understand the behavior of electromagnetic waves propagating through a turbulent medium. In the following discussion, it will be more convenient to factor out the free-space electric permittivity, ε_0, and express the electric permittivity in terms of a *relative* electric permittivity, ε_r:

$$\varepsilon(\mathbf{r}, t) = \varepsilon_0\varepsilon_r(\mathbf{r}, t). \tag{21}$$

Expressing the **D** and **B** fields in terms of the **E** and **H** fields, respectively, using the above constitutive relations, the source-free Maxwell equations then become

$$\nabla \times \mathbf{E}(\mathbf{r}, t) = -\mu_0\frac{\partial}{\partial t}\mathbf{H}(\mathbf{r}, t), \tag{22}$$

$$\nabla \times \mathbf{H}(\mathbf{r}, t) = \varepsilon_0\frac{\partial}{\partial t}\left[\varepsilon_r(\mathbf{r}, t)\mathbf{E}(\mathbf{r}, t)\right], \tag{23}$$

$$\nabla \cdot \left[\varepsilon_r(\mathbf{r}, t)\mathbf{E}(\mathbf{r}, t)\right] = 0, \tag{24}$$

$$\nabla \cdot \mathbf{H}(\mathbf{r}, t) = 0. \tag{25}$$

The next steps involves a technique that is used for deriving the classical wave equation for electromagnetic waves propagating through a homogeneous and stationary medium. Taking the curl of both sides of

Equation (22), Faraday's law becomes

$$\nabla \times \nabla \times \mathbf{E}(\mathbf{r},t) = -\mu_0 \frac{\partial}{\partial t} \left[\nabla \times \mathbf{H}(\mathbf{r},t)\right]. \tag{26}$$

Using Equation (23) to substitute for $\nabla \times \mathbf{H}$ on the right-hand side, Equation (26) can be expressed in terms of $\mathbf{E}(\mathbf{r},t)$ only:

$$\nabla \times \nabla \times \mathbf{E}(\mathbf{r},t) = -\mu_0 \varepsilon_0 \frac{\partial^2}{\partial t^2} \left[\varepsilon_r(\mathbf{r},t)\mathbf{E}(\mathbf{r},t)\right]. \tag{27}$$

Using the vector identity,

$$\nabla \times \nabla \times \mathbf{E} = \nabla(\nabla \cdot \mathbf{E}) - \nabla^2 \mathbf{E}, \tag{28}$$

Equation (27) can then be written as

$$\nabla^2 \mathbf{E}(\mathbf{r},t) - \nabla \left[\nabla \cdot \mathbf{E}(\mathbf{r},t)\right] = \mu_0 \varepsilon_0 \frac{\partial^2}{\partial t^2} \left[\varepsilon_r(\mathbf{r},t)\mathbf{E}(\mathbf{r},t)\right]. \tag{29}$$

Equation (24) can, in turn, be used to derive an expression for $\nabla \cdot \mathbf{E}(\mathbf{r},t)$. Using the product rule of differentiation, Gauss's law for the case of an inhomogeneous medium can be written as

$$\nabla \cdot \left[\varepsilon_r(\mathbf{r},t)\mathbf{E}(\mathbf{r},t)\right] = \varepsilon_r(\mathbf{r},t)\, \nabla \cdot \mathbf{E}(\mathbf{r},t) + \mathbf{E}(\mathbf{r},t) \cdot \nabla \varepsilon_r(\mathbf{r},t) = 0, \tag{30}$$

which can be used to obtain the following relation for $\nabla \cdot \mathbf{E}(\mathbf{r},t)$:

$$\nabla \cdot \mathbf{E}(\mathbf{r},t) = -\mathbf{E}(\mathbf{r},t) \cdot \frac{\nabla \varepsilon_r(\mathbf{r},t)}{\varepsilon_r(\mathbf{r},t)} = -\mathbf{E}(\mathbf{r},t) \cdot \nabla \ln \varepsilon_r(\mathbf{r},t). \tag{31}$$

Using this expression for $\nabla \cdot \mathbf{E}(\mathbf{r},t)$, Equation (29) becomes

$$\nabla^2 \mathbf{E}(\mathbf{r},t) + \nabla \left[\mathbf{E}(\mathbf{r},t) \cdot \nabla \ln \varepsilon_r(\mathbf{r},t)\right] = \mu_0 \varepsilon_0 \frac{\partial^2}{\partial t^2} \left[\varepsilon_r(\mathbf{r},t)\mathbf{E}(\mathbf{r},t)\right]. \tag{32}$$

To compute $\nabla \ln \varepsilon_r(\mathbf{r},t)$ in Equation (32), $\varepsilon_r(\mathbf{r},t)$ can be written as

$$\varepsilon_r(\mathbf{r},t) = \langle \varepsilon_r \rangle + \delta\varepsilon_r(\mathbf{r},t) = \langle \varepsilon_r \rangle \left[1 + \varepsilon_1(\mathbf{r},t)\right], \tag{33}$$

where $\langle \cdot \rangle$ denotes an ensemble average, and

$$\varepsilon_1(\mathbf{r},t) = \frac{\delta\varepsilon_r(\mathbf{r},t)}{\langle \varepsilon_r \rangle}. \tag{34}$$

ε_1 is a stochastic function of position and time and is described by a probability density function. Clearly, $\langle \varepsilon_1(\mathbf{r},t) \rangle = 0$. The first assumption in deriving the parabolic wave equation is that ε_1 has a Gaussian probability distribution. The second assumption is that $\sqrt{\left\langle \left|\varepsilon_1(\mathbf{r},t)\right|^2 \right\rangle} \ll 1$; in other words, $\sqrt{\left\langle \left|\delta\varepsilon_r(\mathbf{r},t)\right|^2 \right\rangle} \ll \langle \varepsilon_r \rangle$. Based on the second assumption, $\ln \varepsilon_r$ can be written as

$$\ln \varepsilon_r = \ln \langle \varepsilon_r \rangle + \ln\left(1 + \varepsilon_1\right) \simeq \ln \langle \varepsilon_r \rangle + \varepsilon_1. \tag{35}$$

It follows that

$$\nabla \ln \varepsilon_r(\mathbf{r},t) \simeq \nabla \varepsilon_1(\mathbf{r},t). \tag{36}$$

Using this expression for $\nabla \ln \varepsilon_r(\mathbf{r}, t)$, Equation (32) becomes

$$\nabla^2 \mathbf{E}(\mathbf{r}, t) + \nabla \left[\mathbf{E}(\mathbf{r}, t) \cdot \nabla \varepsilon_1(\mathbf{r}, t) \right] = \mu_0 \varepsilon_0 \left\langle \varepsilon_r \right\rangle \frac{\partial^2}{\partial t^2} \left[1 + \varepsilon_1(\mathbf{r}, t) \right] \mathbf{E}(\mathbf{r}, t). \tag{37}$$

Next dimensional analysis is employed to to simplify Equation (37). In particular, the terms involving both $\mathbf{E}$ and ε_1 need to be simplified. The term on the right-hand side of Equation (37) is examined first. Using the product rule of differentiation, the second partial derivative of the cross term on the right-hand side with respect to time expands to

$$\frac{\partial^2}{\partial t^2} \left[\varepsilon_1(\mathbf{r}, t) \mathbf{E}(\mathbf{r}, t) \right] = \varepsilon_1 \frac{\partial^2 \mathbf{E}}{\partial t^2} + 2 \frac{\partial \varepsilon_1}{\partial t} \frac{\partial \mathbf{E}}{\partial t} + \mathbf{E} \frac{\partial^2 \varepsilon_1}{\partial t^2}. \tag{38}$$

The derivatives in this expression can be approximated using dimensional analysis arguments. The magnitudes of the first and second time derivatives of $\mathbf{E}$, can be approximated as

$$\left| \frac{\partial \mathbf{E}}{\partial t} \right| \sim \sigma_E \nu \quad \text{and} \quad \left| \frac{\partial^2 \mathbf{E}}{\partial t^2} \right| \sim \sigma_E \nu^2, \tag{39}$$

respectively, where

$$\sigma_E = \sqrt{\left\langle \left\| \mathbf{E}(\mathbf{r}, t) \right\|^2 \right\rangle} \tag{40}$$

denotes the root-mean-square of the variations in the electric field, $\mathbf{E}(\mathbf{r}, t)$, and ν is the dominant frequency of the propagating electromagnetic field. The magnitudes of the first and second time derivatives of ε_1 can, in turn, be approximated as

$$\left| \frac{\partial \varepsilon_1}{\partial t} \right| \sim \frac{\sigma_\varepsilon}{\tau_\varepsilon} \quad \text{and} \quad \left| \frac{\partial^2 \varepsilon_1}{\partial t^2} \right| \sim \frac{\sigma_\varepsilon}{\tau_\varepsilon^2}, \tag{41}$$

respectively, where

$$\sigma_\varepsilon = \sqrt{\left\langle \left\| \varepsilon_1(\mathbf{r}, t) \right\|^2 \right\rangle} \tag{42}$$

denotes the root-mean-square variations in the relative electric permittivity, $\varepsilon_1(\mathbf{r}, t)$, and τ_ε denotes the typical time scale associated with the temporal variations in $\varepsilon_1(\mathbf{r}, t)$. Using these approximations, the magnitudes of the three terms on the right-hand side of Equation (38) can be approximated as follows:

$$\left| \varepsilon_1 \frac{\partial^2 \mathbf{E}}{\partial t^2} \right| \sim \sigma_\varepsilon \sigma_E \nu^2, \tag{43}$$

$$\left| 2 \frac{\partial \varepsilon_1}{\partial t} \frac{\partial \mathbf{E}}{\partial t} \right| \sim \frac{\sigma_\varepsilon \sigma_E \nu}{\tau_\varepsilon}, \tag{44}$$

$$\left| \mathbf{E} \frac{\partial^2 \varepsilon_1}{\partial t^2} \right| \sim \frac{\sigma_E \sigma_\varepsilon}{\tau_\varepsilon^2}. \tag{45}$$

Combining the three terms gives

$$\left| \frac{\partial^2}{\partial t^2} \left[\varepsilon_1(\mathbf{r}, t) \mathbf{E}(\mathbf{r}, t) \right] \right| \sim \sigma_\varepsilon \sigma_E \nu^2 \left(1 + \frac{1}{\tau_\varepsilon \nu} + \frac{1}{\tau_\varepsilon \nu^2} \right). \tag{46}$$

Now if $\tau_\varepsilon \nu \gg 1$ (third assumption), then the last two terms in the parentheses on the right-hand side can be ignored, and the second partial time derivative (38) can be approximated as:

$$\frac{\partial^2}{\partial t^2} \left[\varepsilon_1(\mathbf{r}, t) \mathbf{E}(\mathbf{r}, t) \right] \simeq \varepsilon_1(\mathbf{r}, t) \frac{\partial^2}{\partial t^2} \mathbf{E}(\mathbf{r}, t). \tag{47}$$

In other words, if the temporal variations in $\varepsilon_1(\mathbf{r},t)$, characterized by the time scale τ_ε, are significantly slower than the temporal variations in the electric field $\mathbf{E}(\mathbf{r},t)$, characterized by the time scale ν^{-1}, then $\varepsilon_1(\mathbf{r},t)$ can be treated as a constant as far as the second partial time derivative is concerned. Using this approximation, Equation (37) becomes

$$\nabla^2\mathbf{E}(\mathbf{r},t)+\nabla\left[\mathbf{E}(\mathbf{r},t)\cdot\nabla\varepsilon_1(\mathbf{r},t)\right]=\mu_0\varepsilon_0\left\langle\varepsilon_r\right\rangle\left[1+\varepsilon_1(\mathbf{r},t)\right]\frac{\partial^2}{\partial t^2}\mathbf{E}(\mathbf{r},t). \tag{48}$$

When dealing with time-harmonic electromagnetic fields, the temporal behavior of the fields can often be eliminated from the dynamic equations by resorting to phasor notation. For a monochromatic electric field characterized by a single angular frequency ω ($\omega=2\pi\nu$), the electric field can be written as

$$\mathbf{E}(\mathbf{r},t)=\mathrm{Re}\left\{\underline{\mathbf{E}}(\mathbf{r})e^{j\omega t}\right\}, \tag{49}$$

where $\underline{\mathbf{E}}(\mathbf{r})$, referred to as a phasor, is a complex vector field. For more complicated temporal variations, contributions from a range of angular frequencies must be included. For the general case, the temporal Fourier transform $\underline{\mathbf{E}}(\mathbf{r},\omega)$ of the electric field must therefore be considered:

$$\underline{\mathbf{E}}(\mathbf{r},\omega)=\frac{1}{2\pi}\int_{-\infty}^{\infty}\mathbf{E}(\mathbf{r},t)e^{-j\omega t}\,dt. \tag{50}$$

The next step toward deriving the parabolic wave equation is to take the temporal Fourier transform of Equation (48). The temporal Fourier transform of the cross term on the right-hand side of Equation (48) is examined first. Applying integration by parts twice, the Fourier transform of the cross term becomes

$$\begin{aligned}\int_{-\infty}^{\infty}\varepsilon_1(\mathbf{r},t)\frac{\partial^2}{\partial t^2}\mathbf{E}(\mathbf{r},t)e^{-j\omega t}\,dt=\varepsilon_1\frac{\partial\mathbf{E}}{\partial t}e^{-j\omega t}\Big|_{-\infty}^{\infty}+\left(\frac{\partial\varepsilon_1}{\partial t}-j\omega\varepsilon\right)\mathbf{E}e^{-j\omega t}\Big|_{-\infty}^{\infty}\\+\int_{-\infty}^{\infty}\left(\frac{\partial^2\varepsilon_1}{\partial t^2}-2j\omega\frac{\partial\varepsilon_1}{\partial t}-\omega^2\varepsilon_1\right)\mathbf{E}e^{-j\omega t}\,dt.\end{aligned} \tag{51}$$

The first two terms on the right-side can be set equal to zero since the electric field does not exist (i.e., is equal to zero) at $t=\pm\infty$. Next, applying the approximations for the first and second time derivatives of ε_1 discussed above, the magnitude of the expression in parentheses in the integrand of the integral on the right-hand side can be approximated as

$$\left|\frac{\partial^2\varepsilon_1}{\partial t^2}-2j\omega\frac{\partial\varepsilon_1}{\partial t}-\omega^2\varepsilon_1\right|\sim\frac{\sigma_\varepsilon}{\tau_\varepsilon^2}+\frac{\nu\sigma_\varepsilon}{\tau_\varepsilon}+\nu^2\sigma_\varepsilon=\left(\frac{1}{\tau_\varepsilon^2\nu^2}+\frac{1}{\tau_\varepsilon\nu}+1\right)\nu^2\sigma_\varepsilon. \tag{52}$$

Since $\tau_\varepsilon\nu\gg1$ (third assumption), the first two terms in parentheses on the right-hand side can be safely ignored, and the temporal Fourier transform of the cross term on the right-hand side of Equation (48) can be approximated as

$$\int_{-\infty}^{\infty}\varepsilon_1(\mathbf{r},t)\frac{\partial^2}{\partial t^2}\mathbf{E}(\mathbf{r},t)e^{-j\omega t}\,dt\simeq-\omega^2\int_{-\infty}^{\infty}\varepsilon_1(\mathbf{r},t)\mathbf{E}(\mathbf{r},t)e^{-j\omega t}\,dt. \tag{53}$$

Since the temporal variations in $\varepsilon_1(\mathbf{r},t)$ are much slower than the temporal variations in the electric field $\mathbf{E}(\mathbf{r},t)$ based on the third assumption ($\tau_\varepsilon\nu\gg1$), $\varepsilon_1(\mathbf{r},t)$ can be safely moved outside of the integral:

$$\int_{-\infty}^{\infty}\varepsilon_1(\mathbf{r},t)\mathbf{E}(\mathbf{r},t)e^{-j\omega t}\,dt\simeq\varepsilon_1(\mathbf{r},t)\int_{-\infty}^{\infty}\mathbf{E}(\mathbf{r},t)e^{-j\omega t}\,dt=\varepsilon_1(\mathbf{r},t)\underline{\mathbf{E}}(\mathbf{r},\omega). \tag{54}$$

Similarly, when computing the temporal Fourier transform of the second term involving $\nabla\varepsilon_1(\mathbf{r},t)$ on the left-hand side of Equation (48), $\nabla\varepsilon_1(\mathbf{r},t)$ can be safely moved outside of the integral:

$$\int_{-\infty}^{\infty}\mathbf{E}(\mathbf{r},t)\cdot\nabla\varepsilon_1(\mathbf{r},t)e^{-j\omega t}\,dt \simeq \left[\int_{-\infty}^{\infty}\mathbf{E}(\mathbf{r},t)e^{-j\omega t}\,dt\right]\cdot\nabla\varepsilon_1(\mathbf{r},t) = \underline{\mathbf{E}}(\mathbf{r},\omega)\cdot\nabla\varepsilon_1(\mathbf{r},t). \tag{55}$$

At this point, the explicit time dependence in ε_1 and $\nabla\varepsilon_1$ can be dropped. In other words, the medium can be safely assumed to be *frozen in time* for the time scales of interest. Equipped with these approximations, the temporal Fourier transform of Equation (48) reduces to

$$\nabla^2\underline{\mathbf{E}}(\mathbf{r},\omega) + k^2\left[1+\varepsilon_1(\mathbf{r})\right]\underline{\mathbf{E}}(\mathbf{r},\omega) = -\nabla\left[\underline{\mathbf{E}}(\mathbf{r},\omega)\cdot\nabla\varepsilon_1(\mathbf{r})\right], \tag{56}$$

where

$$k = \omega\sqrt{\mu_0\varepsilon_0\left\langle\varepsilon_r\right\rangle}. \tag{57}$$

Equation (57) is the *dispersion relation*. The average speed of light in the turbulent medium is

$$c = \frac{1}{\sqrt{\mu_0\varepsilon_0\left\langle\varepsilon_r\right\rangle}}. \tag{58}$$

The next step involves the examination of the gradient term on the right-hand side of Equation (56). Bringing all terms involving $\varepsilon_1(\mathbf{r})$ to the right-hand side, Equation (56) can be written as

$$\nabla^2\underline{\mathbf{E}}(\mathbf{r},\omega) + k^2\underline{\mathbf{E}}(\mathbf{r},\omega) = -k^2\varepsilon_1(\mathbf{r})\underline{\mathbf{E}}(\mathbf{r},\omega) - \nabla\left[\underline{\mathbf{E}}(\mathbf{r},\omega)\cdot\nabla\varepsilon_1(\mathbf{r})\right]. \tag{59}$$

Using dimensional arguments, the magnitudes of the gradients of $\mathbf{E}(\mathbf{r},\omega)$ and $\varepsilon_1(\mathbf{r})$ can be approximated as

$$|\nabla\mathbf{E}(\mathbf{r},\omega)| \sim \frac{\sigma_E}{\lambda} \quad \text{and} \quad |\nabla\varepsilon_1(\mathbf{r})| \sim \frac{\sigma_\varepsilon}{\ell_\varepsilon}, \tag{60}$$

where σ_E and σ_ε are defined as before; λ is the wavelength of the propagating electromagnetic wave; and ℓ_ε denotes the typical length scale associated with the spatial variations in $\varepsilon_1(\mathbf{r})$. Using these approximations, the magnitudes of the first and second terms on the right-hand side of Equation (59) can be approximated as

$$\left|-k^2\varepsilon_1(\mathbf{r})\underline{\mathbf{E}}(\mathbf{r},\omega)\right| \sim \frac{\sigma_\varepsilon\sigma_E}{\lambda^2} \tag{61}$$

and

$$\left|-\nabla\left[\underline{\mathbf{E}}(\mathbf{r})\cdot\nabla\varepsilon_1(\mathbf{r})\right]\right| \sim \frac{\sigma_E\sigma_\varepsilon}{\lambda\ell_\varepsilon}, \tag{62}$$

respectively. The ratio of the magnitude of the second term divided by the magnitude of the first term is then given by

$$\left|\frac{\nabla\left[\underline{\mathbf{E}}(\mathbf{r})\cdot\nabla\varepsilon_1(\mathbf{r})\right]}{k^2\varepsilon_1(\mathbf{r})\underline{\mathbf{E}}(\mathbf{r},\omega)}\right| \sim \frac{\lambda}{\ell_\varepsilon}. \tag{63}$$

Now, if $\lambda \ll \ell_\varepsilon$ (fourth assumption), then the magnitude of the second term with the respect to the first term is very small and the second term on the right-hand side of Equation (59) can therefore be safely ignored. Bringing the remaining term on the right-hand side to the left-hand side, Equation (59) then reduces to the classic wave equation:

$$\nabla^2\underline{\mathbf{E}}(\mathbf{r},\omega) + k^2\left[1+\varepsilon_1(\mathbf{r})\right]\underline{\mathbf{E}}(\mathbf{r},\omega) = 0. \tag{64}$$

Since Equation (64) now represents three uncoupled partial differential equations, one for each component of the electric field, $\underline{\mathbf{E}}(\mathbf{r},\omega)$, any arbitrary component of the electric field, denoted by $U(\mathbf{r},\omega)$, can be

considered for further analysis without loss of generality. In other words, it will be sufficient to consider the following equation in place of Equation (64):

$$\nabla^2 U(\mathbf{r},\omega) + k^2\left[1+\varepsilon_1(\mathbf{r})\right]U(\mathbf{r},\omega) = 0. \tag{65}$$

Equation (65) is the classic *Helmholtz equation*. For notational convenience, the explicit dependence on the angular frequency, ω, can be dropped, and $U(\mathbf{r},\omega)$ can be written simply as $U(\mathbf{r})$ in the following.

As alluded to in the beginning of this section, the scattering of electromagnetic waves propagation through a turbulent medium is primarily in the forward direction, with little to no backscattering or reflection. The parabolic wave equation describes how waves are scattered in such a manner. In anticipation of this result, $U(\mathbf{r})$ can be written as

$$U(\mathbf{r}) = \psi(\mathbf{s},z)e^{-jkz}, \tag{66}$$

where the position vector, $\mathbf{r}$, has been decomposed into a transverse component, $\mathbf{s}$, and a longitudinal component, z; that is, $\mathbf{r} = (\mathbf{s},z)$. Here, the scalar wave field, $U(\mathbf{r})$, has been decomposed into a randomly scattered component, $\psi(\mathbf{r},z)$, and a plane wave propagating in the positive z direction. The next step involves substituting Equation (66) for $U(\mathbf{r})$ in the Helmholtz wave Equation (65) to derive a partial differential equation for the scattered wave field, $\psi(\mathbf{s},z)$. To that end, the Laplacian operator in Equation (65) is first decomposed into transverse and longitudinal components:

$$\nabla^2 U(\mathbf{r}) = \nabla_\perp^2 U(\mathbf{r}) + \frac{\partial^2 U(\mathbf{r})}{\partial z^2}, \tag{67}$$

where

$$\nabla_\perp^2 = \frac{\partial^2}{\partial x^2} + \frac{\partial^2}{\partial y^2} \tag{68}$$

denotes the transverse Laplacian operator. The transverse Laplacian of $U(\mathbf{r})$ then becomes

$$\nabla_\perp^2 U(\mathbf{r}) = \left[\nabla_\perp^2 \psi(\mathbf{s},z)\right] e^{-jkz}, \tag{69}$$

while the longitudinal Laplacian can be written as

$$\frac{\partial^2 U(\mathbf{r})}{\partial z^2} = \frac{\partial^2}{\partial z^2}\left[\psi(\mathbf{s},z)e^{-jkz}\right] = \left[\frac{\partial^2\psi(\mathbf{s},z)}{\partial z^2} - 2jk\frac{\partial\psi(\mathbf{s},z)}{\partial z} - k^2\psi(\mathbf{s},z)\right]e^{-jkz}. \tag{70}$$

Using Equation (66), the second term in Equation (65) becomes

$$k^2\left[1+\varepsilon_1(\mathbf{r})\right]U(\mathbf{r}) = \left[k^2\psi(\mathbf{s},z) + k^2\varepsilon_1(\mathbf{s},z)\psi(\mathbf{s},z)\right]e^{-jkz}. \tag{71}$$

Gathering terms and dropping the common e^{-jkz} term, the following partial differential equation is obtained for the scattered wave field, $\psi(\mathbf{r},z)$:

$$\nabla_\perp^2\psi(\mathbf{s},z) + \frac{\partial^2\psi(\mathbf{s},z)}{\partial z^2} - 2jk\frac{\partial\psi(\mathbf{s},z)}{\partial z} + k^2\varepsilon_1(\mathbf{s},z)\psi(\mathbf{s},z) = 0. \tag{72}$$

At this point, the only term standing in the way of arriving at the parabolic wave equation is the second partial derivative of the scattered wave field, $\psi(\mathbf{s},z)$, with respect to z in Equation (72). As before, dimensional analysis is employed to examine the relative contribution of this term to the final result compared to the term involving the first partial derivative of the scattered wave field with respect to z. To that end,

approximations are needed for the magnitudes of terms involving partial derivatives of the scattered wave field with respect to z. However, here, $\partial/\partial z$ can no longer be simply replaced with $1/\lambda$ as was done when deriving the Helmholtz Equation (65). This is because the characteristic length scale of the scattered wave field in the propagation direction, z, is influenced by the turbulent medium. In other words, the desired characteristic length scale that is needed to approximate the partial derivative of the scattered wave field, $\psi(\mathbf{s}, z)$, with respect to z must capture the degree to which the field interacts with the medium. What is needed is a *correlation length* for the scattered wave field along the z direction, which can be obtained by considering a preliminary solution of Equation (72). Such a preliminary solution is derived next. Ignoring the Laplacian terms, Equation (72) reduces to

$$-2jk\frac{\partial\psi(\mathbf{s}, z)}{\partial z} + k^2\varepsilon_1(\mathbf{s}, z)\psi(\mathbf{s}, z) = 0. \tag{73}$$

Ignoring the Laplacian terms in Equation (72) is equivalent to ignoring the effects of diffraction. The goal is merely to derive a typical length scale characterizing the spatial variations of the scattered wave field, $\psi(\mathbf{s}, z)$, in the z direction. This length scale is prescribed by the so-called *optical path length*, influenced mainly by refractive effects in the direction of propagation. Equation (73) therefore meets the need for providing a preliminary solution from which a correlation length for $\psi(\mathbf{s}, z)$ can be derived. Its solution is

$$\psi(\mathbf{s}, z) = \psi(\mathbf{s}, 0)\exp\left(-j\frac{k}{2}\int_0^z \varepsilon_1(\mathbf{s}, \zeta)\, d\zeta\right). \tag{74}$$

Assuming plane waves, $\psi(\mathbf{s}, 0) = 1$. To derive a correlation length, the correlation function of the scattered wave field, $\psi(\mathbf{s}, z)$, along the z direction needs to be computed first. The correlation function of the scattered wave field is given by

$$\langle\psi(\mathbf{s}, z_1)\psi^*(\mathbf{s}, z_2)\rangle = \left\langle\exp\left(-j\frac{k}{2}\left[\int_0^{z_1}\varepsilon_1(\mathbf{s}, \zeta_1)\, d\zeta_1 - \int_0^{z_2}\varepsilon_1(\mathbf{s}, \zeta_1)\, d\zeta_2\right]\right)\right\rangle. \tag{75}$$

Since ε_1 is a zero-mean Gaussian random variable (first assumption), the following identity can be used to compute the above ensemble average (denoted by angular brackets):

$$\left\langle e^{j\theta}\right\rangle = e^{-\frac{1}{2}\langle\theta^2\rangle}. \tag{76}$$

where θ is a zero-mean Gaussian random variable. Applying this identity, the correlation function for the scattered wave field becomes

$$\langle\psi(\mathbf{s}, z_1)\psi^*(\mathbf{s}, z_2)\rangle = \exp\left(-\frac{k^2}{8}\left\langle\left[\int_0^{z_1}\varepsilon_1(\mathbf{s}, \zeta)\, d\zeta - \int_0^{z_2}\varepsilon_1(\mathbf{s}, \zeta)\, d\zeta\right]^2\right\rangle\right). \tag{77}$$

The ensemble average in the exponential can be written as

$$\begin{aligned}\left\langle\left[\int_0^{z_1}\varepsilon_1(\mathbf{s}, \zeta)\, d\zeta - \int_0^{z_2}\varepsilon_1(\mathbf{s}, \zeta)\, d\zeta\right]^2\right\rangle &= \int_0^{z_1}\int_0^{z_1}\langle\varepsilon_1(\mathbf{s}, \zeta_1)\varepsilon_1(\mathbf{s}, \zeta_2)\rangle\, d\zeta_1 d\zeta_2 \\ &\quad - 2\int_0^{z_1}\int_0^{z_2}\langle\varepsilon_1(\mathbf{s}, \zeta_1)\varepsilon_1(\mathbf{s}, \zeta_2)\rangle\, d\zeta_1 d\zeta_2 + \int_0^{z_2}\int_0^{z_2}\langle\varepsilon_1(\mathbf{s}, \zeta_1)\varepsilon_1(\mathbf{s}, \zeta_2)\rangle\, d\zeta_1 d\zeta_2.\end{aligned} \tag{78}$$

Letting $z_1 = z$ and $z_2 = z + \ell_\psi$, the correlation length, ℓ_ψ, can be defined as the point where

$$\langle\psi(\mathbf{s}, z)\psi^*(\mathbf{s}, z + \ell_\psi)\rangle = \frac{1}{2}. \tag{79}$$

Letting $z_1 =$ and $z_2 = z + \ell_\psi$ in Equation (78), the second double integral on the right-hand side of Equation (78) can be decomposed into two double integrals:

$$\int_0^{z_1}\int_0^{z_2} = \int_0^{z}\int_0^{z+\ell_\psi} = \int_0^{z}\int_0^{z} + \int_0^{z}\int_z^{z+\ell_\psi}. \tag{80}$$

Similarly, the second double integral on the right-hand side of Equation (78) can be expanded to

$$\int_0^{z_2}\int_0^{z_2} = \int_0^{z+\ell_\psi}\int_0^{z+\ell_\psi} = \int_0^{z}\int_0^{z} + \int_0^{z}\int_z^{z+\ell_\psi} + \int_z^{z+\ell_\psi}\int_0^{z} + \int_z^{z+\ell_\psi}\int_z^{z+\ell_\psi}. \tag{81}$$

Due to the symmetry of the correlation function, the middle two double integrals on the right-hand side can be combined:

$$\int_0^{z}\int_z^{z+\ell_\psi} + \int_z^{z+\ell_\psi}\int_0^{z} = 2\int_0^{z}\int_z^{z+\ell_\psi}. \tag{82}$$

Using this result, Equation (78) becomes

$$\left\langle \left[\int_0^z \varepsilon_1(\mathbf{s},\zeta)\,d\zeta - \int_0^{z+\ell_\psi} \varepsilon_1(\mathbf{s},\zeta)\,d\zeta\right]^2 \right\rangle = \int_z^{z+\ell_\psi}\int_z^{z+\ell_\psi} \langle \varepsilon_1(\mathbf{s},\zeta_1)\varepsilon_1(\mathbf{s},\zeta_2)\rangle \; d\zeta_1 d\zeta_2. \tag{83}$$

Hence, the correlation length, ℓ_ψ, of the scattered wave field in the z direction can be obtained by solving

$$\langle \psi(\mathbf{s},z)\psi^*(\mathbf{s},z+\ell_\psi)\rangle = \exp\left(-\frac{k^2}{8}\int_z^{z+\ell_\psi}\int_z^{z+\ell_\psi} \langle \varepsilon_1(\mathbf{s},\zeta_1)\varepsilon_1(\mathbf{s},\zeta_2)\rangle \; d\zeta_1 d\zeta_2\right) = \frac{1}{2}. \tag{84}$$

Taking the natural logarithm of both sides of this equation and letting $z = 0$ without loss of generality gives

$$k^2\int_0^{\ell_\psi}\int_0^{\ell_\psi} \langle \varepsilon_1(\mathbf{s},\zeta_1)\varepsilon_1(\mathbf{s},\zeta_2)\rangle \; d\zeta_1 d\zeta_2 = 8\ln 2. \tag{85}$$

The correlation function of the variations in ε_1 along the z direction can be denoted with

$$R_\varepsilon(\mathbf{s},\zeta_1,\zeta_2) = \langle \varepsilon_1(\mathbf{s},\zeta_1)\varepsilon_1(\mathbf{s},\zeta_2)\rangle\,. \tag{86}$$

Since ε_1 is a stationary random field, the correlation function is only a function of the difference between the two points ζ_1 and ζ_2 along the propagation direction; that is,

$$R_\varepsilon(\mathbf{s},\zeta_1,\zeta_2) = R_\varepsilon(\mathbf{s},\zeta_1-\zeta_2). \tag{87}$$

Letting $\zeta = \zeta_1 - \zeta_2$ and integrating Equation (85) over ζ_2 gives

$$k^2\ell_\psi\int_{-\ell_\psi}^{\ell_\psi}\left(1-\frac{|\zeta|}{\ell_\psi}\right) R_\varepsilon(\mathbf{s},\zeta)\,d\zeta = 8\ln 2. \tag{88}$$

Now, if $\ell_\varepsilon \ll \ell_\psi$ (fifth assumption), then

$$\int_{-\ell_\psi}^{\ell_\psi}\left(1-\frac{|\zeta|}{\ell_\psi}\right) R_\varepsilon(\mathbf{s},\zeta)\,d\zeta \simeq \int_{-\infty}^{\infty} R_\varepsilon(\mathbf{s},\zeta)\,d\zeta \sim \sigma_\varepsilon^2\ell_\varepsilon. \tag{89}$$

Ignoring the numerical factors $8\ln 2$ and $4\pi^2$, the correlation length is then given by

$$\ell_\psi \sim \frac{\lambda^2}{\sigma_\varepsilon^2\ell_\varepsilon}. \tag{90}$$

Equipped with a proper length scale characterizing the variations in the scattered wave field, $\psi(\mathbf{s}, z)$, it is now possible to write approximations for the magnitudes of the partial derivatives of the scattered wave field with respect to z in Equation (72). The first and second partial derivatives can be approximated as

$$\left|\frac{\partial\psi(\mathbf{s},z)}{\partial z}\right| \sim \frac{\sigma_\psi}{\ell_\psi} \quad \text{and} \quad \left|\frac{\partial^2\psi(\mathbf{s},z)}{\partial z^2}\right| \sim \frac{\sigma_\psi}{\ell_\psi^2}, \tag{91}$$

where

$$\sigma_\psi = \sqrt{\left\langle |\psi(\mathbf{s},z)|^2 \right\rangle} \tag{92}$$

denotes the root-mean-square variations in the scattered wave field, $\psi(\mathbf{s}, z)$. The magnitudes of the second and third terms in Equation (72) can, in turn, be approximated as

$$\left|\frac{\partial^2\psi(\mathbf{s},z)}{\partial z^2}\right| \sim \frac{\sigma_\psi}{\ell_\psi^2} \sim \frac{\sigma_\psi \sigma_\varepsilon^4 \ell_\varepsilon^2}{\lambda^4} \tag{93}$$

and

$$\left|-2jk\frac{\partial\psi(\mathbf{s},z)}{\partial z}\right| \sim \frac{\sigma_\psi}{\lambda\ell_\psi} \sim \frac{\sigma_\psi \sigma_\varepsilon^2 \ell_\varepsilon}{\lambda^3}, \tag{94}$$

respectively. The ratio of the magnitudes of the second and third terms in Equation (72) then can be approximated as

$$\left|\frac{\partial^2\psi(\mathbf{s},z)/\partial z^2}{-2jk\left[\partial\psi(\mathbf{s},z)/\partial z\right]}\right| \sim \frac{\sigma_\varepsilon^2 \ell_\varepsilon}{\lambda}. \tag{95}$$

It follows that if $\sigma_\varepsilon^2 \ll \lambda/\ell_\varepsilon$ (sixth assumption), then Equation (72) becomes

$$-2jk\frac{\partial\psi(\mathbf{s},z)}{\partial z} + \nabla_\perp^2\psi(\mathbf{s},z) + k^2\varepsilon_1(\mathbf{s},z)\psi(\mathbf{s},z) = 0. \tag{96}$$

Equation (96) is the parabolic wave equation governing the propagation of waves in turbulent media.

The parabolic wave Equation (96) is expressed in terms of the normalized fluctuations, $\varepsilon_1(\mathbf{s}, z)$, of the relative electric permittivity. To tie it back to the results derived in Section 2, it must be expressed in terms of the index of refraction. The relation between the index of refraction and the relative electric permittivity is given by

$$n(\mathbf{s},z) = \sqrt{\varepsilon_r(\mathbf{s},z)} = \sqrt{\langle\varepsilon_r\rangle\left[1+\varepsilon_1(\mathbf{s},z)\right]}. \tag{97}$$

Since $\sqrt{\left\langle |\varepsilon_1(\mathbf{s},z)|^2 \right\rangle} \ll 1$ (second assumption), a first-order Taylor approximation can be applied to obtain

$$n(\mathbf{s},z) \simeq \sqrt{\langle\varepsilon_r\rangle}\left[1+\frac{\varepsilon_1(\mathbf{s},z)}{2}\right]. \tag{98}$$

It follows that

$$\langle n\rangle = \sqrt{\langle\varepsilon_r\rangle} \tag{99}$$

and

$$\varepsilon_1(\mathbf{s},z) = 2n_1(\mathbf{s},z). \tag{100}$$

Substituting this expression for $\varepsilon_1(\mathbf{s}, z)$ into Equation (96), the parabolic wave equation can then be written in terms of the index of refraction:

$$-2jk\frac{\partial\psi(\mathbf{s},z)}{\partial z} + \nabla_\perp^2\psi(\mathbf{s},z) + 2k^2 n_1(\mathbf{s},z)\psi(\mathbf{s},z) = 0. \tag{101}$$

The parabolic wave Equation (101) is the fundamental equation describing the propagation of waves through turbulent media and will be the point of departure in the following discussion[2]. A number assumptions were made to arrive at Equation (101) from the Maxwell equations. All assumptions have been verified by measurements. Before leaving this section, here is a summary of the assumptions that were made to derive the parabolic wave equation:

1. The random fluctuations in the normalized relative permittivity, $\varepsilon_1(\mathbf{r}, t)$, are described by a zero-mean Gaussian probability density function. Since $\varepsilon_1(\mathbf{r}, t) = 2n_1(\mathbf{r}, t)$, the fluctuations in the normalized relative index of refraction, $n_1(\mathbf{s}, z)$, are also described by a zero-mean Gaussian probability density function.

2. The root-mean-square variations in $\varepsilon_1(\mathbf{r}, t)$, and hence the root-mean-square variations in $n_1(\mathbf{r}, t)$, are significantly smaller than unity; that is, $\sigma_\varepsilon = \sqrt{\left\langle |\varepsilon_1(\mathbf{r}, t)|^2 \right\rangle} \ll 1$ and $\sigma_n = \sqrt{\left\langle |n_1(\mathbf{r}, t)|^2 \right\rangle} \ll 1$.

3. The typical time scale of the variations in $\varepsilon_1(\mathbf{r}, t)$, and hence the typical time scale of the variations in $n_1(\mathbf{r}, t)$, is significantly greater that the inverse of the frequency of the propagating electromagnetic wave; that is, $\tau_\varepsilon \nu \gg 1$ and $\tau_n \nu \gg 1$. This assumption allows ε_1 and n_1 to be treated as frozen in time for propagation problems involving time scales that are much smaller than the time scales characterizing the random variations of the turbulent medium. In other words, we can let $\varepsilon_1(\mathbf{r}, t) \to \varepsilon_1(\mathbf{r})$ and $n_1(\mathbf{r}, t) \to n_1(\mathbf{r})$ in propagation equations.

4. The typical length scale of the variations in $\varepsilon_1(\mathbf{r})$, and hence the typical length scale of the variations in $n_1(\mathbf{r})$, is significantly greater than the wavelength of the propagating electromagnetic wave; that is, $\ell_\varepsilon \gg \lambda$ and $\ell_n \gg \lambda$.

5. The correlation length of the variations in the scattered wave field, $\psi(\mathbf{s}, z)$, where $\mathbf{r} = (\mathbf{s}, z)$, is significantly greater that the typical length scale of the variations in $\varepsilon_1(\mathbf{s}, z)$, and hence significantly greater the typical length scale of the variations in $n_1(\mathbf{s}, z)$; that is, $\ell_\psi \gg \ell_\varepsilon$ and $\ell_\psi \gg \ell_\varepsilon$.

[2]Interestingly, letting $z \to t$, $\mathbf{s} \to \mathbf{r}$, $k \to \hbar^{-1}$, $\nabla_\perp \to \nabla$, and $n_1(\mathbf{s}, z) \to -V(\mathbf{r}, t)$, Equation (101) takes the same form as the time-dependent Schrödinger equation describing the motion of a particle of unit mass ($m = 1$) in three-dimensional space:

$$-j\hbar \frac{\partial \psi(\mathbf{r}, t)}{\partial t} + \frac{\hbar^2}{2} \nabla^2 \psi(\mathbf{r}, t) - V(\mathbf{r}, t)\psi(\mathbf{r}, t) = 0.$$

Using operator notation, the time-dependent Schrödinger can be written as

$$-j\hbar \frac{\partial \left|\psi\right\rangle}{\partial t} = H \left|\psi\right\rangle,$$

where

$$H = -\frac{\hbar^2}{2} \nabla^2 + V(\mathbf{r}, t)$$

is the system's Hamiltonian, representing the particle's total energy (kinetic energy *plus* potential energy). The first term is the particle's kinetic energy, while $V(\mathbf{r}, t)$ is the particle's time-dependent potential energy. The momentum operator, $\hat{\mathbf{p}}$ is, in turn, given by

$$\hat{\mathbf{p}} = j\hbar\nabla.$$

Hence, the particle's kinetic energy is given by

$$\frac{\|\hat{\mathbf{p}}\|^2}{2} = -\frac{\hbar^2}{2} \nabla^2.$$

It follows that in an analogy with quantum mechanics, $\nabla_\perp^2/(2k^2) + n_1(\mathbf{s}, z)$ in Equation (101) can be interpreted as a Hamiltonian; $j\nabla_\perp/k$ can be interpreted as a momentum operator; and $n(\mathbf{s}, z)$ can be interpreted as the negative of a potential energy.

6. The mean-square variations in $\varepsilon_1(\mathbf{s}, z)$ is significantly smaller than the ratio of the wavelength of the propagating electromagnetic wave divided by the typical length scale of the variations in $\varepsilon_1(\mathbf{s}, z)$; that is, $\sigma_\varepsilon^2 \ll \lambda/\ell_\varepsilon$. Similarly, the mean-square variations in $n_1(\mathbf{s}, z)$ is significantly smaller than the ratio of the wavelength of the propagating electromagnetic wave divided by the typical length scale of the variations in $n_1(\mathbf{s}, z)$; that is, $\sigma_n^2 \ll \lambda/\ell_n$. These are stronger conditions compared to the conditions $\sigma_\varepsilon \ll 1$ and $\sigma_n \ll 1$ (third assumption).

A major consequence of the fifth assumption ($\ell_\psi \gg \ell_\varepsilon$ or $\ell_\psi \gg \ell_n$) is that the turbulent medium can be assumed to be uncorrelated along the direction of propagation (z direction in our notation). This is the *Markov approximation*. The Markov approximation implies that the scattering caused by a thin layer of the random medium along the propagation direction is independent of the scattering caused by the layers of the random medium behind this layer. This result is consistent with the small-angle forward scattering of waves governed by the parabolic wave equation. The Markov approximation simplifies the derivation of formal solutions of parabolic wave equation, which is the subject of the next section.

4 Formal Solutions

In this section, two formal solutions of the parabolic wave Equation (101) are derived for two limiting scenarios. Section 4.1 addresses the case where the turbulent medium is concentrated in a thin layer perpendicular to the direction of propagation. Many propagation effects be can be explained with a fairly high degree of accuracy using such a "thin screen" model of the medium, such as scenarios involving electromagnetic waves propagating through "clumps" of turbulent regions in the atmosphere. The thin medium layer acts effectively as a phase screen that corrugates the wavefronts of the propagating electromagnetic waves. The statistical properties of such a phase screen are discussed in Section 4.2. The solution to the thin screen problem also provides a convenient basis for deriving the formal solution for the case of an extended medium—the second limiting scenario—that can be regarded as a superposition of many thin screens. The formal solution for the case of wave propagation through extended media is derived in Section 4.3.

4.1 The Thin Screen Problem

In this section, a formal solution of the parabolic wave Equation (101) is derived for the limiting case of the turbulent medium being concentrated in a thin screen of thickness δz located at $z = 0$. The geometry of this propagation scenario is illustrated in Figure 4.

Although thin, the screen's thickness is assumed to be still significantly greater than the typical length scale of the normalized relative index of refraction fluctuations of the medium, $n_1(\mathbf{s}, z)$; that is, $\delta z \ll \ell_n$. Yet, the screen is assumed to be thin enough to allow for solving the parabolic wave Equation (101) in two more simplified steps. In the first step, the diffractive effects modeled by the transverse Laplacian, $\nabla_\perp^2$, in the parabolic wave Equation (101) are ignored. This results in the so-called geometric optics solution that captures the effect the turbulent medium will have in modifying the phase of waves propagating through the thin screen. In the second step, the parabolic wave equation is solved by ignoring the third term involving the index of refraction, $n_1(\mathbf{s}, z)$, in Equation (101). In other words, the second step compensates for the diffractive effects that were ignored in the first step. In the second step, the geometrical optics solution from the first step becomes the initial condition for solving the free-space version ($n_1 = 0$) of the parabolic

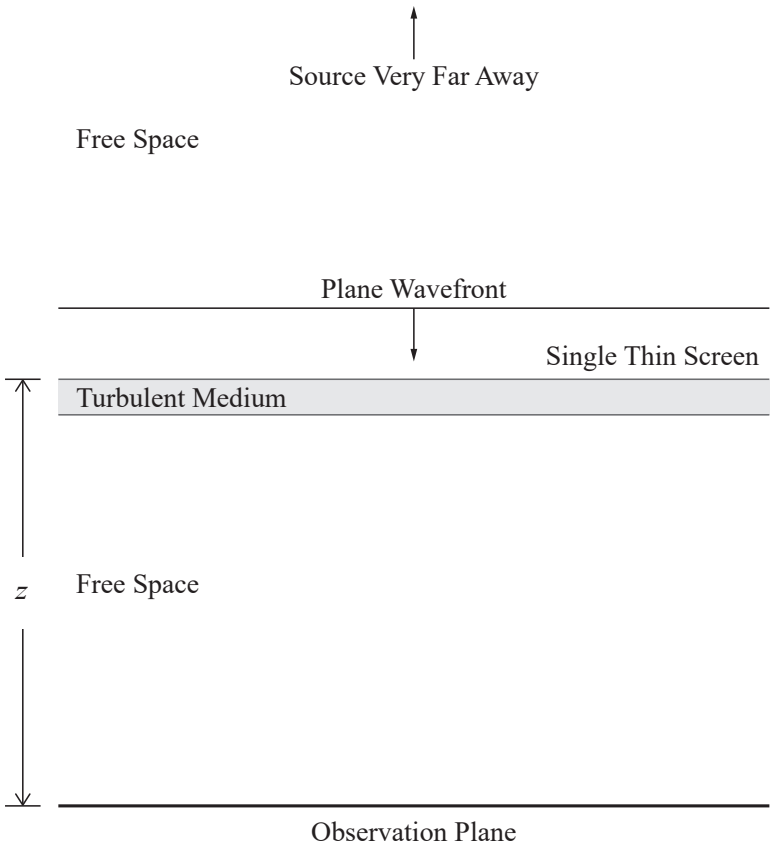

Figure 4: Geometry of the thin screen propagation problem. The radiation source is assumed to lie very far away from the observer. The turbulent medium is assumed to be concentrated into a thin layer at $z = 0$.

wave equation. This technique for solving the parabolic wave equation is often referred to as the *split-step algorithm*. The split-step technique can be applied only if the medium layer is sufficiently thin.

In the first step of the split-step algorithm, the geometric optics solution associated with the scattered wave field immediately exiting the screen of thickness δz located at $z = 0$ (see Figure 4) is desired; that is, the aim is to obtain $\psi(\mathbf{s}, \delta z)$. Within the screen ($0 \leq z < \delta z$), ignoring the Laplacian term, $\nabla_\perp^2 \psi(\mathbf{s}, z)$, in Equation (101), the parabolic wave equation becomes

$$-2jk\frac{\partial \psi(\mathbf{s}, z)}{\partial z} + 2k^2 n_1(\mathbf{s}, z)\psi(\mathbf{s}, z) = 0. \tag{102}$$

This is a trivial differential equation that can be easily solved to give

$$\psi(\mathbf{s}, \delta z) = \psi(\mathbf{s}, 0) \exp\left(-jk \int_0^{\delta z} n_1(\mathbf{s}, \zeta)\, d\zeta\right), \tag{103}$$

where $\psi(\mathbf{s}, 0)$ is the wave field immediately prior to entering the thin screen. For a point source at a distance very far away from the observer, the wave impinging on the thin screen is effectively a plane wave; that is, $\psi(\mathbf{s}, 0) = 1$ (see Figure 4). Letting

$$\varphi(\mathbf{s}) = k \int_0^{\delta z} n_1(\mathbf{s}, \zeta)\, d\zeta, \tag{104}$$

the solution can be written as

$$\psi(\mathbf{s}, \delta z) = \psi(\mathbf{s}, 0) e^{-j\varphi(\mathbf{s})}. \tag{105}$$

Here, $\varphi(\mathbf{s})$ denotes the random phase variations induced by the medium as the wave propagates through it.

In the second step of the split-step algorithm, the diffractive effects captured by the Laplacian term, $\nabla_\perp^2 \psi(\mathbf{s}, z)$, in the parabolic wave Equation (101) that were ignored in deriving the geometric optics solution (105) are included. Letting $n_1(\mathbf{s}, z) = 0$ in Equation (101), the parabolic wave equation becomes

$$-2jk \frac{\partial \psi(\mathbf{s}, z)}{\partial z} + \nabla_\perp^2 \psi(\mathbf{s}, z) = 0. \tag{106}$$

The geometric optics solution (105) serves as the initial condition for solving this partial differential equation. Since after exiting the thin screen, the wave propagates through free space until it reaches the observation plane (see Figure 4), the solution to the free-space parabolic wave Equation (106) with initial condition (105) can be applied to any $z > 0$ and is therefore not limited to only within the thin screen (i.e., $0 < z < \delta z$). Fourier analysis can be used to solve Equation (106). The following Fourier relations are assumed (see also Appendix A)[3]:

$$\psi(\mathbf{s}, z) = \int_{\mathbb{R}^2} \Psi(\boldsymbol{\kappa}, z) e^{-j\boldsymbol{\kappa}\cdot\mathbf{s}} \, d^2\boldsymbol{\kappa}, \tag{107}$$

$$\Psi(\boldsymbol{\kappa}, z) = \frac{1}{(2\pi)^2} \int_{\mathbb{R}^2} \psi(\mathbf{s}, z) e^{j\boldsymbol{\kappa}\cdot\mathbf{s}} \, d^2\mathbf{s}. \tag{108}$$

Taking the two-dimensional Fourier transform of Equation (106) and noting that

$$\nabla_\perp^2 \psi(\mathbf{s}, z) = \int_{\mathbb{R}^2} \left[- \|\boldsymbol{\kappa}\|^2 \Psi(\boldsymbol{\kappa}, z) \right] e^{-j\boldsymbol{\kappa}\cdot\mathbf{s}} \, d^2\boldsymbol{\kappa}, \tag{109}$$

the parabolic wave equation becomes

$$-2jk \frac{\partial \Psi(\boldsymbol{\kappa}, z)}{\partial z} - \|\boldsymbol{\kappa}\|^2 \Psi(\boldsymbol{\kappa}, z) = 0. \tag{110}$$

This again is a trivial differential equation that can be easily solved to give

$$\Psi(\boldsymbol{\kappa}, z) = \Psi(\boldsymbol{\kappa}, \delta z) \exp\left(\frac{j \|\boldsymbol{\kappa}\|^2}{2k} \int_0^z d\zeta \right), \tag{111}$$

where $\Psi(\boldsymbol{\kappa}, \delta z)$ is the two-dimensional Fourier transform of the geometrical optics solution, $\psi(\mathbf{s}, \delta z)$, which serves as the initial condition for the free-space parabolic wave Equation (106). The exponential term in Equation (111) is a Gaussian function. Its inverse Fourier transform is therefore also a Gaussian function:

$$\int_{\mathbb{R}^2} \exp\left(\frac{jz}{2k} \|\boldsymbol{\kappa}\|^2 \right) e^{-j\boldsymbol{\kappa}\cdot\mathbf{s}} \, d^2\boldsymbol{\kappa} = \frac{jk}{2\pi z} \exp\left(-\frac{jk}{2z} \|\mathbf{s}\|^2 \right). \tag{112}$$

The inverse Fourier transform of Equation (111) is therefore the convolution of this Gaussian function and the initial condition $\psi(\mathbf{s}, \delta z)$:

$$\psi(\mathbf{s}, z) = \psi(\mathbf{s}, \delta z) * \frac{jk}{2\pi z} \exp\left(-\frac{jk}{2z} \|\mathbf{s}\|^2 \right). \tag{113}$$

[3]Since the function $\psi(\mathbf{s}, z)$ is stochastic, the Fourier integral is not guaranteed to be absolutely integrable. Any discontinuities of $\psi(\mathbf{s}, z)$ are also not guaranteed to be finite. More formally, the stochastic *Fourier–Stieltjes integral* must be used instead of the conventional Fourier integral. However, the same result as derived in this section is obtained when applying the Fourier–Stieltjes integral. As a result, this subtlety is often ignored in the literate. For more information on Fourier–Stieltjes integral see [1].

Expanding the convolution integral, $\psi(\mathbf{s}, z)$ can be written as

$$\psi(\mathbf{s}, z) = \frac{jk}{2\pi z} \int_{\mathbb{R}^2} \psi\left(\mathbf{s}', 0\right)\ e^{-j\varphi(\mathbf{s}')} \exp\left(-\frac{jk}{2z}\left\|\mathbf{s}' - \mathbf{s}\right\|^2\right)\ d^2\mathbf{s}'. \tag{114}$$

This is the formal solution for the scattered wave field, $\psi(\mathbf{s}, z)$, propagating through a thin screen. Equation (114) can also be written as

$$\psi(\mathbf{s}, z) = \int_{\mathbb{R}^2} \psi\left(\mathbf{s}', 0\right) G\left(\mathbf{s}, \mathbf{s}', z\right)\ d^2\mathbf{s}', \tag{115}$$

where

$$G(\mathbf{s}, \mathbf{s}', z) = e^{-j\varphi(\mathbf{s}')} G^f(\mathbf{s}, \mathbf{s}', z) \tag{116}$$

is the *Green function* for the wave propagation problem through the turbulent thin screen. The second factor on the right-hand side is, in turn, the *free-space Green function*:

$$G^f\left(\mathbf{s}, \mathbf{s}', z\right) = \frac{jk}{2\pi z} \exp\left(-\frac{jk}{2z}\left\|\mathbf{s}' - \mathbf{s}\right\|^2\right). \tag{117}$$

4.2 Phase Statistics

The statistical properties of the phase fluctuations induced by the thin layer of random medium of thickness δz (see Figure 4),

$$\varphi(\mathbf{s}) = k \int_0^{\delta z} n_1(\mathbf{s}, \zeta)\, d\zeta, \tag{118}$$

play a direct role in characterizing the average behavior of the scattered wave field, $\psi(\mathbf{s}, z)$, in the observation plane. In this section, the key statistical parameters characterizing the random behavior of these phase fluctuations are derived and expressed in terms of the corresponding statistical parameters associated with the fluctuations of the normalized relative index of fraction of the turbulent medium. Specifically, expressions are derived for characterizing the second-order statistical behavior of the phase function specified in Equation (118), corresponding to the correlation function of $\varphi(\mathbf{s})$, or, equivalently, its power spectral density.

The two-point correlation function of the random phase fluctuation, $\varphi(\mathbf{s})$, is defined by

$$R_\varphi(\mathbf{s}_1, \mathbf{s}_2) = \left\langle \left[\varphi(\mathbf{s}_1) - \langle\varphi(\mathbf{s}_1)\rangle\right] \left[\varphi(\mathbf{s}_2) - \langle\varphi(\mathbf{s}_2)\rangle\right] \right\rangle, \tag{119}$$

where the angular brackets, $\langle\cdot\rangle$, denote the ensemble average. The ensemble average of $\varphi(\mathbf{s})$ can be easily computed from Equation (118) to obtain

$$\langle\varphi(\mathbf{s})\rangle = k \int_0^{\delta z} \langle n_1(\mathbf{s}, \zeta)\rangle\ d\zeta = 0. \tag{120}$$

It follows that the correlation function, $R_\varphi(\mathbf{s}_1, \mathbf{s}_2)$, can be expressed as

$$R_\varphi(\mathbf{s}_1, \mathbf{s}_2) = \langle\varphi(\mathbf{s}_1)\varphi(\mathbf{s}_2)\rangle = k^2 \int_0^{\delta z} \int_0^{\delta z} \langle n_1(\mathbf{s}_1, \zeta_1) n_1(\mathbf{s}_2, \zeta_2)\rangle\ d\zeta_1 d\zeta_2. \tag{121}$$

Now, since $n_1(\mathbf{s}, z)$ is a homogeneous scalar random field, its two-point correlation function is only a function of the difference between the two points; that is,

$$\langle n_1(\mathbf{s}_1, z_1) n_1(\mathbf{s}_2, z_2)\rangle = R_n(\mathbf{s}_1 - \mathbf{s}_2, z_1 - z_2). \tag{122}$$

Using this expression, the expression for $R_\varphi(\mathbf{s}_1, \mathbf{s}_2)$ becomes

$$R_\varphi(\mathbf{s}_1, \mathbf{s}_2) = k^2 \int_0^{\delta z} \int_0^{\delta z} R_n(\mathbf{s}_1 - \mathbf{s}_2, \zeta_1 - \zeta_2)\, d\zeta_1 d\zeta_2. \tag{123}$$

It follows that

$$R_\varphi(\mathbf{s}_1, \mathbf{s}_2) = R_\varphi(\mathbf{s}_1 - \mathbf{s}_2) = R_\varphi(\mathbf{s}), \tag{124}$$

is also a function of the difference vector, $\mathbf{s} = \mathbf{s}_1 - \mathbf{s}_2$. Letting $\zeta = \zeta_1 - \zeta_2$ and integrating over ζ_2, $R_\varphi(\mathbf{s})$ becomes

$$R_\varphi(\mathbf{s}) = k^2 \delta z \int_{-\delta z}^{\delta z} \left(1 - \frac{|\zeta|}{\delta z}\right) R_n(\mathbf{s}, \zeta)\, d\zeta. \tag{125}$$

Since the screen thickness, δz, is assumed to be significantly greater than the typical length, ℓ_n, of the variations in $n_1(\mathbf{s}, z)$, $R_\varphi(\mathbf{s})$ can be written as

$$R_\varphi(\mathbf{s}) \simeq k^2 \delta z \int_{-\infty}^{\infty} R_n(\mathbf{s}, \zeta)\, d\zeta. \tag{126}$$

Taking the two-dimensional Fourier transform (with respect to $\mathbf{s}$) of $R_n(\mathbf{s}, \zeta)$, $R_n(\mathbf{s}, \zeta)$ can be written in terms of the power spectral density of the normalized index of refraction fluctuations:

$$R_n(\mathbf{s}, z) = \int_{-\infty}^{\infty} \int_{\mathbb{R}^2} P_n(\boldsymbol{\kappa}, q_z) e^{-j\boldsymbol{\kappa}\cdot\mathbf{s}} e^{-jq_z z}\, d^2\boldsymbol{\kappa}\, dq_z. \tag{127}$$

$R_\varphi(\mathbf{s})$ can therefore be written as

$$R_\varphi(\mathbf{s}) = k^2 \delta z \int_{-\infty}^{\infty} \left[\int_{-\infty}^{\infty} \int_{\mathbb{R}^2} P_n(\boldsymbol{\kappa}, q_z) e^{-j\boldsymbol{\kappa}\cdot\mathbf{s}} e^{-jq_z \zeta}\, d^2\boldsymbol{\kappa}\, dq_z \right] d\zeta. \tag{128}$$

Since

$$\int_{-\infty}^{\infty} e^{-jq_z\zeta}\, d\zeta = 2\pi\delta(q_z), \tag{129}$$

where $\delta(\cdot)$ is the Dirac delta function, it follows that

$$R_\varphi(\mathbf{s}) = 2\pi k^2 \delta z \int_{\mathbb{R}^2} P_n(\boldsymbol{\kappa}, 0) e^{-j\boldsymbol{\kappa}\cdot\mathbf{s}}\, d^2\boldsymbol{\kappa}. \tag{130}$$

Since the correlation function, $R_\phi(\mathbf{s})$, can also be expressed as the two-dimensional Fourier transform of the power spectral density, $P_\varphi(\boldsymbol{\kappa})$, of the phase fluctuations induced by the thin screen,

$$R_\varphi(\mathbf{s}) = \int_{\mathbb{R}^2} P_\varphi(\boldsymbol{\kappa}) e^{-j\boldsymbol{\kappa}\cdot\mathbf{s}}\, d^2\boldsymbol{\kappa}, \tag{131}$$

it follows that

$$P_\varphi(\boldsymbol{\kappa}) = 2\pi k^2 \delta z P_n(\boldsymbol{\kappa}, 0). \tag{132}$$

Equation (132) provides a direct relation between the power spectral density of the phase fluctuations induced by the thin screen and the power spectral density of the fluctuations in the index of refraction of the turbulent medium. Substituting the general expression for the power spectral density of the index of refraction fluctuations discussed in Section 2 into Equation (132), the following expression is obtained for the power spectral density of the phase fluctuations induced by the thin screen:

$$P_\varphi(\kappa) = \frac{C_\varphi^2}{(\kappa^2 + \kappa_o^2)^{\beta/2}} \exp\left(-\frac{\kappa^2}{\kappa_i^2}\right), \tag{133}$$

where $\kappa = \|\boldsymbol{\kappa}\| = \sqrt{q_x^2 + q_y^2}$ denotes the magnitude of the two-dimensional wavenumber, $\boldsymbol{\kappa}$, and

$$C_\varphi^2 = 2\pi k^2 f(\beta) C_n^2 \delta z \tag{134}$$

is hereafter referred to as the *phase structure constant*.

Beside the power spectral density, another important function characterizing the second-order statistical behavior of a random field is the *structure function*. The general definition of the structure function (expressed here for the random phase fluctuations, $\varphi(\mathbf{s})$) is given by

$$D_\varphi(\mathbf{s}_1, \mathbf{s}_2) = \left\langle \left\{ [\varphi(\mathbf{s}_1) - \langle \varphi(\mathbf{s}_1) \rangle] - [\varphi(\mathbf{s}_2) - \langle \varphi(\mathbf{s}_2) \rangle] \right\}^2 \right\rangle = \left\langle [\varphi(\mathbf{s}_1) - \varphi(\mathbf{s}_2)]^2 \right\rangle. \tag{135}$$

Structure functions are useful for describing the statistical properties of random fields that are only locally homogeneous (see [1] for a more detailed discussion on structure functions and inhomogeneous random fields). For stationary random fields, expanding the right-hand side of Equation (135), the structure function can be directly related to the correlation function:

$$D_\varphi(\mathbf{s}) = 2\left[R_\varphi(\mathbf{0}) - R_\varphi(\mathbf{s})\right], \tag{136}$$

where $\mathbf{s} = \mathbf{s}_1 - \mathbf{s}_2$. Clearly, $D_\varphi(\mathbf{0}) = \mathbf{0}$. Using this relationship, the structure function of the phase fluctuations can also be expressed in terms of their power spectral density:

$$D_\varphi(\mathbf{s}) = 2\int_{\mathbb{R}^2} P_\varphi(\boldsymbol{\kappa}) \left[1 - e^{-j\boldsymbol{\kappa}\cdot\mathbf{s}}\right] d^2\boldsymbol{\kappa}. \tag{137}$$

4.3 Extended Media

The thin screen solution derived in Section 4.1 forms the basis for deriving a formal solution for the extended medium scenario. The extended medium can be modeled as a superposition of a large number of thin phase screens stacked on top of each other. Due to the Markov approximation discussed at the end of Section 3, the propagation problem through each phase screen can be treated independently. The wave exiting one phase screen becomes the input to the next phase screen along the propagation direction. The formal solution for the extended medium scenario is obtained by dividing the extended medium into ever larger number of phase screens.

The geometry relevant to the discussion in this section is shown in Figure 5. Specifically, the extended medium is divided into N phase screens, each of thickness δz, along the z-axis (direction of propagation), such that

$$z_{k+1} = z_k + \delta z, \tag{138}$$

where $k = 0, 1, 2, \ldots, N-1$, with $z_0 = 0$ and $z_N = N\delta z = z$ (the observation plane). The initial aim will be to derive the formal solution associated with the kth screen using the same split-step technique employed in Section 4.1. Subsequently, the results will be combined using recursion to obtain the formal solution for N screens.

The random phase variations induced by the kth screen are given by

$$\varphi_k(\mathbf{s}_k) = k\int_{z_k}^{z_{k+1}} n_1(\mathbf{s}_k, \zeta)\, d\zeta. \tag{139}$$

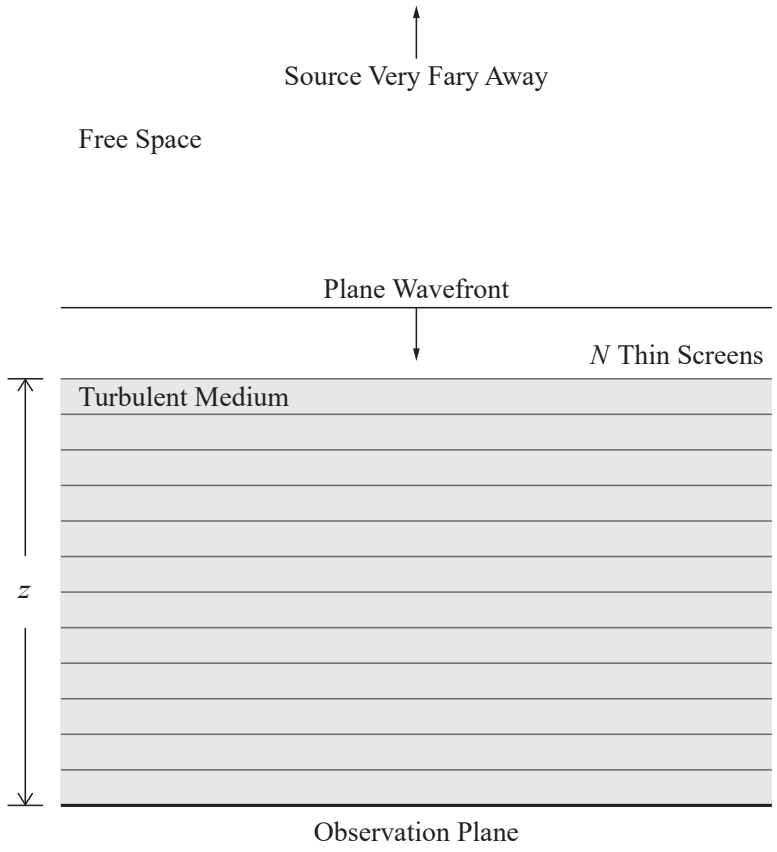

Figure 5: Extended medium propagation geometry. The radiation source is assumed to lie very far away from the observer. The turbulent medium is divided into N thin screens along the direction of propagation.

Here, $\mathbf{s}_k = (x_k, y_k)$ denotes the coordinates of the plane perpendicular to the direction of propagating at $z = z_k$. The kth phase screen corrugates the wavefront of the scattered wave field exiting the screen:

$$\psi_k^-(\mathbf{s}_k, z_{k+1}) = \psi_k^+(\mathbf{s}_k, z_k)\, e^{-j\varphi_k(\mathbf{s}_k)}, \tag{140}$$

where $\psi_k^+(\mathbf{s}_k, z_k)$ denotes the wave field entering the screen at $z = z_k$, and $\psi_k^-(\mathbf{s}_k, z_{k+1})$ denotes the wave field exiting the phase screen prior to taking the diffractive effect of the free-space Green function into account. This is the first step of the split-step solution. Next, to include the effect of diffraction, $\psi_k^-(\mathbf{s}_k, z_{k+1})$ is multiplied by the free-space Green function,

$$G^f(\mathbf{s}_k, \mathbf{s}_{k+1}, \delta z) = \frac{jk}{2\pi\delta z} \exp\left(-\frac{jk}{2\delta z}\left\|\mathbf{s}_{k+1} - \mathbf{s}_k\right\|^2\right), \tag{141}$$

and integrated over $\mathbf{s}_k$. The scattered wave field at $z = z_{k+1}$ with the diffractive effect included is then given by

$$\psi_{k+1}^+(\mathbf{s}_{k+1}, z_{k+1}) = \frac{jk}{2\pi\delta z}\int_{\mathbb{R}^2} \psi_k^-(\mathbf{s}_k, z_{k+1}) \exp\left(-j\frac{k\left\|\mathbf{s}_{k+1} - \mathbf{s}_k\right\|^2}{2\delta z}\right) d^2\mathbf{s}_k. \tag{142}$$

This is the second step of the split-step algorithm. Combining the two steps and dropping the now redundant "+" and "−" superscripts, the following recursion relation expressing the scattered wave field at $z = z_{k+1}$

in terms of the scattered wave field at $z = z_k$ is obtained:

$$\psi_{k+1}(\mathbf{s}_{k+1}, z_{k+1}) = \frac{jk}{2\pi\delta z} \int_{\mathbb{R}^2} \psi_k(\mathbf{s}_k, z_k)\, e^{-j\varphi_k(\mathbf{s}_k)} \exp\left(-j\frac{k\left\|\mathbf{s}_{k+1} - \mathbf{s}_k\right\|^2}{2\delta z}\right) d^2\mathbf{s}_k. \tag{143}$$

Applying Equation (142) recursively, the expression for the scattered wave field at $z = z_N = N\delta z$ is then given by

$$\psi(\mathbf{s}_N, z_N) = \left(\frac{jk}{2\pi\delta z}\right)^{N-1} \int_{\mathbb{R}^2} \cdots \int_{\mathbb{R}^2} \psi(\mathbf{s}_1, z_1) \exp\left(-j\sum_{k=1}^{N-1}\left[\varphi(\mathbf{s}_k) + \frac{k\left\|\mathbf{s}_{k+1} - \mathbf{s}_k\right\|^2}{2\delta z}\right]\right) d^2\mathbf{s}_{N-1} \cdots d^2\mathbf{s}_1. \tag{144}$$

This is the formal solution for the wave field propagating through N phase screens.

Letting

$$\frac{k\left\|\mathbf{s}_{k+1} - \mathbf{s}_k\right\|^2}{2\delta z} = \frac{k}{2}\left\|\frac{\mathbf{s}_{k+1} - \mathbf{s}_k}{\delta z}\right\|^2 \delta z, \tag{145}$$

and noting that δz is very small, $\varphi(\mathbf{s})$ can be approximated as

$$\varphi(\mathbf{s}_k) \simeq k n_1(\mathbf{s}_k, z_k)\delta z. \tag{146}$$

Subsequently, the argument of the exponential in Equation (144) can be written as

$$-j\sum_{k=1}^{N-1}\left[\varphi(\mathbf{s}_k) + \frac{k\left\|\mathbf{s}_{k+1} - \mathbf{s}_k\right\|^2}{2\delta z}\right] = -jk\sum_{k=1}^{N-1}\left[n_1(\mathbf{s}_k, z_k) + \frac{1}{2}\left\|\frac{\mathbf{s}_{k+1} - \mathbf{s}_k}{\delta z}\right\|^2\right]\delta z. \tag{147}$$

As $N \to \infty$ (and therefore as $\delta z \to 0$), the summation is replaced with an integral:

$$\lim_{N\to\infty}\sum_{k=1}^{N-1}\left[n_1(\mathbf{s}_k, z_k) + \frac{1}{2}\left\|\frac{\mathbf{s}_{k+1} - \mathbf{s}_k}{\delta z_k}\right\|^2\right]\delta z_k = \int_0^z \left[n_1\left(\mathbf{s}(\zeta), \zeta\right) + \frac{1}{2}\left\|\frac{d\mathbf{s}(\zeta)}{d\zeta}\right\|^2\right] d\zeta, \tag{148}$$

where $z = z_N$ (observer location). The scattered wave field is, in turn, given by

$$\psi(\mathbf{s}, z) = \lim_{N\to\infty}\psi(\mathbf{s}_N, z_N) = \int \psi(\mathbf{s}(0), 0) \exp\left(-jk\int_0^z L(\mathbf{s}(\zeta), \zeta)\, d\zeta\right) D\mathbf{s}(z), \tag{149}$$

where

$$L(\mathbf{s}(\zeta), \zeta) = \frac{1}{2}\left\|\frac{d\mathbf{s}(\zeta)}{d\zeta}\right\|^2 + n_1(\mathbf{s}(\zeta), \zeta), \tag{150}$$

and $D\mathbf{s}(z)$ denotes a "functional differential" that is defined such that

$$\int D\mathbf{s}(z) = \lim_{N\to\infty}\left[\left(\frac{jk}{2\pi\delta z}\right)^{N-1}\int_{\mathbb{R}^2}\cdots\int_{\mathbb{R}^2} d^2\mathbf{s}_{N-1}\cdots d^2\mathbf{s}_1\right]. \tag{151}$$

Equation (149) is recognized as the *Feynman path integral* (see [5]). It is the formal solution of the parabolic wave Equation (101) for an extended medium[4].

[4]Following the footnote discussion in Section 3, letting $\mathbf{s}(\zeta) \to \mathbf{r}$, $\zeta \to t$, and interpreting $n_1(\mathbf{s}(\zeta), \zeta) \to -V(\mathbf{r}, t)$ as a potential energy in analogy with quantum mechanics, the expression in the square brackets in the integral in Equation (149) can be interpreted as a Lagrangian (kinetic energy *minus* potential energy):

$$L(\mathbf{s}(\zeta), \zeta) = \frac{1}{2}\left\|\frac{d\mathbf{s}(\zeta)}{d\zeta}\right\| + n_1(\mathbf{s}(\zeta), \zeta) \quad \to \quad L(\mathbf{r}, t) = \frac{1}{2}\left\|\dot{\mathbf{r}}\right\|^2 - V(\mathbf{r}, t).$$

5 Second-Order Statistics

The formal solutions derived in Section 4 represent the random realizations of the scattered wave field. One must resort to statistical analyses in order to gain a better understanding of the propagation problem at hand. Statistical moments describe key average properties associated with the observed scattered wave fields. In this section and the next, following the formulation of [6], expressions are derived for the *second* and *fourth* statistical moments of the scattered wave field, respectively, that are of particular importance. These expressions are used in Section 7 to derive few useful parameters characterizing the statistical behavior of the observed scattered wave fields. The turbulent medium is assumed to be concentrated in a thin layer located at a distance z from the observation plane. The solution of the parabolic wave equation given by Equation (114) is used to derive the expressions for the second and fourth statistical moments for the thin screen problem. Although not discussed, the Feynman path integral (149) can be used in a similar manner to derive expressions for the second and fourth statistical moments for waves propagating through extended media (see [6] for further detail).

5.1 Second Moment

The second statistical moment of the scattered wave field is defined as

$$\Gamma_2(\mathbf{s}_1, \mathbf{s}_2, z) = \langle \psi(\mathbf{s}_1, z) \psi^*(\mathbf{s}_2, z) \rangle \,. \tag{152}$$

The second moment represents the *mutual coherence function* of the scattered wave field. Its Fourier transform, in turn, represents the *brightness distribution function* of the scattered wave field. The brightness distribution is used to characterize the degree of angular scattering experienced by the wave propagating through the turbulent medium.

Substituting Equation (114)—or, equivalently, Equation (115)—for the scattered wave field into Equation (152), the second statistical moment for a wave propagating through a thin turbulent medium layer located at a distance z from the observation plane can be written as

$$\Gamma_2(\mathbf{s}_1, \mathbf{s}_2, z) = \int_{\mathbb{R}^2} \int_{\mathbb{R}^2} \Gamma_2 \left(\mathbf{s}_1', \mathbf{s}_2', 0\right) G_2 \left(\mathbf{s}_1, \mathbf{s}_2, \mathbf{s}_1', \mathbf{s}_2', z\right) \, d^2\mathbf{s}_1' d^2\mathbf{s}_2', \tag{153}$$

where

$$G_2 \left(\mathbf{s}_1, \mathbf{s}_2, \mathbf{s}_1', \mathbf{s}_2', z\right) = \left\langle G \left(\mathbf{s}_1, \mathbf{s}_1', z\right) G^* \left(\mathbf{s}_2, \mathbf{s}_2', z\right) \right\rangle . \tag{154}$$

Substituting Equation (116) for the Green function, G, associated with the scattered wave field, the Green function, G_2, for the second moment can be written as

$$G_2 \left(\mathbf{s}_1, \mathbf{s}_2, \mathbf{s}_1', \mathbf{s}_2', z\right) = \left\langle e^{-j[\varphi(\mathbf{s}_1') - \varphi(\mathbf{s}_2')]} \right\rangle G_2^f \left(\mathbf{s}_1, \mathbf{s}_2, \mathbf{s}_1', \mathbf{s}_2', z\right) , \tag{155}$$

where

$$G_2^f \left(\mathbf{s}_1, \mathbf{s}_2, \mathbf{s}_1', \mathbf{s}_2', z\right) = G^f \left(\mathbf{s}_1, \mathbf{s}_1', z\right) G^{f*} \left(\mathbf{s}_2, \mathbf{s}_2', z\right) . \tag{156}$$

Substituting Equation (117) for the free space Green function, G^f, associated with the scattered wave field into Equation (156), the free space Green function, G_2^f, for the second moment becomes

$$G_2^f \left(\mathbf{s}_1, \mathbf{s}_2, \mathbf{s}_1', \mathbf{s}_2', z\right) = \left(\frac{k}{2\pi z}\right)^2 \exp\left(-\frac{jk}{2z}\left(\left\|\mathbf{s}_1' - \mathbf{s}_1\right\|^2 - \left\|\mathbf{s}_2' - \mathbf{s}_2\right\|^2\right)\right) \tag{157}$$

If θ is a zero-mean Gaussian random variable, then

$$\left\langle e^{j\theta} \right\rangle = e^{-\frac{1}{2}\langle \theta^2 \rangle}. \tag{158}$$

Using this identity, the term in angular brackets in Equation (155) can be expressed as

$$\left\langle e^{-j\left[\varphi(\mathbf{s}_1')-\varphi(\mathbf{s}_2')\right]} \right\rangle = e^{-\frac{1}{2}\left\langle \left[\varphi(\mathbf{s}_1')-\varphi(\mathbf{s}_2')\right]^2 \right\rangle} = \exp\left(-\frac{1}{2} D_\varphi\left(\mathbf{s}_1' - \mathbf{s}_2'\right)\right). \tag{159}$$

It follows from equations (157) and (159) that

$$\begin{aligned}\Gamma_2(\mathbf{s}_1, \mathbf{s}_2, z) = \left(\frac{k}{2\pi z}\right)^2 \int_{\mathbb{R}^2}\int_{\mathbb{R}^2} \Gamma_2\left(\mathbf{s}_1', \mathbf{s}_2', 0\right) \exp\left(-\frac{1}{2} D_\varphi\left(\mathbf{s}_1' - \mathbf{s}_2'\right)\right) \\ \times \exp\left(-\frac{jk}{2z}\left(\left\|\mathbf{s}_1' - \mathbf{s}_1\right\|^2 - \left\|\mathbf{s}_2' - \mathbf{s}_2\right\|^2\right)\right) d^2\mathbf{s}_1' d^2\mathbf{s}_2'.\end{aligned} \tag{160}$$

To simplify Equation (160), the following change of variables is introduced:

$$\begin{aligned}\boldsymbol{\sigma}' &= \mathbf{s}_1' - \mathbf{s}_1', \\ \boldsymbol{\rho}' &= \frac{\mathbf{s}_1' + \mathbf{s}_2'}{2}.\end{aligned} \tag{161}$$

Equivalently, $\mathbf{s}_1'$ and $\mathbf{s}_2'$ can be expressed in terms of $\boldsymbol{\sigma}'$ and $\boldsymbol{\rho}'$:

$$\begin{aligned}\mathbf{s}_1' &= \boldsymbol{\rho}' + \frac{\boldsymbol{\sigma}'}{2}, \\ \mathbf{s}_2' &= \boldsymbol{\rho}' - \frac{\boldsymbol{\sigma}'}{2}.\end{aligned} \tag{162}$$

Similar relationships hold between $(\boldsymbol{\sigma}, \boldsymbol{\rho})$ and $(\mathbf{s}_1, \mathbf{s}_2)$. Using the algebraic identity $a^2 - b^2 = (a+b)(a-b)$, it follows that

$$\begin{aligned}\left\|\mathbf{s}_1 - \mathbf{s}_1'\right\|^2 - \left\|\mathbf{s}_2 - \mathbf{s}_2'\right\|^2 &= \left(\mathbf{s}_1 - \mathbf{s}_1' + \mathbf{s}_2 - \mathbf{s}_2'\right) \cdot \left(\mathbf{s}_1 - \mathbf{s}_1' - \mathbf{s}_2 + \mathbf{s}_2'\right) \\ &= \left[\left(\mathbf{s}_1 + \mathbf{s}_2\right) - \left(\mathbf{s}_1' + \mathbf{s}_2'\right)\right] \cdot \left[\left(\mathbf{s}_1 - \mathbf{s}_2\right) - \left(\mathbf{s}_1' - \mathbf{s}_2'\right)\right] \\ &= 2\left(\boldsymbol{\rho} - \boldsymbol{\rho}'\right) \cdot \left(\boldsymbol{\sigma} - \boldsymbol{\sigma}'\right).\end{aligned} \tag{163}$$

The free space Green function for the second moment can then be expressed in terms of the new variables:

$$G_2^f(\boldsymbol{\sigma}, \boldsymbol{\rho}, \boldsymbol{\sigma}', \boldsymbol{\rho}', z) = \left(\frac{k}{2\pi z}\right)^2 \exp\left(-\frac{jk}{z}\left(\boldsymbol{\rho}' - \boldsymbol{\rho}\right) \cdot \left(\boldsymbol{\sigma}' - \boldsymbol{\sigma}\right)\right). \tag{164}$$

The relationship between the differential elements is given by

$$d^2\mathbf{s}_1' d^2\mathbf{s}_2' = \left|\frac{\partial\left(\mathbf{s}_1', \mathbf{s}_2'\right)}{\partial\left(\boldsymbol{\sigma}', \boldsymbol{\rho}'\right)}\right| d^2\boldsymbol{\sigma}' d^2\boldsymbol{\rho}'. \tag{165}$$

The Jacobian is, in turn, given by

$$\left|\frac{\partial\left(\mathbf{s}_1', \mathbf{s}_2'\right)}{\partial\left(\boldsymbol{\sigma}', \boldsymbol{\rho}'\right)}\right| = \begin{vmatrix} \frac{1}{2} & 1 \\ -\frac{1}{2} & 1 \end{vmatrix} = 1. \tag{166}$$

It follows that the second moment (160) can be written as

$$\begin{aligned}\Gamma_2(\boldsymbol{\sigma}, \boldsymbol{\rho}, z) = \left(\frac{k}{2\pi z}\right)^2 \int_{\mathbb{R}^2}\int_{\mathbb{R}^2} \Gamma_2(\boldsymbol{\sigma}', \boldsymbol{\rho}', 0) \exp\left(-\frac{1}{2} D_\varphi(\boldsymbol{\sigma}')\right) \\ \times \exp\left(-\frac{jk}{z}\left(\boldsymbol{\rho}' - \boldsymbol{\rho}\right) \cdot \left(\boldsymbol{\sigma}' - \boldsymbol{\sigma}\right)\right) d^2\boldsymbol{\sigma}' d^2\boldsymbol{\rho}'.\end{aligned} \tag{167}$$

5.2 Plane Waves

For plane waves,

$$\psi\left(\mathbf{s}', 0\right) = 1. \tag{168}$$

It follows that

$$\Gamma_2\left(\mathbf{s}_1', \mathbf{s}_2', 0\right) = \left\langle \psi\left(\mathbf{s}_1', 0\right) \psi^*\left(\mathbf{s}_2', 0\right) \right\rangle = 1. \tag{169}$$

Therefore, Equation (167) for the second moment becomes

$$\Gamma_2(\boldsymbol{\sigma}, \boldsymbol{\rho}, z) = \left(\frac{k}{2\pi z}\right)^2 \int_{\mathbb{R}^2} \int_{\mathbb{R}^2} \exp\left(-\frac{1}{2} D_\varphi(\boldsymbol{\sigma}')\right) \exp\left(-\frac{jk}{z}\left(\boldsymbol{\rho}' - \boldsymbol{\rho}\right) \cdot \left(\boldsymbol{\sigma}' - \boldsymbol{\sigma}\right)\right) d^2\boldsymbol{\sigma}' d^2\boldsymbol{\rho}'. \tag{170}$$

Integration with respect to $\boldsymbol{\rho}'$ gives

$$\left(\frac{k}{2\pi z}\right)^2 \int_{\mathbb{R}^2} \exp\left(-\frac{jk}{z}\left(\boldsymbol{\rho}' - \boldsymbol{\rho}\right) \cdot \left(\boldsymbol{\sigma}' - \boldsymbol{\sigma}\right)\right) d^2\boldsymbol{\rho}' = \delta\left(\boldsymbol{\sigma}' - \boldsymbol{\sigma}\right). \tag{171}$$

Substituting this results into Equation (170), the second moment reduces to

$$\Gamma_2(\boldsymbol{\sigma}, \boldsymbol{\rho}, z) = \int_{\mathbb{R}^2} \exp\left(-\frac{1}{2} D_\varphi(\boldsymbol{\sigma}')\right) \delta\left(\boldsymbol{\sigma}' - \boldsymbol{\sigma}\right) d^2\boldsymbol{\sigma}' = \exp\left(-\frac{1}{2} D_\varphi(\boldsymbol{\sigma})\right). \tag{172}$$

Since the second moment does not explicitly depend on $\boldsymbol{\rho}$ or z, it can be written as

$$\Gamma_2(\mathbf{s}) = \exp\left(-\frac{1}{2} D_\varphi(\mathbf{s})\right). \tag{173}$$

6 Fourth-Order Statistics

In this section, expressions for the fourth moment and the associated intensity correlation function (or, equivalently, the intensity spectrum) are derived for the thin screen problem; that is, the case when the turbulent medium is modeled as a thin phase screen located at a distance z from the observation plane. As in the case of the second moment, the Feynman path integral can be used to derive the corresponding expressions for the case of waves propagating through an extended turbulent medium (see [6] for further detail).

6.1 Fourth Moment

The fourth statistical moment of the scattered wave field is defined as

$$\Gamma_4(\mathbf{s}_1, \mathbf{s}_2, \mathbf{s}_3, \mathbf{s}_4, z) = \langle \psi(\mathbf{s}_1, z) \psi^*(\mathbf{s}_2, z) \psi(\mathbf{s}_3, z) \psi^*(\mathbf{s}_4, z) \rangle. \tag{174}$$

The intensity correlation function (or, equivalently, the intensity spectrum) is related to the fourth moment. The intensity of the scattered wave field is given by

$$S(\mathbf{s}, z) = \psi(\mathbf{s}, z) \psi^*(\mathbf{s}, z). \tag{175}$$

The intensity correlation function is then related to the fourth moment via the relation:

$$R_S(\mathbf{s}_1, \mathbf{s}_2, z) = \langle S(\mathbf{s}_1, z) S(\mathbf{s}_2, z) \rangle = \Gamma_4(\mathbf{s}_1, \mathbf{s}_1, \mathbf{s}_2, \mathbf{s}_2, z). \tag{176}$$

Substituting Equation (114)—or, equivalently, Equation (115)—for the scattered wave field into Equation (174), the fourth statistical moment for a wave propagating through a thin turbulent medium layer located at a distance z from the observation plane can be written as

$$\Gamma_4(\mathbf{s}_1,\mathbf{s}_2,\mathbf{s}_3,\mathbf{s}_4,z)=\int_{\mathbb{R}^2}\int_{\mathbb{R}^2}\int_{\mathbb{R}^2}\int_{\mathbb{R}^2}\Gamma_4\left(\mathbf{s}_1',\mathbf{s}_2',\mathbf{s}_3',\mathbf{s}_4',0\right)G_4\left(\mathbf{s}_1,\mathbf{s}_2,\mathbf{s}_3,\mathbf{s}_4,\mathbf{s}_1',\mathbf{s}_2',\mathbf{s}_3',\mathbf{s}_4',z\right)\\ d^2\mathbf{s}_1'd^2\mathbf{s}_2'd^2\mathbf{s}_3'd^2\mathbf{s}_4', \quad (177)$$

where

$$G_4\left(\mathbf{s}_1,\mathbf{s}_2,\mathbf{s}_3,\mathbf{s}_4,\mathbf{s}_1',\mathbf{s}_2',\mathbf{s}_3',\mathbf{s}_4',z\right)=\left\langle G\left(\mathbf{s}_1,\mathbf{s}_1',z\right)G^*\left(\mathbf{s}_2,\mathbf{s}_2',z\right)G\left(\mathbf{s}_3,\mathbf{s}_3',z\right)G^*\left(\mathbf{s}_4,\mathbf{s}_4',z\right)\right\rangle. \quad (178)$$

Substituting Equation (116) for the Green function, G, associated with the scattered wave field and letting

$$\left(\mathbf{s}_i,\mathbf{s}_i',z\right)=\left(\mathbf{s}_1,\mathbf{s}_2,\mathbf{s}_3,\mathbf{s}_4,\mathbf{s}_1',\mathbf{s}_2',\mathbf{s}_3',\mathbf{s}_4',z\right) \quad (179)$$

for notational convenience, the Green function, G_4, for the fourth moment can be written as

$$G_4\left(\mathbf{s}_i,\mathbf{s}_i',z\right)=\left\langle e^{-j\left[\varphi\left(\mathbf{s}_1'\right)-\varphi\left(\mathbf{s}_2'\right)+\varphi\left(\mathbf{s}_3'\right)-\varphi\left(\mathbf{s}_4'\right)\right]}\right\rangle G_4^f\left(\mathbf{s}_i,\mathbf{s}_i',z\right), \quad (180)$$

where

$$G_4^f\left(\mathbf{s}_i,\mathbf{s}_i',z\right)=G^f\left(\mathbf{s}_1,\mathbf{s}_1',z\right)G^{f*}\left(\mathbf{s}_2,\mathbf{s}_2',z\right)G^f\left(\mathbf{s}_3,\mathbf{s}_3',z\right)G^{f*}\left(\mathbf{s}_4,\mathbf{s}_4',z\right). \quad (181)$$

Substituting Equation (117) for the free Green function, G^f, associated with the scattered wave field into Equation (181), the free space Green function, G_4^f, for the fourth moment becomes

$$G_4^f(\mathbf{s}_i,\mathbf{s}_i',z)=\left(\frac{k}{2\pi z}\right)^4\exp\left(-\frac{jk}{2z}\left(\left\|\mathbf{s}_1-\mathbf{s}_1'\right\|^2-\left\|\mathbf{s}_2-\mathbf{s}_2'\right\|^2+\left\|\mathbf{s}_3-\mathbf{s}_3'\right\|^2-\left\|\mathbf{s}_4-\mathbf{s}_4'\right\|^2\right)\right). \quad (182)$$

Using the identity given in Equation (158), the term in angular brackets in Equation (180) can be expressed as

$$\left\langle e^{-j\left[\varphi\left(\mathbf{s}_1'\right)-\varphi\left(\mathbf{s}_2'\right)+\varphi\left(\mathbf{s}_3'\right)-\varphi\left(\mathbf{s}_4'\right)\right]}\right\rangle=e^{-\frac{1}{2}\left\langle\left[\varphi\left(\mathbf{s}_1'\right)-\varphi\left(\mathbf{s}_2'\right)+\varphi\left(\mathbf{s}_3'\right)-\varphi\left(\mathbf{s}_4'\right)\right]^2\right\rangle}. \quad (183)$$

The ensemble average in the exponent on the right-hand side of Equation (183) can be expanded to give

$$\begin{aligned}&\left\langle\left[\varphi\left(\mathbf{s}_1'\right)-\varphi\left(\mathbf{s}_2'\right)+\varphi\left(\mathbf{s}_3'\right)-\varphi\left(\mathbf{s}_4'\right)\right]^2\right\rangle=\\ &\quad\left\langle\left[\varphi\left(\mathbf{s}_1'\right)-\varphi\left(\mathbf{s}_2'\right)\right]^2\right\rangle+2\left\langle\left[\varphi\left(\mathbf{s}_1'\right)-\varphi\left(\mathbf{s}_2'\right)\right]\left[\varphi\left(\mathbf{s}_3'\right)-\varphi\left(\mathbf{s}_4'\right)\right]\right\rangle+\left\langle\left[\varphi\left(\mathbf{s}_3'\right)-\varphi\left(\mathbf{s}_4'\right)\right]^2\right\rangle=\\ &\qquad D_\varphi\left(\mathbf{s}_1'-\mathbf{s}_2'\right)+2\left\langle\left[\varphi\left(\mathbf{s}_1'\right)-\varphi\left(\mathbf{s}_2'\right)\right]\left[\varphi\left(\mathbf{s}_3'\right)-\varphi\left(\mathbf{s}_4'\right)\right]\right\rangle+D_\varphi\left(\mathbf{s}_3'-\mathbf{s}_4'\right). \quad (184)\end{aligned}$$

The cross term can be expanded to give

$$\begin{aligned}&2\left\langle\left[\varphi\left(\mathbf{s}_1'\right)-\varphi\left(\mathbf{s}_2'\right)\right]\left[\varphi\left(\mathbf{s}_3'\right)-\varphi\left(\mathbf{s}_4'\right)\right]\right\rangle=\\ &\quad 2\left\langle\varphi\left(\mathbf{s}_1'\right)\varphi\left(\mathbf{s}_3'\right)\right\rangle-2\left\langle\varphi\left(\mathbf{s}_1'\right)\varphi\left(\mathbf{s}_4'\right)\right\rangle-2\left\langle\varphi\left(\mathbf{s}_2'\right)\varphi\left(\mathbf{s}_3'\right)\right\rangle+2\left\langle\varphi\left(\mathbf{s}_2'\right)\varphi\left(\mathbf{s}_4'\right)\right\rangle=\\ &\qquad 2R_\varphi\left(\mathbf{s}_1'-\mathbf{s}_3'\right)-2R_\varphi\left(\mathbf{s}_1'-\mathbf{s}_4'\right)-2R_\varphi\left(\mathbf{s}_2'-\mathbf{s}_3'\right)+2R_\varphi\left(\mathbf{s}_2'-\mathbf{s}_4'\right). \quad (185)\end{aligned}$$

Since

$$D_\varphi\left(\mathbf{s}_m'-\mathbf{s}_n'\right)=2\left[R_\varphi(\mathbf{0})-R_\varphi\left(\mathbf{s}_m'-\mathbf{s}_n'\right)\right], \quad (186)$$

with $m = 1, 2$ and $n = 3, 4$, the cross term can be written as

$$2\left\langle \left[\varphi\left(\mathbf{s}_1'\right) - \varphi\left(\mathbf{s}_2'\right)\right]\left[\varphi\left(\mathbf{s}_3'\right) - \varphi\left(\mathbf{s}_4'\right)\right]\right\rangle = D_\varphi\left(\mathbf{s}_1' - \mathbf{s}_4'\right) + D_\varphi\left(\mathbf{s}_2' - \mathbf{s}_3'\right) - D_\varphi\left(\mathbf{s}_1' - \mathbf{s}_3'\right) - D_\varphi\left(\mathbf{s}_2' - \mathbf{s}_4'\right). \quad (187)$$

It follows that Equation (183) can be written as

$$\left\langle e^{-j\left[\varphi\left(\mathbf{s}_1'\right) - \varphi\left(\mathbf{s}_2'\right) + \varphi\left(\mathbf{s}_3'\right) - \varphi\left(\mathbf{s}_4'\right)\right]}\right\rangle = \exp\left(-\frac{1}{2}V_\varphi\left(\mathbf{s}_1', \mathbf{s}_2', \mathbf{s}_3', \mathbf{s}_4'\right)\right), \quad (188)$$

where

$$V_\varphi\left(\mathbf{s}_1', \mathbf{s}_2', \mathbf{s}_3', \mathbf{s}_4'\right) = D_\varphi\left(\mathbf{s}_1' - \mathbf{s}_2'\right) + D_\varphi\left(\mathbf{s}_3' - \mathbf{s}_4'\right) + D_\varphi\left(\mathbf{s}_1' - \mathbf{s}_4'\right) + D_\varphi\left(\mathbf{s}_2' - \mathbf{s}_3'\right) - D_\varphi\left(\mathbf{s}_1' - \mathbf{s}_3'\right) - D_\varphi\left(\mathbf{s}_2' - \mathbf{s}_4'\right). \quad (189)$$

Substituting equations (182) and (188) into Equation (177), the fourth moment can then be written as

$$\Gamma_4(\mathbf{s}_1, \mathbf{s}_2, \mathbf{s}_3, \mathbf{s}_4, z) = \left(\frac{k}{2\pi z}\right)^4 \int_{\mathbb{R}^2}\int_{\mathbb{R}^2}\int_{\mathbb{R}^2}\int_{\mathbb{R}^2} \Gamma_4\left(\mathbf{s}_1', \mathbf{s}_2', \mathbf{s}_3', \mathbf{s}_4', 0\right) \exp\left(-\frac{1}{2}V_\varphi\left(\mathbf{s}_1', \mathbf{s}_2', \mathbf{s}_3', \mathbf{s}_4'\right)\right) \times \exp\left(-\frac{jk}{2z}\left(\left\|\mathbf{s}_1 - \mathbf{s}_1'\right\|^2 - \left\|\mathbf{s}_2 - \mathbf{s}_2'\right\|^2 + \left\|\mathbf{s}_3 - \mathbf{s}_3'\right\|^2 - \left\|\mathbf{s}_4 - \mathbf{s}_4'\right\|^2\right)\right) d^2\mathbf{s}_1' d^2\mathbf{s}_2' d^2\mathbf{s}_3' d^2\mathbf{s}_4'. \quad (190)$$

To simplify Equation (190), the following change of variables is introduced: Change of variables:

$$\begin{aligned} \boldsymbol{\alpha}' &= \frac{\mathbf{s}_1' + \mathbf{s}_2'}{2} + \frac{\mathbf{s}_3' + \mathbf{s}_4'}{2}, \\ \boldsymbol{\beta}' &= \frac{\mathbf{s}_1' + \mathbf{s}_2'}{2} - \frac{\mathbf{s}_3' + \mathbf{s}_4'}{2}, \\ \boldsymbol{\gamma}' &= \frac{\mathbf{s}_1' - \mathbf{s}_2'}{2} - \frac{\mathbf{s}_3' - \mathbf{s}_4'}{2}, \\ \boldsymbol{\delta}' &= \frac{\mathbf{s}_1' - \mathbf{s}_2'}{2} + \frac{\mathbf{s}_3' - \mathbf{s}_4'}{2}. \end{aligned} \quad (191)$$

Equivalently, $\mathbf{s}_1'$, $\mathbf{s}_2'$, $\mathbf{s}_3'$, and $\mathbf{s}_4'$ can be expressed in terms of $\boldsymbol{\alpha}'$, $\boldsymbol{\beta}'$, $\boldsymbol{\gamma}'$, and $\boldsymbol{\delta}'$:

$$\begin{aligned} \mathbf{s}_1' &= \frac{\boldsymbol{\alpha}' + \boldsymbol{\beta}'}{2} + \frac{\boldsymbol{\gamma}' + \boldsymbol{\delta}'}{2}, \\ \mathbf{s}_2' &= \frac{\boldsymbol{\alpha}' + \boldsymbol{\beta}'}{2} - \frac{\boldsymbol{\gamma}' + \boldsymbol{\delta}'}{2}, \\ \mathbf{s}_3' &= \frac{\boldsymbol{\alpha}' - \boldsymbol{\beta}'}{2} - \frac{\boldsymbol{\gamma}' - \boldsymbol{\delta}'}{2}, \\ \mathbf{s}_4' &= \frac{\boldsymbol{\alpha}' - \boldsymbol{\beta}'}{2} + \frac{\boldsymbol{\gamma}' - \boldsymbol{\delta}'}{2}. \end{aligned} \quad (192)$$

Similar relationships hold between $(\boldsymbol{\alpha}, \boldsymbol{\beta}, \boldsymbol{\gamma}, \boldsymbol{\delta})$ and $(\mathbf{s}_1, \mathbf{s}_2, \mathbf{s}_3, \mathbf{s}_4)$. Using the algebraic identity $a^2 - b^2 = (a + b)(a - b)$, it follows that

$$\left\|\mathbf{s}_1 - \mathbf{s}_1'\right\|^2 - \left\|\mathbf{s}_2 - \mathbf{s}_2'\right\|^2 + \left\|\mathbf{s}_3 - \mathbf{s}_3'\right\|^2 - \left\|\mathbf{s}_4 - \mathbf{s}_4'\right\|^2 = 2\left(\boldsymbol{\alpha} - \boldsymbol{\alpha}'\right)\cdot\left(\boldsymbol{\delta} - \boldsymbol{\delta}'\right) + 2\left(\boldsymbol{\beta} - \boldsymbol{\beta}'\right)\cdot\left(\boldsymbol{\gamma} - \boldsymbol{\gamma}'\right). \quad (193)$$

The free space Green function for the fourth moment can then be expressed in terms of the new variables:

$$G_4^f(\boldsymbol{\alpha},\boldsymbol{\beta},\boldsymbol{\gamma},\boldsymbol{\delta},\boldsymbol{\alpha}',\boldsymbol{\beta}',\boldsymbol{\gamma}',\boldsymbol{\delta}',z) = \exp\left(-\frac{jk}{z}\left[(\boldsymbol{\alpha}-\boldsymbol{\alpha}')\cdot(\boldsymbol{\delta}-\boldsymbol{\delta}')+(\boldsymbol{\beta}-\boldsymbol{\beta}')\cdot(\boldsymbol{\gamma}-\boldsymbol{\gamma}')\right]\right). \quad (194)$$

The relationship between the differential elements is given by

$$d^2\mathbf{s}_1' d^2\mathbf{s}_2' d^2\mathbf{s}_3' d^2\mathbf{s}_4' = \left|\frac{\partial(\mathbf{s}_1',\mathbf{s}_2',\mathbf{s}_3',\mathbf{s}_4')}{\partial(\boldsymbol{\alpha}',\boldsymbol{\beta}',\boldsymbol{\gamma}',\boldsymbol{\delta}')}\right| d^2\boldsymbol{\alpha}' d^2\boldsymbol{\beta}' d^2\boldsymbol{\gamma}' d^2\boldsymbol{\delta}'. \quad (195)$$

The Jacobian is, in turn, given by

$$\left|\frac{\partial(\mathbf{s}_1',\mathbf{s}_2',\mathbf{s}_3',\mathbf{s}_4')}{\partial(\boldsymbol{\alpha}',\boldsymbol{\beta}',\boldsymbol{\gamma}',\boldsymbol{\delta}')}\right| = \left|\frac{1}{2}\begin{pmatrix} 1 & 1 & 1 & 1 \\ 1 & 1 & -1 & -1 \\ 1 & -1 & -1 & 1 \\ 1 & -1 & 1 & -1 \end{pmatrix}\right| = 1. \quad (196)$$

Expressing $V_\varphi(\mathbf{s}_1',\mathbf{s}_2',\mathbf{s}_3',\mathbf{s}_4')$ in terms of $\boldsymbol{\alpha}'$, $\boldsymbol{\beta}'$, $\boldsymbol{\gamma}'$, and $\boldsymbol{\delta}'$,

$$V_\varphi(\boldsymbol{\beta}',\boldsymbol{\gamma}',\boldsymbol{\delta}') = D_\varphi(\boldsymbol{\gamma}'+\boldsymbol{\delta}') + D_\varphi(\boldsymbol{\gamma}'-\boldsymbol{\delta}') + D_\varphi(\boldsymbol{\beta}'+\boldsymbol{\delta}') + D_\varphi(\boldsymbol{\beta}'-\boldsymbol{\delta}') - D_\varphi(\boldsymbol{\beta}'+\boldsymbol{\gamma}') - D_\varphi(\boldsymbol{\beta}'-\boldsymbol{\gamma}'), \quad (197)$$

it follows that V_φ does not depend on $\boldsymbol{\alpha}'$. In terms of the new variables, the fourth moment can then be written as

$$\Gamma_4(\boldsymbol{\alpha},\boldsymbol{\beta},\boldsymbol{\gamma},\boldsymbol{\delta},z) = \left(\frac{k}{2\pi z}\right)^4 \int_{\mathbb{R}^2}\int_{\mathbb{R}^2}\int_{\mathbb{R}^2}\int_{\mathbb{R}^2} \Gamma_4(\boldsymbol{\alpha}',\boldsymbol{\beta}',\boldsymbol{\gamma}',\boldsymbol{\delta}',0)\exp\left(-\frac{1}{2}V_\varphi(\boldsymbol{\beta}',\boldsymbol{\gamma}',\boldsymbol{\delta}')\right) \times \exp\left(-\frac{jk}{z}\left[(\boldsymbol{\alpha}-\boldsymbol{\alpha}')\cdot(\boldsymbol{\delta}-\boldsymbol{\delta}')+(\boldsymbol{\beta}-\boldsymbol{\beta}')\cdot(\boldsymbol{\gamma}-\boldsymbol{\gamma}')\right]\right) d^2\boldsymbol{\alpha}' d^2\boldsymbol{\beta}' d^2\boldsymbol{\gamma}' d^2\boldsymbol{\delta}'. \quad (198)$$

6.2 Series Representation

The expression for the fourth moment given by Equation (198) is very complicated and cannot be computed analytically. In this section, a series representation is derived for the fourth moment that allows inference of asymptotic solutions for the intensity correlation function (or, equivalently, the intensity spectrum). It follows directly from the definition (174) that the fourth moment has the following symmetry property:

$$\Gamma_4(\mathbf{s}_1,\mathbf{s}_2,\mathbf{s}_3,\mathbf{s}_4,z) = \Gamma_4(\mathbf{s}_1,\mathbf{s}_4,\mathbf{s}_3,\mathbf{s}_2,z). \quad (199)$$

From the relationship between the intensity correlation function and the fourth moment, namely,

$$R_S(\mathbf{s}_1,\mathbf{s}_2,z) = \langle S(\mathbf{s}_1,z)S(\mathbf{s}_2,z)\rangle = \Gamma_4(\mathbf{s}_1,\mathbf{s}_1,\mathbf{s}_2,\mathbf{s}_2,z), \quad (200)$$

and the symmetry property (199), it follows that the intensity correlation function can also be obtained from

$$R_S(\mathbf{s}_1,\mathbf{s}_2,z) = \Gamma_4(\mathbf{s}_1,\mathbf{s}_2,\mathbf{s}_2,\mathbf{s}_1,z). \quad (201)$$

In other words, there are two ways to arriving at the intensity correlation function from the fourth moment: either via $\mathbf{s}_2 \to \mathbf{s}_1$ and $\mathbf{s}_4 \to \mathbf{s}_3$ (and then setting $\mathbf{s}_3$ equal to $\mathbf{s}_2$ without loss of generality), or via $\mathbf{s}_4 \to \mathbf{s}_1$

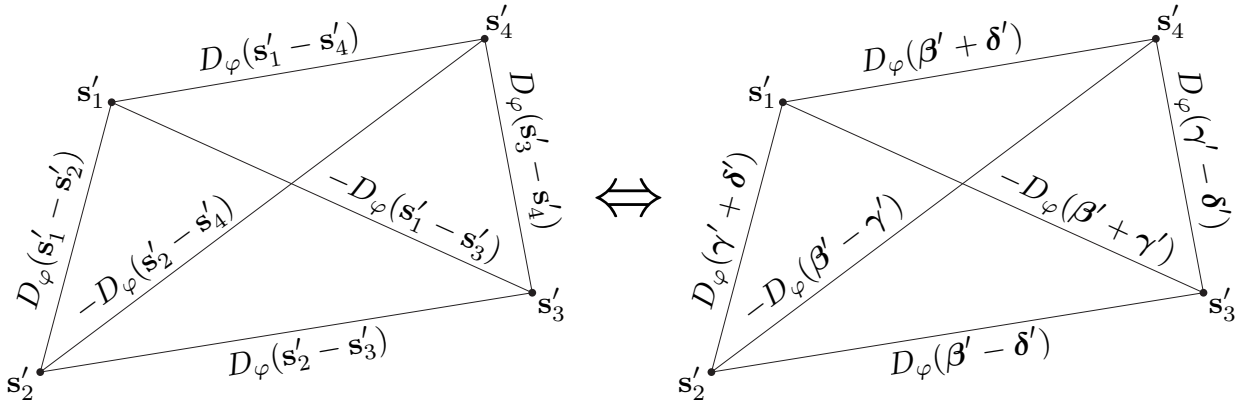

Figure 6: The phase structure functions appearing in Equation (189) (left) and in Equation (197) (right).

and $\mathbf{s}_3 \to \mathbf{s}_2$. This symmetry property can be exploited to obtain alternative series representations for the fourth moment.

The exponential term involving V_φ in Equation (198) is particularly cumbersome. The six structure functions in Equation (189) that combine to give V_φ are shown in Figure 6. The diagram on the left expresses the structure functions in terms of the original variables, $(\mathbf{s}'_1, \mathbf{s}'_2, \mathbf{s}'_3, \mathbf{s}'_4)$, while the diagram on the right expresses the structure functions in terms of the new variables $(\boldsymbol{\beta}', \boldsymbol{\gamma}', \boldsymbol{\delta}')$, where there is no dependence on $\boldsymbol{\alpha}'$. In the first case of arriving at the intensity correlation function (i.e., via $\mathbf{s}'_2 \to \mathbf{s}'_1$ and $\mathbf{s}'_4 \to \mathbf{s}'_3$), the combination

$$D_\varphi\left(\boldsymbol{\beta}' + \boldsymbol{\delta}'\right) + D_\varphi\left(\boldsymbol{\beta}' - \boldsymbol{\delta}'\right) - D_\varphi\left(\boldsymbol{\beta}' + \boldsymbol{\gamma}'\right) - D_\varphi\left(\boldsymbol{\beta}' - \boldsymbol{\gamma}'\right) \tag{202}$$

becomes small since as $\mathbf{s}'_2 \to \mathbf{s}'_1$ and $\mathbf{s}'_4 \to \mathbf{s}'_3$, these four structure functions, as illustrated by the middle diagram in Figure 7, become nearly equal to one another and nearly cancel out. It is therefore convenient to write V_φ as

$$V_\varphi\left(\boldsymbol{\beta}', \boldsymbol{\gamma}', \boldsymbol{\delta}'\right) = D_\varphi\left(\boldsymbol{\gamma}' + \boldsymbol{\delta}'\right) + D_\varphi(\boldsymbol{\gamma}' - \boldsymbol{\delta}') + Q\left(\boldsymbol{\beta}', \boldsymbol{\gamma}', \boldsymbol{\delta}'\right), \tag{203}$$

where

$$Q\left(\boldsymbol{\beta}', \boldsymbol{\gamma}', \boldsymbol{\delta}'\right) = D_\varphi\left(\boldsymbol{\beta}' + \boldsymbol{\delta}'\right) + D_\varphi\left(\boldsymbol{\beta}' - \boldsymbol{\delta}'\right) - D_\varphi\left(\boldsymbol{\beta}' + \boldsymbol{\gamma}'\right) - D_\varphi\left(\boldsymbol{\beta}' - \boldsymbol{\gamma}'\right) \tag{204}$$

becomes vanishingly small as $\mathbf{s}'_2 \to \mathbf{s}'_1$ and $\mathbf{s}'_4 \to \mathbf{s}'_3$. In the second way of arriving at the intensity correlation function (i.e., via $\mathbf{s}'_4 \to \mathbf{s}'_1$ and $\mathbf{s}'_3 \to \mathbf{s}'_2$), the combination

$$D_\varphi\left(\boldsymbol{\gamma}' + \boldsymbol{\delta}'\right) + D_\varphi\left(\boldsymbol{\gamma}' - \boldsymbol{\delta}'\right) - D_\varphi\left(\boldsymbol{\gamma}' + \boldsymbol{\beta}'\right) - D_\varphi\left(\boldsymbol{\beta}' - \boldsymbol{\gamma}'\right), \tag{205}$$

becomes, in turn, small, as illustrated by the diagram on the right in Figure 7. In this case, it is therefore convenient to write V_φ as

$$V_\varphi\left(\boldsymbol{\beta}', \boldsymbol{\gamma}', \boldsymbol{\delta}'\right) = D_\varphi\left(\boldsymbol{\beta}' + \boldsymbol{\delta}'\right) + D_\varphi\left(\boldsymbol{\beta}' - \boldsymbol{\delta}'\right) + Q'\left(\boldsymbol{\beta}', \boldsymbol{\gamma}', \boldsymbol{\delta}'\right), \tag{206}$$

where

$$Q'\left(\boldsymbol{\beta}', \boldsymbol{\gamma}', \boldsymbol{\delta}'\right) = D_\varphi\left(\boldsymbol{\gamma}' + \boldsymbol{\delta}'\right) + D_\varphi\left(\boldsymbol{\gamma}' - \boldsymbol{\delta}'\right) - D_\varphi\left(\boldsymbol{\gamma}' + \boldsymbol{\beta}'\right) - D_\varphi\left(\boldsymbol{\gamma}' - \boldsymbol{\beta}'\right) \tag{207}$$

is now vanishingly small as $\mathbf{s}'_4 \to \mathbf{s}'_1$ and $\mathbf{s}'_3 \to \mathbf{s}'_2$. Comparing Equation (207) with Equation (204) reveals that Q' can be obtained from Q by simply exchanging $\boldsymbol{\beta}'$ and $\boldsymbol{\gamma}'$. From the relation,

$$D_\varphi(\mathbf{s}) = 2\int_{\mathbb{R}^2} P_\varphi(\boldsymbol{\kappa})\left(1 - e^{-j\boldsymbol{\kappa}\cdot\mathbf{s}}\right)\, d^2\boldsymbol{\kappa}, \tag{208}$$

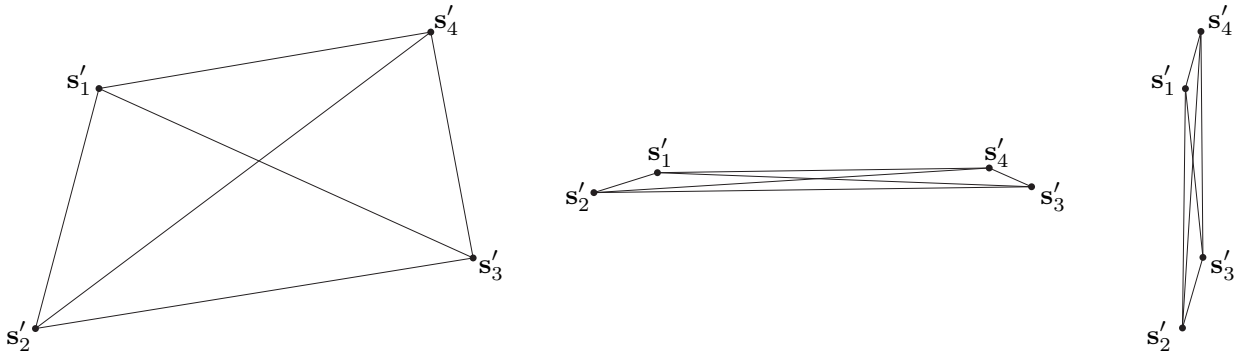

Figure 7: Two ways of arriving at the intensity correlation function: via $\mathbf{s}'_2 \to \mathbf{s}'_1$ and $\mathbf{s}'_4 \to \mathbf{s}'_3$ (middle); or via $\mathbf{s}'_4 \to \mathbf{s}'_1$ and $\mathbf{s}'_3 \to \mathbf{s}'_2$ (right).

Q can be expressed in terms of P_φ:

$$Q\left(\boldsymbol{\beta}', \boldsymbol{\gamma}', \boldsymbol{\delta}'\right) = 4 \int_{\mathbb{R}^2} P_\varphi(\boldsymbol{\kappa}) \left[\cos\left(\boldsymbol{\kappa} \cdot \boldsymbol{\gamma}'\right) - \cos\left(\boldsymbol{\kappa} \cdot \boldsymbol{\delta}'\right)\right] e^{-j\boldsymbol{\kappa} \cdot \boldsymbol{\beta}'} \, d^2\boldsymbol{\kappa}. \tag{209}$$

Similarly,

$$Q'\left(\boldsymbol{\beta}', \boldsymbol{\gamma}', \boldsymbol{\delta}'\right) = 4 \int_{\mathbb{R}^2} P_\varphi(\boldsymbol{\kappa}) \left[\cos\left(\boldsymbol{\kappa} \cdot \boldsymbol{\beta}'\right) - \cos\left(\boldsymbol{\kappa} \cdot \boldsymbol{\delta}'\right)\right] e^{-j\boldsymbol{\kappa} \cdot \boldsymbol{\gamma}'} \, d^2\boldsymbol{\kappa}. \tag{210}$$

Taking the route $\mathbf{s}'_2 \to \mathbf{s}'_1$ and $\mathbf{s}'_4 \to \mathbf{s}'_3$ to arrive at the intensity correlation function from the general expression for the fourth moment, the Green function for the fourth moment can be expressed as

$$G_4\left(\mathbf{s}_i, \mathbf{s}'_i, z\right) = G_4^f\left(\mathbf{s}_i, \mathbf{s}'_i, z\right) \exp\left(-\frac{1}{2}\left[D_\varphi\left(\boldsymbol{\gamma}' + \boldsymbol{\delta}'\right) + D_\varphi\left(\boldsymbol{\gamma}' - \boldsymbol{\delta}'\right) + Q\left(\boldsymbol{\beta}', \boldsymbol{\gamma}', \boldsymbol{\delta}'\right)\right]\right), \tag{211}$$

where the free space Green function for the fourth moment is given by

$$G_4^f\left(\mathbf{s}_i, \mathbf{s}'_i, z\right) = \left(\frac{k}{2\pi z}\right)^4 \exp\left(-\frac{jk}{z}\left[\left(\boldsymbol{\alpha} - \boldsymbol{\alpha}'\right) \cdot \left(\boldsymbol{\delta} - \boldsymbol{\delta}'\right) + \left(\boldsymbol{\beta} - \boldsymbol{\beta}'\right) \cdot \left(\boldsymbol{\gamma} - \boldsymbol{\gamma}'\right)\right]\right). \tag{212}$$

Since Q is small, it makes sense to consider the following Taylor series expansion:

$$\begin{aligned}
\exp\left(-\frac{Q\left(\boldsymbol{\beta}', \boldsymbol{\gamma}', \boldsymbol{\delta}'\right)}{2}\right) &= \sum_{n=0}^{\infty} \frac{1}{n!} \left[-\frac{Q\left(\boldsymbol{\beta}', \boldsymbol{\gamma}', \boldsymbol{\delta}'\right)}{2}\right]^n = \\
&\sum_{n=0}^{\infty} \frac{1}{n!} \left(2 \int_{\mathbb{R}^2} P_\varphi\left(\boldsymbol{\kappa}'\right) \left[\cos\left(\boldsymbol{\kappa}' \cdot \boldsymbol{\delta}'\right) - \cos\left(\boldsymbol{\kappa}' \cdot \boldsymbol{\gamma}'\right)\right] e^{-j\boldsymbol{\kappa}' \cdot \boldsymbol{\beta}'} \, d^2\boldsymbol{\kappa}'\right)^n = \\
&1 + \sum_{n=1}^{\infty} \frac{2^n}{n!} \int_{\mathbb{R}^2} \cdots \int_{\mathbb{R}^2} \left\{\prod_{m=1}^{n} P_\varphi\left(\boldsymbol{\kappa}'_m\right) \left[\cos\left(\boldsymbol{\kappa}'_m \cdot \boldsymbol{\delta}'\right) - \cos\left(\boldsymbol{\kappa}'_m \cdot \boldsymbol{\gamma}'\right)\right]\right\} \\
&\qquad \times \exp\left(-j \sum_{m=1}^{n} \boldsymbol{\kappa}'_m \cdot \boldsymbol{\beta}'\right) d^2\boldsymbol{\kappa}'_1 \cdots d^2\boldsymbol{\kappa}'_n.
\end{aligned} \tag{213}$$

Equipped with this expression, the Green function for the fourth moment can then be represented as a series:

$$G_4\left(\mathbf{s}_i, \mathbf{s}_i', z\right) = \sum_{n=0}^{\infty} G_4^{(n)}\left(\mathbf{s}_i, \mathbf{s}_i', z\right). \tag{214}$$

The zeroth-order term ($n = 0$) is given by

$$G_4^{(0)}\left(\mathbf{s}_i, \mathbf{s}_i', z\right) = G_4^f\left(\mathbf{s}_i, \mathbf{s}_i', z\right) \exp\left(-\frac{1}{2}\left[D_\varphi(\boldsymbol{\gamma}' + \boldsymbol{\delta}') + D_\varphi(\boldsymbol{\gamma}' - \boldsymbol{\delta}')\right]\right). \tag{215}$$

The first-order term ($n = 1$) is given by

$$\begin{aligned} G_4^{(1)}\left(\mathbf{s}_i, \mathbf{s}_i', z\right) = 2\, G_4^f\left(\mathbf{s}_i, \mathbf{s}_i', z\right) \exp\left(-\frac{1}{2}\left[D_\varphi\left(\boldsymbol{\gamma}' + \boldsymbol{\delta}'\right) + D_\varphi\left(\boldsymbol{\gamma}' - \boldsymbol{\delta}'\right)\right]\right) \\ \times \int_{\mathbb{R}^2} P_\varphi\left(\boldsymbol{\kappa}'\right)\left[\cos\left(\boldsymbol{\kappa}' \cdot \boldsymbol{\delta}'\right) - \cos\left(\boldsymbol{\kappa}' \cdot \boldsymbol{\gamma}'\right)\right] e^{-j\boldsymbol{\kappa}' \cdot \boldsymbol{\beta}'}\, d^2\boldsymbol{\kappa}'. \end{aligned} \tag{216}$$

6.3 Intensity Spectra

The series representation of the Green function for the fourth moment derived in Section 6.1 can, in turn, be used to derive two series expansions for the intensity correlation function, R_S, one valid at low wavenumbers (or low spatial frequencies), R_S^{LF}, and one valid at high wavenumbers (or high spatial frequencies), R_S^{HF}. The total correlation function is then obtained from

$$R_S = \sum_{n=0}^{\infty} R_S^{\text{LF}(n)} + \sum_{n=0}^{\infty} R_S^{\text{HF}(n)}. \tag{217}$$

6.3.1 Low-Wavenumber Approximation

The series expansion (213) can be truncated for small values of n if $Q(\boldsymbol{\beta}', \boldsymbol{\gamma}', \boldsymbol{\delta}')$ is small. The middle diagram in Figure 7 illustrates the case when $Q(\boldsymbol{\beta}', \boldsymbol{\gamma}', \boldsymbol{\delta}')$ is small, corresponding to the case where the structure functions associated with the two baselines represented by the diagonal lines connecting the four corners of the quadrangles shown in Figure 6 nearly cancel the structure functions associated with the baselines represented by the top and bottom edges of the quadrangles. From this starting point (the middle diagram in Figure 7), letting $\mathbf{s}_2 = \mathbf{s}_1$ and $\mathbf{s}_4 = \mathbf{s}_3$, the baseline $\|\mathbf{s}_1 - \mathbf{s}_3\|$ will be relatively large, corresponding to a relatively low wavenumber (or low spatial frequency). Furthermore, it follows from (191) that $\boldsymbol{\gamma} = \boldsymbol{\delta} = \mathbf{0}$. The intensity correlation function is then given by

$$R_S^{\text{LF}}(\mathbf{s}_1, \mathbf{s}_3, z) = \Gamma_4(\mathbf{s}_1, \mathbf{s}_1, \mathbf{s}_3, \mathbf{s}_3, z), \tag{218}$$

or equivalently,

$$R_S^{\text{LF}}(\boldsymbol{\alpha}, \boldsymbol{\beta}, z) = \Gamma_4(\boldsymbol{\alpha}, \boldsymbol{\beta}, \mathbf{0}, \mathbf{0}, z). \tag{219}$$

The free space Green's function, in turn, becomes

$$G_4^{f^{\text{LF}}}\left(\boldsymbol{\alpha}, \boldsymbol{\alpha}', \boldsymbol{\beta}, \boldsymbol{\beta}', \boldsymbol{\gamma}', \boldsymbol{\delta}', z\right) = \left(\frac{k}{2\pi z}\right)^4 \exp\left(-\frac{jk}{z}\left[\left(\boldsymbol{\alpha}' - \boldsymbol{\alpha}\right) \cdot \boldsymbol{\delta}' + \left(\boldsymbol{\beta}' - \boldsymbol{\beta}\right) \cdot \boldsymbol{\gamma}'\right]\right). \tag{220}$$

The intensity correlation function is then given by

$$R_S^{\text{LF}}(\boldsymbol{\alpha},\boldsymbol{\beta},z) = \left(\frac{k}{2\pi z}\right)^4 \int_{\mathbb{R}^2}\int_{\mathbb{R}^2}\int_{\mathbb{R}^2}\int_{\mathbb{R}^2} \Gamma_4\left(\boldsymbol{\alpha}',\boldsymbol{\beta}',\boldsymbol{\gamma}',\boldsymbol{\delta}',0\right) \times \exp\left(-\frac{jk}{z}\left[(\boldsymbol{\alpha}'-\boldsymbol{\alpha})\cdot\boldsymbol{\delta}' + (\boldsymbol{\beta}'-\boldsymbol{\beta})\cdot\boldsymbol{\gamma}'\right]\right) \exp\left(-\frac{1}{2}\left[D_\varphi\left(\boldsymbol{\gamma}'+\boldsymbol{\delta}'\right) + D_\varphi\left(\boldsymbol{\gamma}'-\boldsymbol{\delta}'\right)\right]\right) \times \exp\left(-\frac{1}{2}Q\left(\boldsymbol{\beta}',\boldsymbol{\gamma}',\boldsymbol{\delta}'\right)\right) d^2\boldsymbol{\alpha}' d^2\boldsymbol{\beta}' d^2\boldsymbol{\gamma}' d^2\boldsymbol{\delta}'. \quad (221)$$

It is often more convenient to consider the intensity spectrum instead of the intensity correlation function. The intensity spectrum, which is the Fourier transform of the intensity correlation function, is given by

$$P_S^{\text{LF}}(\boldsymbol{\alpha},\boldsymbol{\kappa},z) = \frac{1}{(2\pi)^2}\int_{\mathbb{R}^2} R_S^{\text{LF}}(\boldsymbol{\alpha},\boldsymbol{\beta},z)\, e^{j\boldsymbol{\kappa}\cdot\boldsymbol{\beta}}\, d^2\boldsymbol{\beta}. \quad (222)$$

Based on the Taylor expansion (213), the intensity correlation function at low wavenumbers can be represented as a series:

$$R_S^{\text{LF}}(\boldsymbol{\alpha},\boldsymbol{\beta},z) = \sum_{n=0}^{\infty} R_S^{\text{LF}^{(n)}}(\boldsymbol{\alpha},\boldsymbol{\beta},z). \quad (223)$$

The zeroth-order term ($n=0$) is given by

$$R_S^{\text{LF}^{(0)}}(\boldsymbol{\alpha},\boldsymbol{\beta},z) = \left(\frac{k}{2\pi z}\right)^4 \int_{\mathbb{R}^2}\int_{\mathbb{R}^2}\int_{\mathbb{R}^2}\int_{\mathbb{R}^2} \Gamma_4\left(\boldsymbol{\alpha}',\boldsymbol{\beta}',\boldsymbol{\gamma}',\boldsymbol{\delta}',0\right) \times \exp\left(-\frac{jk}{z}\left[(\boldsymbol{\alpha}'-\boldsymbol{\alpha})\cdot\boldsymbol{\delta}' + (\boldsymbol{\beta}'-\boldsymbol{\beta})\cdot\boldsymbol{\gamma}'\right]\right) \exp\left(-\frac{1}{2}\left[D_\varphi\left(\boldsymbol{\gamma}'+\boldsymbol{\delta}'\right) + D_\varphi\left(\boldsymbol{\gamma}'-\boldsymbol{\delta}'\right)\right]\right) d^2\boldsymbol{\alpha}' d^2\boldsymbol{\beta}' d^2\boldsymbol{\gamma}' d^2\boldsymbol{\delta}'. \quad (224)$$

The first-order term ($n=1$) is given by

$$R_S^{\text{LF}^{(1)}}(\boldsymbol{\alpha},\boldsymbol{\beta},z) = 2\left(\frac{k}{2\pi z}\right)^4 \int_{\mathbb{R}^2}\int_{\mathbb{R}^2}\int_{\mathbb{R}^2}\int_{\mathbb{R}^2} \Gamma_4\left(\boldsymbol{\alpha}',\boldsymbol{\beta}',\boldsymbol{\gamma}',\boldsymbol{\delta}',0\right) \times \exp\left(-\frac{jk}{z}\left[(\boldsymbol{\alpha}'-\boldsymbol{\alpha})\cdot\boldsymbol{\delta}' + (\boldsymbol{\beta}'-\boldsymbol{\beta})\cdot\boldsymbol{\gamma}'\right]\right) \exp\left(-\frac{1}{2}\left[D_\varphi\left(\boldsymbol{\gamma}'+\boldsymbol{\delta}'\right) + D_\varphi\left(\boldsymbol{\gamma}'-\boldsymbol{\delta}'\right)\right]\right) P_\varphi\left(\boldsymbol{\kappa}'\right)\left[\cos\left(\boldsymbol{\kappa}'\cdot\boldsymbol{\delta}'\right) - \cos\left(\boldsymbol{\kappa}'\cdot\boldsymbol{\gamma}'\right)\right] e^{-j\boldsymbol{\kappa}'\cdot\boldsymbol{\beta}'}\, d^2\boldsymbol{\alpha}' d^2\boldsymbol{\beta}' d^2\boldsymbol{\gamma}' d^2\boldsymbol{\delta}' d^2\boldsymbol{\kappa}'. \quad (225)$$

Higher order terms need to be considered as the baseline $\|\mathbf{s}_1 - \mathbf{s}_3\|$ becomes small.

6.3.2 High-Wavenumber Approximation

Returning to the middle diagram of Figure 7, now letting $\mathbf{s}_4 = \mathbf{s}_1$ and $\mathbf{s}_3 = \mathbf{s}_2$, the baseline $\|\mathbf{s}_1 - \mathbf{s}_2\|$ will be relatively small, corresponding to a relatively high wavenumber (or high spatial frequency). Furthermore, it follows from (191) that $\boldsymbol{\beta} = \boldsymbol{\delta} = \mathbf{0}$. The intensity correlation function is then given by

$$R_S^{\text{HF}}(\mathbf{s}_1,\mathbf{s}_2,z) = \Gamma_4(\mathbf{s}_1,\mathbf{s}_2,\mathbf{s}_2,\mathbf{s}_1,z), \quad (226)$$

or equivalently,

$$R_S^{\text{HF}}(\boldsymbol{\alpha},\boldsymbol{\gamma},z) = \Gamma_4(\boldsymbol{\alpha},\mathbf{0},\boldsymbol{\gamma},\mathbf{0},z). \quad (227)$$

The free space Green's function, in turn, becomes

$$G_4^{f^{\text{HF}}}\left(\boldsymbol{\alpha},\boldsymbol{\alpha}',\boldsymbol{\beta}',\boldsymbol{\gamma},\boldsymbol{\gamma}',\boldsymbol{\delta}',z\right)=\left(\frac{k}{2\pi z}\right)^4\exp\left(-\frac{jk}{z}\left[\left(\boldsymbol{\alpha}'-\boldsymbol{\alpha}\right)\cdot\boldsymbol{\delta}'+\boldsymbol{\beta}'\cdot\left(\boldsymbol{\gamma}'-\boldsymbol{\gamma}\right)\right]\right). \tag{228}$$

The intensity correlation function is then given by

$$\begin{aligned}R_S^{\text{HF}}(\boldsymbol{\alpha},\boldsymbol{\gamma},z)=&\left(\frac{k}{2\pi z}\right)^4\int_{\mathbb{R}^2}\int_{\mathbb{R}^2}\int_{\mathbb{R}^2}\int_{\mathbb{R}^2}\Gamma_4\left(\boldsymbol{\alpha}',\boldsymbol{\beta}',\boldsymbol{\gamma}',\boldsymbol{\delta}',0\right)\\&\times\exp\left(-\frac{jk}{z}\left[\left(\boldsymbol{\alpha}'-\boldsymbol{\alpha}\right)\cdot\boldsymbol{\delta}'+\boldsymbol{\beta}'\cdot\left(\boldsymbol{\gamma}'-\boldsymbol{\gamma}\right)\right]\right)\exp\left(-\frac{1}{2}\left[D_\varphi\left(\boldsymbol{\gamma}'+\boldsymbol{\delta}'\right)+D_\varphi\left(\boldsymbol{\gamma}'-\boldsymbol{\delta}'\right)\right]\right)\\&\times\exp\left(-\frac{1}{2}Q\left(\boldsymbol{\beta}',\boldsymbol{\gamma}',\boldsymbol{\delta}'\right)\right)\,d^2\boldsymbol{\alpha}'d^2\boldsymbol{\beta}'d^2\boldsymbol{\gamma}'d^2\boldsymbol{\delta}'.\end{aligned} \tag{229}$$

The intensity spectrum is, in turn, given by

$$P_S^{\text{HF}}(\boldsymbol{\alpha},\boldsymbol{\kappa},z)=\frac{1}{(2\pi)^2}\int_{\mathbb{R}^2}R_S^{\text{HF}}(\boldsymbol{\alpha},\boldsymbol{\gamma},z)\,e^{j\boldsymbol{\kappa}\cdot\boldsymbol{\gamma}}\,d^2\boldsymbol{\gamma}. \tag{230}$$

As in the low wavenumber scenario, the Taylor expansion (213) can be used to represent the intensity correlation function at high wavenumbers as a series:

$$R_S^{\text{HF}}(\boldsymbol{\alpha},\boldsymbol{\gamma},z)=\sum_{n=0}^{\infty}R_S^{\text{HF}(n)}(\boldsymbol{\alpha},\boldsymbol{\gamma},z). \tag{231}$$

The zeroth-order term ($n=0$) is given by

$$\begin{aligned}R_S^{\text{HF}(0)}(\boldsymbol{\alpha},\boldsymbol{\gamma},z)=&\left(\frac{k}{2\pi z}\right)^4\int_{\mathbb{R}^2}\int_{\mathbb{R}^2}\int_{\mathbb{R}^2}\int_{\mathbb{R}^2}\Gamma_4\left(\boldsymbol{\alpha}',\boldsymbol{\beta}',\boldsymbol{\gamma}',\boldsymbol{\delta}',0\right)\\&\times\exp\left(-\frac{jk}{z}\left[\left(\boldsymbol{\alpha}'-\boldsymbol{\alpha}\right)\cdot\boldsymbol{\delta}'+\boldsymbol{\beta}'\cdot\left(\boldsymbol{\gamma}'-\boldsymbol{\gamma}\right)\right]\right)\exp\left(-\frac{1}{2}\left[D_\varphi\left(\boldsymbol{\gamma}'+\boldsymbol{\delta}'\right)+D_\varphi\left(\boldsymbol{\gamma}'-\boldsymbol{\delta}'\right)\right]\right)\\&d^2\boldsymbol{\alpha}'d^2\boldsymbol{\beta}'d^2\boldsymbol{\gamma}'d^2\boldsymbol{\delta}'.\end{aligned} \tag{232}$$

The first-order term ($n=1$) is given by

$$\begin{aligned}R_S^{\text{HF}(1)}(\boldsymbol{\alpha},\boldsymbol{\gamma},z)=&2\left(\frac{k}{2\pi z}\right)^4\int_{\mathbb{R}^2}\int_{\mathbb{R}^2}\int_{\mathbb{R}^2}\int_{\mathbb{R}^2}\Gamma_4\left(\boldsymbol{\alpha}',\boldsymbol{\beta}',\boldsymbol{\gamma}',\boldsymbol{\delta}',0\right)\\&\times\exp\left(-\frac{jk}{z}\left[\left(\boldsymbol{\alpha}'-\boldsymbol{\alpha}\right)\cdot\boldsymbol{\delta}'+\boldsymbol{\beta}'\cdot\left(\boldsymbol{\gamma}'-\boldsymbol{\gamma}\right)\right]\right)\exp\left(-\frac{1}{2}\left[D_\varphi\left(\boldsymbol{\gamma}'+\boldsymbol{\delta}'\right)+D_\varphi\left(\boldsymbol{\gamma}'-\boldsymbol{\delta}'\right)\right]\right)\\&P_\varphi\left(\boldsymbol{\kappa}'\right)\left[\cos\left(\boldsymbol{\kappa}'\cdot\boldsymbol{\delta}'\right)-\cos\left(\boldsymbol{\kappa}'\cdot\boldsymbol{\gamma}'\right)\right]e^{-j\boldsymbol{\kappa}'\cdot\boldsymbol{\beta}'}\,d^2\boldsymbol{\alpha}'d^2\boldsymbol{\beta}'d^2\boldsymbol{\gamma}'d^2\boldsymbol{\delta}'d^2\boldsymbol{\kappa}'.\end{aligned} \tag{233}$$

Higher-order terms need to be considered as the baseline $\|\mathbf{s}_1-\mathbf{s}_2\|$ becomes large.

6.4 Plane Waves

For plane waves, $\Gamma_4(\mathbf{s}_1,\mathbf{s}_2,\mathbf{s}_3,\mathbf{s}_4,0)=1$, and the first few terms of the low- and high-wavenumber series expansions for the intensity correlation function (or, equivalently, the intensity spectrum) simplify significantly. The first two terms associated with the low- and high-wavenumber series are derived in the following sections.

6.4.1 Low-Wavenumber Approximation

For plane waves, the zeroth-order term ($n = 0$) of the low-wavenumber series expansion of the intensity correlation function becomes

$$R_S^{\mathrm{LF}(0)}(\boldsymbol{\alpha}, \boldsymbol{\beta}, z) = \left(\frac{k}{2\pi z}\right)^4 \int_{\mathbb{R}^2}\int_{\mathbb{R}^2}\int_{\mathbb{R}^2}\int_{\mathbb{R}^2} \times \exp\left(-\frac{jk}{z}\left[(\boldsymbol{\alpha}' - \boldsymbol{\alpha})\cdot\boldsymbol{\delta}' + (\boldsymbol{\beta}' - \boldsymbol{\beta})\cdot\boldsymbol{\gamma}'\right]\right) \exp\left(-\frac{1}{2}\left[D_\varphi\left(\boldsymbol{\gamma}' + \boldsymbol{\delta}'\right) + D_\varphi\left(\boldsymbol{\gamma}' - \boldsymbol{\delta}'\right)\right]\right) d^2\boldsymbol{\alpha}' d^2\boldsymbol{\beta}' d^2\boldsymbol{\gamma}' d^2\boldsymbol{\delta}'. \quad (234)$$

The integration with respect to $\boldsymbol{\alpha}'$ gives

$$\left(\frac{k}{2\pi z}\right)^2 \int_{\mathbb{R}^2} \exp\left(-\frac{jk}{z}\left(\boldsymbol{\alpha}' - \boldsymbol{\alpha}\right)\cdot\boldsymbol{\delta}'\right) d^2\boldsymbol{\alpha}' = \delta\left(\boldsymbol{\delta}'\right). \quad (235)$$

Similarly, the integration with respect to $\boldsymbol{\beta}'$ gives

$$\left(\frac{k}{2\pi z}\right)^2 \int_{\mathbb{R}^2} \exp\left(-\frac{jk}{z}\left(\boldsymbol{\beta}' - \boldsymbol{\beta}\right)\cdot\boldsymbol{\gamma}'\right) d^2\boldsymbol{\beta}' = \delta\left(\boldsymbol{\gamma}'\right). \quad (236)$$

Substituting these results into Equation (234), the zeroth-order term reduces to

$$R_S^{\mathrm{LF}(0)} = e^{-D_\varphi(\mathbf{0})} = 1. \quad (237)$$

The intensity spectrum associated with the zeroth-order term is, in turn, given by

$$P_S^{\mathrm{LF}(0)}(\boldsymbol{\kappa}) = \delta(\boldsymbol{\kappa}). \quad (238)$$

For plane waves, the first-order term ($n = 1$) of the low-wavenumber series expansion of the intensity correlation function becomes

$$R_S^{\mathrm{LF}(1)}(\boldsymbol{\alpha}, \boldsymbol{\beta}, z) = 2\left(\frac{k}{2\pi z}\right)^4 \int_{\mathbb{R}^2}\int_{\mathbb{R}^2}\int_{\mathbb{R}^2}\int_{\mathbb{R}^2}\int_{\mathbb{R}^2} \times \exp\left(-\frac{jk}{z}\left[(\boldsymbol{\alpha}' - \boldsymbol{\alpha})\cdot\boldsymbol{\delta}' + (\boldsymbol{\beta}' - \boldsymbol{\beta})\cdot\boldsymbol{\gamma}'\right]\right) \exp\left(-\frac{1}{2}\left[D_\varphi\left(\boldsymbol{\gamma}' + \boldsymbol{\delta}'\right) + D_\varphi\left(\boldsymbol{\gamma}' - \boldsymbol{\delta}'\right)\right]\right) P_\varphi\left(\boldsymbol{\kappa}'\right)\left[\cos\left(\boldsymbol{\kappa}'\cdot\boldsymbol{\delta}'\right) - \cos\left(\boldsymbol{\kappa}'\cdot\boldsymbol{\gamma}'\right)\right] e^{-j\boldsymbol{\kappa}'\cdot\boldsymbol{\beta}'} d^2\boldsymbol{\alpha}' d^2\boldsymbol{\beta}' d^2\boldsymbol{\gamma}' d^2\boldsymbol{\delta}' d^2\boldsymbol{\kappa}'. \quad (239)$$

The integration with respect to $\boldsymbol{\alpha}'$ is as before. The integration with respect to $\boldsymbol{\beta}'$, however, now gives

$$\left(\frac{k}{2\pi z}\right)^2 \int_{\mathbb{R}^2} \exp\left(-\frac{jk}{z}\boldsymbol{\beta}'\cdot\left(\boldsymbol{\gamma}' + \frac{z}{k}\boldsymbol{\kappa}'\right)\right) d^2\boldsymbol{\beta}' = \delta\left(\boldsymbol{\gamma}' + \frac{z}{k}\boldsymbol{\kappa}'\right). \quad (240)$$

Substituting these results into Equation (239), the first-order term then reduces to

$$R_S^{\mathrm{LF}(1)}(\boldsymbol{\beta}, z) = 2\int_{\mathbb{R}^2} P_\varphi\left(\boldsymbol{\kappa}'\right) \exp\left(-D_\varphi\left(\frac{z}{k}\boldsymbol{\kappa}'\right)\right)\left[1 - \cos\left(\frac{z}{k}\left\|\boldsymbol{\kappa}'\right\|^2\right)\right] e^{-j\boldsymbol{\kappa}'\cdot\boldsymbol{\beta}} d^2\boldsymbol{\kappa}'. \quad (241)$$

Using the trigonometric identity,

$$\cos(x) = \cos^2\left(\frac{x}{2}\right) - \sin^2\left(\frac{x}{2}\right), \tag{242}$$

the $1 - \cos(\cdot)$ term in Equation (241) can be written as

$$1 - \cos\left(\frac{z}{k}\left\|\boldsymbol{\kappa}'\right\|^2\right) = 2\sin^2\left(\frac{z}{2k}\left\|\boldsymbol{\kappa}'\right\|^2\right). \tag{243}$$

It follows that

$$R_S^{\text{LF}(1)}(\boldsymbol{\beta}, z) = 4\int_{\mathbb{R}^2} P_\varphi\left(\boldsymbol{\kappa}'\right) \exp\left(-D_\varphi\left(\frac{z}{k}\boldsymbol{\kappa}'\right)\right) \sin^2\left(\frac{z}{2k}\left\|\boldsymbol{\kappa}'\right\|^2\right) e^{-j\boldsymbol{\kappa}'\cdot\boldsymbol{\beta}}\, d^2\boldsymbol{\kappa}'. \tag{244}$$

The intensity spectrum associated with the first-order term is then given by

$$P_S^{\text{LF}(1)}(\boldsymbol{\kappa}, z) = 4P_\varphi\left(\boldsymbol{\kappa}\right) \exp\left(-D_\varphi\left(\frac{z}{k}\boldsymbol{\kappa}\right)\right) \sin^2\left(\frac{z}{2k}\left\|\boldsymbol{\kappa}\right\|^2\right). \tag{245}$$

6.4.2 High-Wavenumber Approximation

For plane waves, the zeroth-order term ($n = 0$) of the high-wavenumber series expansion of the intensity correlation becomes

$$\begin{aligned} R_S^{\text{HF}(0)}(\boldsymbol{\alpha}, \boldsymbol{\gamma}, z) = &\left(\frac{k}{2\pi z}\right)^4 \int_{\mathbb{R}^2}\int_{\mathbb{R}^2}\int_{\mathbb{R}^2}\int_{\mathbb{R}^2} \\ &\times \exp\left(-\frac{jk}{z}\left[\left(\boldsymbol{\alpha}' - \boldsymbol{\alpha}\right)\cdot\boldsymbol{\delta}' + \boldsymbol{\beta}'\cdot\left(\boldsymbol{\gamma}' - \boldsymbol{\gamma}\right)\right]\right) \exp\left(-\frac{1}{2}\left[D_\varphi\left(\boldsymbol{\gamma}' + \boldsymbol{\delta}'\right) + D_\varphi\left(\boldsymbol{\gamma}' - \boldsymbol{\delta}'\right)\right]\right) \\ &d^2\boldsymbol{\alpha}' d^2\boldsymbol{\beta}' d^2\boldsymbol{\gamma}' d^2\boldsymbol{\delta}'. \end{aligned} \tag{246}$$

The integration with respect to $\boldsymbol{\alpha}'$ gives the same result as in the case of low-wavenumber approximation:

$$\left(\frac{k}{2\pi z}\right)^2 \int_{\mathbb{R}^2} \exp\left(-\frac{jk}{z}\left(\boldsymbol{\alpha}' - \boldsymbol{\alpha}\right)\cdot\boldsymbol{\delta}'\right) d^2\boldsymbol{\alpha}' = \delta\left(\boldsymbol{\delta}'\right). \tag{247}$$

The integration with respect to $\boldsymbol{\beta}'$ gives

$$\left(\frac{k}{2\pi z}\right)^2 \int_{\mathbb{R}^2} \exp\left(-\frac{jk}{z}\boldsymbol{\beta}'\cdot\left(\boldsymbol{\gamma}' - \boldsymbol{\gamma}\right)\right) d^2\boldsymbol{\beta}' = \delta\left(\boldsymbol{\gamma}' - \boldsymbol{\gamma}\right). \tag{248}$$

Substituting these results into Equation (246), the zeroth-order term reduces to

$$R_S^{\text{HF}(0)}(\boldsymbol{\gamma}) = e^{-D_\varphi(\boldsymbol{\gamma})} = \Gamma_2^2(\boldsymbol{\gamma}). \tag{249}$$

In other words, the zeroth-order term of the low-wavenumber series expansion of the intensity correlation function is simply the square of the second statistical moment of the scattered wave field. The intensity spectrum associated with the zeroth-order term is, in turn, obtained from

$$P_S^{\text{HF}(0)}(\boldsymbol{\kappa}) = \frac{1}{(2\pi)^2}\int_{\mathbb{R}^2} e^{-D_\varphi(\boldsymbol{\gamma})} e^{j\boldsymbol{\kappa}\cdot\boldsymbol{\gamma}}\, d^2\boldsymbol{\gamma}. \tag{250}$$

For plane waves, the first-order term ($n = 1$) of the high-wavenumber series expansion of the intensity correlation function becomes

$$R_S^{\text{HF}(1)}(\boldsymbol{\alpha}, \boldsymbol{\gamma}, z) = 2\left(\frac{k}{2\pi z}\right)^4 \int_{\mathbb{R}^2}\int_{\mathbb{R}^2}\int_{\mathbb{R}^2}\int_{\mathbb{R}^2} \times \exp\left(-\frac{jk}{z}\left[(\boldsymbol{\alpha}' - \boldsymbol{\alpha})\cdot\boldsymbol{\delta}' + \boldsymbol{\beta}'\cdot(\boldsymbol{\gamma}' - \boldsymbol{\gamma})\right]\right)\exp\left(-\frac{1}{2}\left[D_\varphi\left(\boldsymbol{\gamma}' + \boldsymbol{\delta}'\right) + D_\varphi\left(\boldsymbol{\gamma}' - \boldsymbol{\delta}'\right)\right]\right) P_\varphi\left(\boldsymbol{\kappa}'\right)\left[\cos\left(\boldsymbol{\kappa}'\cdot\boldsymbol{\delta}'\right) - \cos\left(\boldsymbol{\kappa}'\cdot\boldsymbol{\gamma}'\right)\right] e^{-j\boldsymbol{\kappa}'\cdot\boldsymbol{\beta}'}\, d^2\boldsymbol{\alpha}' d^2\boldsymbol{\beta}' d^2\boldsymbol{\gamma}' d^2\boldsymbol{\delta}' d^2\boldsymbol{\kappa}'. \quad (251)$$

The integration with respect to $\boldsymbol{\alpha}'$ is as before. The integration with respect to $\boldsymbol{\beta}'$, however, now gives

$$\left(\frac{k}{2\pi z}\right)^2 \int_{\mathbb{R}^2} \exp\left(-\frac{jk}{z}\left(\boldsymbol{\gamma}' - \boldsymbol{\gamma} + \frac{z}{k}\boldsymbol{\kappa}'\right)\cdot\boldsymbol{\beta}'\right) d^2\boldsymbol{\beta}' = \delta\left(\boldsymbol{\gamma}' - \boldsymbol{\gamma} + \frac{z}{k}\boldsymbol{\kappa}\right). \quad (252)$$

Substituting these results into Equation (251), the first-order term then reduces to

$$R_S^{\text{HF}(1)}(\boldsymbol{\gamma}, z) = 4\int_{\mathbb{R}^2} P_\varphi\left(\boldsymbol{\kappa}'\right)\exp\left(-D_\varphi\left(\boldsymbol{\gamma} - \frac{z}{k}\boldsymbol{\kappa}'\right)\right)\sin^2\left(\frac{\boldsymbol{\kappa}'}{2}\cdot\left(\boldsymbol{\gamma} - \frac{z}{k}\boldsymbol{\kappa}'\right)\right) d^2\boldsymbol{\kappa}'. \quad (253)$$

The trigonometric identity (242) was used to arrive at the $\sin^2(\cdot)$ term in Equation (253). The intensity spectrum associated with the first-order term is, in turn, obtained from

$$P_S^{\text{HF}(1)}(\boldsymbol{\kappa}, z) = \frac{1}{(2\pi)^2}\int_{\mathbb{R}^2} R_S^{\text{HF}(1)}(\boldsymbol{\gamma}, z) e^{j\boldsymbol{\kappa}\cdot\boldsymbol{\gamma}}\, d^2\boldsymbol{\gamma}. \quad (254)$$

Substituting Equation (253) for $R_S^{\text{HF}(1)}(\boldsymbol{\gamma}, z)$ in Equation (254) and letting

$$\boldsymbol{\mu} = \boldsymbol{\gamma} - \frac{z}{k}\boldsymbol{\kappa}', \quad (255)$$

the intensity spectrum associated with the first-order term then becomes

$$P_S^{\text{HF}(1)}(\boldsymbol{\kappa}, z) = 4\int_{\mathbb{R}^2} P_\varphi\left(\boldsymbol{\kappa}'\right)\Phi\left(\boldsymbol{\kappa}, \boldsymbol{\kappa}'\right)\exp\left(\frac{jz}{k}\boldsymbol{\kappa}\cdot\boldsymbol{\kappa}'\right) d^2\boldsymbol{\kappa}', \quad (256)$$

where

$$\Phi\left(\boldsymbol{\kappa}, \boldsymbol{\kappa}'\right) = \frac{1}{(2\pi)^2}\int_{\mathbb{R}^2} e^{-D_\varphi(\boldsymbol{\mu})}\sin^2\left(\frac{\boldsymbol{\kappa}'\cdot\boldsymbol{\mu}}{2}\right) e^{j\boldsymbol{\kappa}\cdot\boldsymbol{\mu}}\, d^2\boldsymbol{\mu}. \quad (257)$$

7 Characteristic Scales

The expressions for the second and fourth statistical moments of the scattered wave field that were derived in Sections 5 and 6 allow, in turn, derivations of useful parameters for characterizing the statistical behavior of the scattered wave field. In Section 5, it was shown that the second moment—or the mutual coherence function—of the scattered wave field for the case of a plane wave propagating through a thin phase screen is given by

$$\Gamma_2(\mathbf{s}) = \exp\left(-\frac{1}{2}D_\varphi(\mathbf{s})\right). \quad (258)$$

The *field coherence length*, s_0, is defined as the point where

$$D_\varphi(\mathbf{s}_0) = 1. \quad (259)$$

In other words, the field coherence length is the point where the mutual field coherence function has the value $1/\sqrt{e}$. The phase structure function can be obtained from the power spectral density of the phase fluctuations induced by the thin screen:

$$D_\varphi(\mathbf{s}) = 2\int_{\mathbb{R}^2} P_\varphi(\boldsymbol{\kappa})\left[1 - e^{-j\boldsymbol{\kappa}\cdot\mathbf{s}}\right]\, d^2\boldsymbol{\kappa}. \tag{260}$$

For isotropic media, this relationship becomes

$$D_\varphi(s) = 4\pi\int_0^\infty P_\varphi(\kappa)\left[1 - J_0(\kappa s)\right]\kappa\, d\kappa. \tag{261}$$

In Section 4.2 it was shown that the power spectral density of the phase fluctuations induced by the thin screen are related to the power spectral density of the index of refraction fluctuations via the relation:

$$P_\varphi(\boldsymbol{\kappa}) = 2\pi k^2 \delta z P_n(\boldsymbol{\kappa}, 0). \tag{262}$$

For the simple power law model (6), the power spectral density of the phase fluctuations is given by

$$P_\varphi(\kappa) = C_\varphi^2 \kappa^{-\beta}, \tag{263}$$

where

$$C_\varphi^2 = 2\pi k^2 f(\beta) C_n^2 \delta z. \tag{264}$$

Substituting Equation (263) into Equation (261), the phase structure function can be written as

$$D_\varphi(s) = 4\pi C_\varphi^2 \int_0^\infty \kappa^{-\alpha-1}\left[1 - J_0(\kappa s)\right]\, d\kappa, \tag{265}$$

where $\alpha = \beta - 2$. The integral on the right-hand side of the above equation can be looked up in the standard table of integrals (e.g., Equation 11.4.18 of [7]):

$$\int_0^\infty \kappa^{-\alpha-1}\left[1 - J_0(\kappa s)\right]\, d\kappa = \frac{s^\alpha}{\alpha 2^\alpha}\frac{\Gamma\left(1-\alpha/2\right)}{\Gamma\left(1+\alpha/2\right)}. \tag{266}$$

It follows that for the simple power law model (263), the phase structure function is simply

$$D_\varphi(s) = 4\pi g(\alpha) C_\varphi^2 s^\alpha, \tag{267}$$

where

$$g(\alpha) = \frac{1}{\alpha 2^\alpha}\frac{\Gamma\left(1-\alpha/2\right)}{\Gamma\left(1+\alpha/2\right)}. \tag{268}$$

Since $D_\varphi(s_0) = 1$, it follows that for the simple power model (263),

$$s_0 = \left[4\pi g(\alpha) C_\varphi^2\right]^{-\frac{1}{\alpha}}, \tag{269}$$

or, equivalently,

$$s_0 = \left[8\pi^2 k^2 h(\alpha) C_n^2 \delta z\right]^{-\frac{1}{\alpha}}, \tag{270}$$

where

$$h(\alpha) = f(\alpha+2) g(\alpha). \tag{271}$$

It follows that for the simple power model (263), the phase structure function can also be written as

$$D_\varphi(s) = \left(\frac{s}{s_0}\right)^\alpha. \tag{272}$$

The angular scattering caused by the turbulent medium is characterized by the brightness distribution function, $B(\boldsymbol{\theta})$, which is related to the mutual coherence function via the Fourier relation:

$$B(\boldsymbol{\theta}) = \frac{1}{(2\pi)^2}\int_{\mathbb{R}^2}\Gamma_2(\mathbf{s})e^{jk\boldsymbol{\theta}\cdot\mathbf{s}}\,d^2\mathbf{s} = \frac{1}{(2\pi)^2}\int_{\mathbb{R}^2}\exp\left(-\frac{D_\varphi(\mathbf{s})}{2}\right)e^{jk\boldsymbol{\theta}\cdot\mathbf{s}}\,d^2\mathbf{s}, \tag{273}$$

where $\boldsymbol{\theta} = (\theta_x, \theta_y)$ denotes the two-dimensional angular vector. For a plane wave propagating through a thin phase screen characterized by a simple power law power spectral density, with the phase structure function (272), characterized by s_0, the Fourier relation between the mutual coherence function and the brightness distribution implies that the characteristic *scattering angle*, θ_s, can be defined as

$$\theta_s = \frac{1}{ks_0}. \tag{274}$$

The characteristic length scales associated with the observed *intensity fluctuations* can, in turn, be obtained from the expressions for the intensity spectrum that were derived in Section 6. In Section 6, it was shown that the first two terms of the low-wavenumber series expansion of the intensity spectrum for a plane wave propagating through a thin phase screen are given by

$$P_S^{\text{LF}(0)}(\boldsymbol{\kappa}) = \delta(\boldsymbol{\kappa}) \tag{275}$$

and

$$P_S^{\text{LF}(1)}(\boldsymbol{\kappa}, z) = 4P_\varphi(\boldsymbol{\kappa})\exp\left(-D_\varphi\left(r_F^2\boldsymbol{\kappa}'\right)\right)\sin^2\left(\frac{r_F^2\left\|\boldsymbol{\kappa}\right\|^2}{2}\right), \tag{276}$$

where

$$r_F = \sqrt{\frac{z}{k}} \tag{277}$$

is the *Fresnel scale* associated with the phase screen located at a distance z from the observation plane. For the purpose of obtaining the characteristic length scales for the observed intensity fluctuations, the zeroth-order term, $P_S^{\text{LF}(0)}(\boldsymbol{\kappa}) = \delta(\boldsymbol{\kappa})$ can be ignored since it corresponds to a constant correlation function. The first-order term, $P_S^{\text{LF}(1)}$, however, is very useful. Close inspection of Equation (276) reveals that the first-order term—assuming a very large outer scale and a very small inner scale of turbulence—is characterized by two scales. Clearly, the $\sin^2$ term in Equation (276) is dominated by the Fresnel scale, r_F. The characteristic scale of the exponential term can, in turn, be defined as the point, κ_r, where $D_\varphi\left(r_F^2\kappa_r\right) = 1$. Since $D_\varphi(s_0) = 1$, it follows that $r_F^2\kappa_r = s_0$. Hence, the two scales characterizing the correlation function of the intensity fluctuations at low wavenumbers (or large spatial scales), which is the Fourier transform of the first-order low-wavenumber approximation (276), are the Fresnel scale, r_F, and

$$s_R = \kappa_r^{-1} = \frac{r_F^2}{s_0}. \tag{278}$$

Comparing equations (274) and (278), s_R can be written as

$$s_R = z\theta_s. \tag{279}$$

Hence, s_R can be regarded as the size of the *scattering disk* associated with the scattering angle, θ_s, observed at a distance z from the phase screen.

If $r_F \gg s_R$, then the $\sin^2$ term is the dominant term in Equation (276), whereas if $r_F \ll s_R$, then the exponential term is the dominant term in Equation (276). If the Fresnel scale, r_F, is significantly greater than the scattering disk size, s_R, then the intensity fluctuations are small, and Equation (276) can be approximated with

$$P_S^B(\boldsymbol{\kappa}, z) = 4P_\varphi(\boldsymbol{\kappa}) \sin^2\left(\frac{r_F^2 \|\boldsymbol{\kappa}\|^2}{2}\right). \tag{280}$$

Equation (280) is referred to as the *Born* or *Rytov approximation*. The Born approximation is valid in the *weak scintillation* regime (small intensity fluctuations) when $r_F \gg s_R$. From Equation (278), $r_F \gg s_R$ is equivalent to $r_F \ll s_0$. The condition $r_F \ll s_0$ therefore defines the weak scintillation regime. By contrast, the condition $r_F \gg s_0$ defines the *strong scintillation* regime. It is convenient to introduce a strength of scintillation parameter, u, defined as

$$u = \frac{r_F}{s_0}, \tag{281}$$

with $u \ll 1$ corresponding to the weak scintillation condition and $u \gg 1$ corresponding to the strong scintillation condition. Plots of the intensity spectra given by equations (276) and (280) versus the normalized wavenumber (wavenumber times the Fresnel scale) for a range of strength of scintillation parameters, u, are shown in Figure 8. The simple power model (263) with $\beta = 11/3$ (Kolmogorov spectral index) is assumed for the power spectral density of the phase fluctuations induced by the thin phase screen. The y-axis in Figure 8 is multiplied by the wavenumber, κ, to amplify the peaks near the Fresnel scale (equal to 1 on the normalized x-axis). As u becomes significantly smaller than 1, the low-wavenumber approximation (276) approaches the Born approximation (280).

It is evident from Equation (280) that in weak scintillation, the characteristic length scale associated with the observed intensity fluctuations is the Fresnel scale, r_F. In strong scintillation, the situation is more complicated. The scattering disk size, s_R, clearly plays a role. In strong scintillation, we must also take into account the effect of intensity fluctuations at high wavenumbers (small spatial scales). In Section 6, we showed that the first term of the high-wavenumber series expansion of the intensity correlation function for a plane wave propagating through a thin phase screen is given by

$$R_S^{\text{HF}(0)}(\mathbf{s}) = e^{-D_\varphi(\mathbf{s})}. \tag{282}$$

The associated intensity spectrum, in turn, is given by the Fourier relation:

$$P_S^{\text{HF}(0)}(\boldsymbol{\kappa}) = \frac{1}{(2\pi)^2} \int_{\mathbb{R}^2} e^{-D_\varphi(\mathbf{s})} e^{j\boldsymbol{\kappa}\cdot\mathbf{s}}\, d^2\mathbf{s}. \tag{283}$$

For an isotropic medium,

$$P_S^{\text{HF}(0)}(\kappa) = \frac{1}{2\pi} \int_0^\infty e^{-D_\varphi(s)} J_0(\kappa s) s\, ds. \tag{284}$$

Clearly, the dominant spatial scale in high-wavenumber intensity fluctuations is the field coherence length s_0. It follows that in strong scintillation, intensity fluctuations are dominated by two scales: s_R at low wavenumbers (large spatial scales) and s_0 at high wavenumbers (small spatial scales). The low-wavenumber fluctuations with characteristic length scale s_R are referred to as *refractive scintillation*, whereas the high-wavenumber fluctuations with characteristic length scale s_0 are referred to as *diffractive scintillation*. In

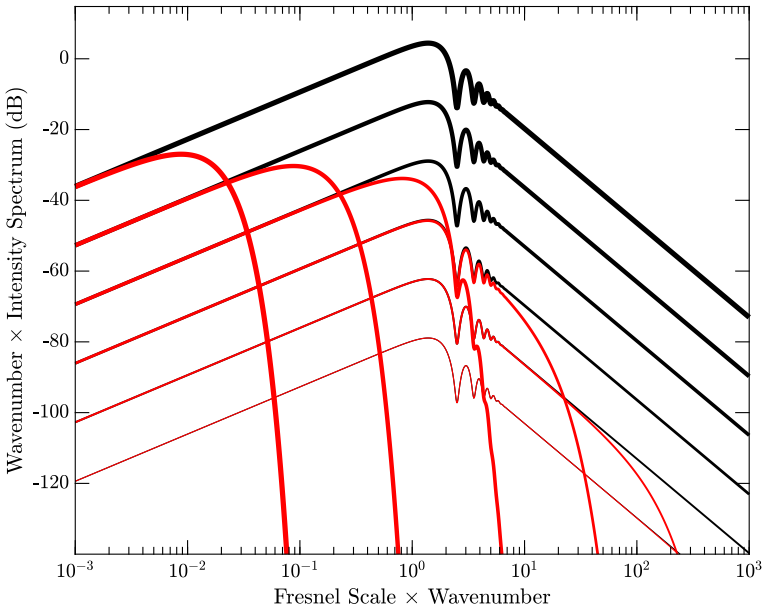

Figure 8: Intensity spectra versus the normalized wavenumber, $r_F\kappa$, for waves propagating through a thin phase screen. The simple power model (263) with $\beta = 11/3$ (Kolmogorov spectral index) is assumed for the power spectral density of the phase fluctuations induced by the thin screen. The y-axis is multiplied by the wavenumber, κ, to amplify the peaks near the Fresnel scale. The red lines correspond to the first-order term of the low-wavenumber approximation (276) of the intensity spectrum, while the black lines correspond to the Born approximation (280). The six lines, from the thinnest to the thickest, correspond to six values of the strength of scintillation parameter, u: 0.001, 0.01, 0.1, 1, 10, and 100. In weak scintillation ($u \ll 1$), intensity fluctuations are dominated by spatial scales on the order of the Fresnel scale, r_F, and the low-wavenumber approximation (276) approaches the Born approximation (280). The ringing observed in the middle of the plots are due to the $\sin^2$ terms in equations (276) and (280).

other words, the high-wavenumber "diffractive" fluctuations with relatively small characteristic length scale s_0 can be regarded as being modulated by the low-wavenumber "refractive" fluctuations with relatively large characteristic length scale s_R.

The intensity spectrum can be expressed as the sum of the low-wavenumber and high-wavenumber series expansions derived in Section 6:

$$P_S(\boldsymbol{\kappa}, z) = \sum_{n=0}^{\infty} P_S^{\mathrm{LF}(n)}(\boldsymbol{\kappa}, z) + \sum_{n=0}^{\infty} P_S^{\mathrm{HF}(n)}(\boldsymbol{\kappa}, z). \tag{285}$$

In strong scintillation (when $u \gg 1$ or $r_F \gg s_0$),

$$P_S(\boldsymbol{\kappa}, z) \simeq P_S^{\mathrm{LF}(0)}(\boldsymbol{\kappa}) + P_S^{\mathrm{LF}(1)}(\boldsymbol{\kappa}, z) + P_S^{\mathrm{HF}(0)}(\boldsymbol{\kappa}). \tag{286}$$

Again, for the purpose of examining the characteristic length scales of the observed intensity variations, the zeroth-order term, $P_S^{\mathrm{LF}(0)}(\boldsymbol{\kappa}) = \delta(\boldsymbol{\kappa})$, can be ignored since it corresponds to a constant correlation function.

To that end, it is sufficient to consider the "relative" intensity spectrum:

$$P_{\delta S}(\boldsymbol{\kappa}, z) = P_S^{\mathrm{LF}(1)}(\boldsymbol{\kappa}, z) + P_S^{\mathrm{HF}(0)}(\boldsymbol{\kappa}). \tag{287}$$

Plots of the relative intensity spectrum (287) versus the normalized wavenumber (wavenumber times the Fresnel scale) for a range of strength of scintillation parameters, u, are shown in Figure 9. The simple power law model (263) with $\beta = 11/3$ (Kolmogorov spectral index) is assumed for the power spectral density of the phase fluctuations induced by the thin screen. The y-axis in Figure 9 is again multiplied by the wavenumber, κ, to amplify the peaks near the refractive (left peak) and diffractive (right peak) scintillation length scales. As u becomes large, the separation between the refractive and diffractive scintillation length scales increases.

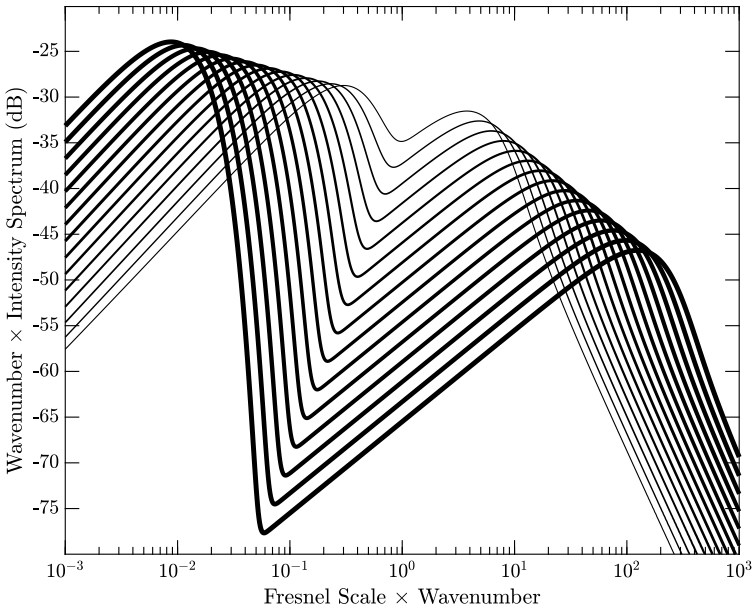

Figure 9: Intensity spectra versus the normalized wavenumber, $r_F\kappa$, in strong scintillation for waves propagating through a thin phase screen. The simple power law model (263) with $\beta = 11/3$ (Kolmogorov spectral index) is assumed for the power spectral density of the phase fluctuations induced by the thin screen. The y-axis is multiplied by the wavenumber, κ, to amplify the peaks near the refractive (left peak) and diffractive (right peak) scintillation length scales. The fifteen lines, from the thinnest to the thickest, correspond to fifteen values of the strength of scintillation parameter, u, ranging from 3 to 100, spaced evenly in logarithmic space.

In summary, in weak scintillation, the characteristic length scale, ℓ_S, for intensity fluctuations is the Fresnel scale:

$$\ell_S = r_F. \tag{288}$$

In strong scintillation, intensity fluctuations are characterized by two distinct length scales, the low-wavenumber, refractive scale given by the scattering disk size:

$$\ell_S = s_R = z\theta_s = \frac{r_F^2}{s_0} = r_F u, \tag{289}$$

and the high-wavenumber, diffractive scale given by the field coherence length:

$$\ell_S = s_0 = \frac{r_F}{u}. \tag{290}$$

A plot of the normalized characteristic length scale of the intensity fluctuations, ℓ_S/r_F, versus the strength of scintillation parameter, u, is shown in Figure 10. As u increases, the separation between the refractive and diffractive scintillation length scales increases. At some point, the separation becomes so large that the large-scale variations of refractive scintillation are no longer perceptible. At this point, the intensity spectrum is dominated by the zeroth-order term (284) of the high-wavenumber series expansion of the intensity spectrum. Higher-order terms in the series expansions in Equation (285) must be included to compute ℓ_S in the transition region from weak to strong scintillation.

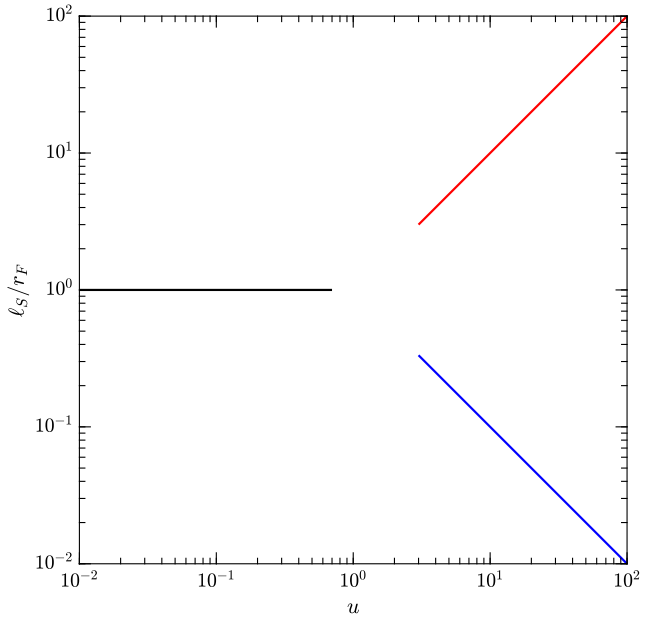

Figure 10: Normalized characteristic length scale of intensity fluctuations, ℓ_S/r_F, versus the strength of scintillation parameter, u. The black line corresponds to the weak scintillation length scale, r_F; the red line corresponds to the refractive scintillation length scale, $s_r = r_F^2/s_0 = r_F u$; and the blue line corresponds to the diffractive scintillation length scale, $s_0 = r_F/u$. The space in between the lines corresponds to the transition region from weak to strong scintillation.

Another important parameter characterizing the statistical behavior of the intensity fluctuations is the *modulation* or *scintillation index*, which is defined as

$$m^2 = \frac{\langle S^2 \rangle - \langle S \rangle^2}{\langle S \rangle^2} = \frac{\langle S^2 \rangle}{\langle S \rangle^2} - 1 = \frac{R_S(\mathbf{0}, z)}{\langle S \rangle^2} - 1. \tag{291}$$

For plane waves, with $\langle S \rangle = 1$,

$$m^2 = R_S(\mathbf{0}, z) - 1. \tag{292}$$

Equivalently,

$$m^2 = \int_{\mathbb{R}^2} P_S(\boldsymbol{\kappa})\, d^2\boldsymbol{\kappa} - 1. \tag{293}$$

In weak scintillation (when $u \ll 1$ or $r_F \ll s_0$), the *weak scintillation index* or the *Born variance* is then given by

$$m_B^2 = 4 \int_{\mathbb{R}^2} P_\varphi(\boldsymbol{\kappa}) \sin^2\left(\frac{r_F^2 \|\boldsymbol{\kappa}\|^2}{2}\right) d^2\boldsymbol{\kappa}. \tag{294}$$

For the simple power law model (263),

$$m_B^2 = 8\pi C_\varphi^2 \int_0^\infty \kappa^{-\alpha-1} \sin^2\left(\frac{r_F^2 \kappa^2}{2}\right) d\kappa, \tag{295}$$

where $\alpha = \beta - 2$. The integral can be looked up in the standard table of integrals (e.g., Equation 3.761-9 of [8]), giving

$$m_B^2 = \frac{4\pi C_\varphi^2}{\alpha} \Gamma\left(1 - \frac{\alpha}{2}\right) \cos\left(\frac{\alpha\pi}{4}\right) r_F^\alpha, \tag{296}$$

which can be rewritten as

$$m_B^2 = K(\alpha) D_\varphi(r_F), \tag{297}$$

where

$$K(\alpha) = 2^\alpha \Gamma\left(1 + \frac{\alpha}{2}\right) \cos\left(\frac{\alpha\pi}{4}\right), \tag{298}$$

and D_φ in Equation (297) is the phase structure function associated with the simple power law model (263); that is, $D_\varphi(r_F) = (r_F/s_0)^\alpha$. In other words,

$$m_B^2 = K(\alpha) \left(\frac{r_F}{s_0}\right)^\alpha = K(\alpha) u^\alpha. \tag{299}$$

Hence, the Born variance, m_B^2, can also be used as a convenient parameter to specify the strength of scintillation, with $m_B^2 \ll 1$ (corresponding to $u \ll 1$) signifying weak scintillation and $m_B^2 \gg 1$ (corresponding to $u \gg 1$) signifying strong scintillation.

In strong scintillation (when $u \gg 1$ or $r_F \gg s_0$), the scintillation index can be obtained from

$$m^2 \simeq m_R^2 + m_D^2, \tag{300}$$

where the *refractive scintillation index* is given by

$$m_R^2 = \int_{\mathbb{R}^2} P_S^{\text{LF}(1)}(\boldsymbol{\kappa}, z)\, d^2\boldsymbol{\kappa} = R_S^{\text{LF}(1)}(\mathbf{0}, z), \tag{301}$$

and the *diffractive scintillation index* is given by

$$m_D^2 = \int_{\mathbb{R}^2} P_S^{\text{HF}(0)}(\boldsymbol{\kappa})\, d^2\boldsymbol{\kappa} = R_S^{\text{HF}(0)}(\mathbf{0}). \tag{302}$$

Clearly,

$$m_D^2 = \frac{e^{-D_\varphi(\mathbf{0})}}{2} = \frac{1}{2}. \tag{303}$$

For the simple power model (263), the refractive scintillation index is given by

$$m_R^2 = 4\pi C_\varphi^2 \int_0^\infty \kappa^{-\alpha-1} e^{-(s_R\kappa)^\alpha} \sin^2\left(\frac{r_F^2\kappa^2}{2}\right) d\kappa, \tag{304}$$

which can be computed numerically[5]. Plots of the scintillation index, m^2, versus the Born variance, m_B^2, in weak and strong scintillation regimes for plane waves propagating through a thin screen are shown in Figure 11. The simple power law model with $\beta = 11/3$ (Kolmogorov spectral index) is assumed for the power spectral density of the random phase fluctuations induced by the thin screen. In weak scintillation, m^2 is computed from Equation (297), whereas in strong scintillation, m^2 is computed from Equation (300). Higher-order terms in the series expansions in Equation (285) must be included in order to obtain values of m^2 in the transition region from weak to strong scintillation.

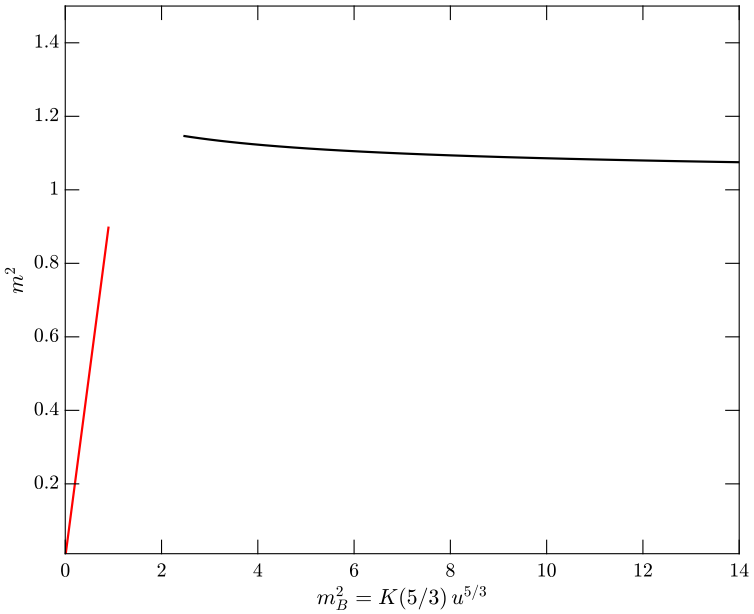

Figure 11: Plots of the scintillation index, m^2, versus the Born variance, m_B^2, characterizing the strength of scintillation for a plane wave propagating through a thin phase screen. The simple power law model with $\beta = 11/3$ (Kolmogorov spectral index) is assumed for the power spectral density of the phase fluctuations introduced by the thin screen. The red line corresponds to the weak scintillation index (297), whereas the black line corresponds to the strong scintillation index (300). The space in between the red and black lines corresponds to the transition region from weak to strong scintillation.

[5]Since the $\sin^2$ term in the integrand of Equation (304) oscillates ever more rapidly as κ increases due to the κ^2 dependence, it can be modified in the following manner to ensure a more stable numerical integration:

$$\sin^2\left(\frac{r_F^2\kappa^2}{2}\right) \to \left[\sin^2\left(\frac{r_F^2\kappa^2}{2}\right) - \frac{1}{2}\right] \exp\left(-\frac{r_F^4\kappa^4}{4a^2}\right) + \frac{1}{2}, \tag{305}$$

with a relatively large, say, $a = 10$. Here, as κ becomes large, the $\sin^2$ term gracefully approaches its mean value of $1/2$ without changing the numerical integration result.

8 Numerical Simulation

The analytical expressions derived in Sections 5, 6, and 7, although useful, do not provide a complete picture of the physics underlying the propagation of waves in turbulent media. For example, the expressions derived in Section 7 for the characteristic length scales of the observed intensity fluctuations do not address the transition region from weak to strong scintillation. Also, the characteristic scales derived in Section 7 focused on plane waves propagating through a thin phase screen. Furthermore, the simple power law model (263) was assumed for the power spectral density of the phase fluctuations induced by the thin screen. For more general scenarios, one must resort to numerical simulations of waves propagating through turbulent media to fully appreciate the observed behavior of waves. In this section, a split-step technique—similar to the technique applied in Section 4.3 to derive the Feynman path integral solution of the parabolic wave equation for extended media—using the fast Fourier transform (FFT) algorithm is applied to simulate the propagation of waves in turbulent media.

The recursion relation (143) derived in Section 4.3 expressing the scattered wave field existing the phase screen at $z = z_{k+1}$ in terms of the scattered wave field exiting the phase screen at $z = z_k$ serves as a starting point, which is repeated here for convenience:

$$\psi_{k+1}(\mathbf{s}_{k+1}, z_{k+1}) = \frac{jk}{2\pi\delta z} \int_{\mathbb{R}^2} \psi_k(\mathbf{s}_k, z_k)\, e^{-j\varphi_k(\mathbf{s}_k)} \exp\left(-j\frac{k\left\|\mathbf{s}_{k+1} - \mathbf{s}_k\right\|^2}{2\delta z}\right) d^2\mathbf{s}_k. \tag{306}$$

Expression (306) is a convolution integral that can be rewritten as

$$\psi(\mathbf{s}_{k+1}, z_{k+1}) = \mathfrak{F}_2^{-1}\left\{\mathfrak{F}_2\left\{\psi(\mathbf{s}_k, z_k)\, e^{-j\varphi_k(\mathbf{s}_k)}\right\} \exp\left(j\frac{\delta z\left\|\boldsymbol{\kappa}\right\|^2}{2k}\right)\right\}, \tag{307}$$

where $\mathfrak{F}_2\{\cdot\}$ denotes the two-dimensional Fourier transform. With the extended medium of thickness z divided evenly into N_z phase screens, the thickness of each phase screen is given by

$$\delta z = \frac{z}{N_z}. \tag{308}$$

Equation (307) represents the numerical approximation of the Feynman path integral (149) discussed in Section 4.3 and can be computed iteratively to propagate a wave through an extended turbulent medium.

The two-dimensional Fourier transform of the function, $f(\mathbf{s})$, given by

$$F(\boldsymbol{\kappa}) = \frac{1}{(2\pi)^2} \int_{\mathbb{R}^2} f(\mathbf{s}) e^{j\boldsymbol{\kappa}\cdot\mathbf{s}}\, d^2\boldsymbol{\kappa}, \tag{309}$$

can be approximated with the two-dimensional discrete Fourier transform (DFT):

$$F_{pq} \simeq \frac{1}{(2\pi)^2} \sum_{m=0}^{N_x-1} \sum_{n=0}^{N_y-1} f_{mn} W_x^{mp} W_y^{nq}\, \Delta\kappa_x \Delta\kappa_y, \tag{310}$$

where

$$F_{pq} = F(p\Delta\kappa_x, q\Delta\kappa_y), \tag{311}$$

with $p = 0, \ldots, N_x - 1$ and $q = 0, \ldots, N_y - 1$; and

$$f_{mn} = f(m\Delta x, n\Delta y), \tag{312}$$

with $m = 0, \ldots, N_x - 1$ and $n = 0, \ldots, N_y - 1$. Here, $\Delta\kappa_x$ and $\Delta\kappa_y$ are evenly spaced sampling intervals along the κ_x-axis and κ_y-axis, respectively. Similarly, Δx and Δy are evenly spaced sampling intervals along the x-axis and y-axis, respectively. The so-called *twiddle factors* are given by

$$W_x = e^{j\Delta x \Delta\kappa_x} \quad \text{and} \quad W_y = e^{j\Delta y \Delta\kappa_y}. \tag{313}$$

Since $\Delta\kappa_x = 2\pi/(N_x\Delta x)$ and $\Delta\kappa_y = 2\pi/(N_y\Delta y)$, it follows that

$$W_x = e^{j\frac{2\pi}{N_x}} \quad \text{and} \quad W_y = e^{j\frac{2\pi}{N_y}}. \tag{314}$$

The inverse Fourier transform, given by

$$f(\mathbf{s}) = \int_{\mathbb{R}^2} F(\boldsymbol{\kappa}) e^{-j\boldsymbol{\kappa}\cdot\mathbf{s}}\, d^{\mathbf{s}}, \tag{315}$$

can, in turn, be approximated with the inverse DFT:

$$f_{mn} \simeq \sum_{p=0}^{N_x-1} \sum_{q=0}^{N_y-1} F_{pq} W_x^{-mp} W_y^{-nq}\, \Delta x \Delta y. \tag{316}$$

The efficient FFT algorithm can be used to compute the DFTs in equations (310) and (316).

Equation (307) requires realizations of phase screens with phase fluctuation $\varphi(\mathbf{s})$. The Wiener–Khinchin theorem can be used to relate the power spectral density of the phase fluctuations induced by a phase screen to the Fourier transform of the phase fluctuations:

$$P_\varphi(\kappa_x, \kappa_y) = \lim_{\substack{L_x\to\infty \\ L_y\to\infty}} \frac{4\pi^2}{L_x L_y}\, \mathbb{E}_{L_x,L_y}\left\{ |\Phi(\kappa_x, \kappa_y)|^2 \right\}, \tag{317}$$

where $\mathbb{E}_{L_x,L_y}\{\cdot\}$ denotes the expectation operation computed over a rectangular region of size L_x-by-L_y. The two-dimensional Fourier transform of $\varphi(\mathbf{s})$ can, in turn, be realized from

$$\Phi_{pq} = \sigma_{pq} r_{pq}, \tag{318}$$

where

$$\sigma_{pq} = \sqrt{\frac{L_x L_y}{4\pi^2}\, P_\varphi(p\Delta\kappa_x, q\Delta\kappa_y)}, \tag{319}$$

and

$$r_{pq} = \frac{1}{\sqrt{2}} \left(g_{pq} + j h_{pq} \right), \tag{320}$$

where g_{pq} and h_{pq} are Gaussian random numbers obtained from a pseudo random number generator. The phase fluctuations are then obtained from the inverse DFT:

$$\varphi_{mn} = \sum_{m=0}^{\infty} \sum_{n=0}^{\infty} \Phi_{pq} W_x^{-mp} W_y^{-nq}\, \Delta x \Delta y, \tag{321}$$

where $m = 0, \ldots, N_x - 1$ and $n = 0, \ldots, N_y - 1$. N_x and N_y are chosen to be powers of 2 in order to use the FFT algorithm to compute Equation (321).

The power spectral density of the phase fluctuations induced by a single phase screen corresponding to the general power spectral density of the index of refraction fluctuations (11) with inner and out scales presented in Section 2 is given by

$$P_\varphi(\kappa) = \frac{C_\varphi^2}{(\kappa^2 + \kappa_o^2)^{\beta/2}} \exp\left(-\frac{\kappa^2}{\kappa_i^2}\right), \tag{322}$$

where

$$C_\varphi^2 = 2\pi k^2 f(\beta) C_n^2 \delta z. \tag{323}$$

The spectral index, β, the inner scale, $\ell_i = 2\pi/\kappa_i$, and the outer scale, $\ell_o = 2\pi/\kappa_o$, can be easily specified as simulation parameters. However, because of its awkward dimension (length$^{-2/3}$ in case of the Kolmogorov power spectral density with $\beta = 11/3$) and its awkward numerical values (in the range of 10^{-18} m$^{-2/3}$ to 10^{-16} m$^{-2/3}$), it is more convenient to specify the turbulence structure constant, C_n^2, determining the strength of turbulence, in terms of the Born variance, m_B^2, which is often used to characterize the strength of intensity fluctuations. As discussed in Section 7, in weak scintillation, $m_B^2 \ll 1$, while in strong scintillation, $m_B^2 \gg 1$.

The general expression for the Born variance associated with a phase screen of thickness δz located at z can be written as

$$\delta m_B^2 = m_B^2(z)\delta z = 4 \int_{\mathbb{R}^2} P_\varphi(\boldsymbol{\kappa}) \sin^2\left(\frac{z \|\boldsymbol{\kappa}\|^2}{2k}\right) d^2\boldsymbol{\kappa}, \tag{324}$$

where $P_\varphi(\boldsymbol{\kappa})$ depends implicitly on the screen thickness, δz. For the general isotropic expression (322) for the power spectral density, the Born variance becomes

$$\delta m_B^2 = m_B^2(z)\delta z = 16\pi^2 k^2 f(\beta) C_n^2 \delta z \int_0^\infty \frac{1}{(\kappa^2 + \kappa_o^2)^{\beta/2}} \exp\left(-\frac{\kappa^2}{\kappa_i^2}\right) \sin^2\left(\frac{z\kappa^2}{2k}\right) \kappa \, d\kappa. \tag{325}$$

For an extended medium composed of a continuum of phase screens stacked on top of each other, the total Born variance can be obtained by simply integrating Equation (324) along z:

$$m_B^2 = \int_0^z m_B^2(\zeta) \, d\zeta, \tag{326}$$

where now z represents the thickness of the extended medium. Integrating Equation (325) for the Born variance along z gives[6]

$$m_B^2 = 8\pi^2 k^2 f(\beta) C_n^2 z \int_0^\infty \frac{1}{(\kappa^2 + \kappa_o^2)^{\beta/2}} \exp\left(-\frac{\kappa^2}{\kappa_i^2}\right) \left[1 - \frac{\sin\left(r_F^2\kappa^2\right)}{r_F^2\kappa^2}\right] d\kappa, \tag{327}$$

where

$$r_F = \sqrt{\frac{z}{k}}. \tag{328}$$

[6]Only the $\sin^2$ term in Equation (297) is dependent on z. Computing the integral of this term with respect to z gives

$$\int_0^z \sin^2\left(\frac{\zeta\kappa^2}{2k}\right) dz = \frac{z}{2}\left[1 - \frac{\sin\left(r_F^2\kappa^2\right)}{r_F^2\kappa^2}\right],$$

where $r_F = \sqrt{z/k}$.

The integral

$$\mathfrak{M}(r_F, \beta, \kappa_i, \kappa_o) = \int_0^\infty \frac{1}{(\kappa^2 + \kappa_o^2)^{\beta/2}} \exp\left(-\frac{\kappa^2}{\kappa_i^2}\right) \left[1 - \frac{\sin\left(r_F^2\kappa^2\right)}{r_F^2\kappa^2}\right] d\kappa, \tag{329}$$

which is dependent on r_F, β, κ_i, and κ_o, can be computed numerically. Subsequently, C_n^2 can be expressed as

$$C_n^2 = \frac{m_B^2}{8\pi^2 k^2 f(\beta) z\, \mathfrak{M}(r_F, \beta, \kappa_i, \kappa_o)}. \tag{330}$$

Once C_n^2 has been computed, the phase structure constant, C_φ^2, for a single phase screen of thickness δz can be obtained from Equation (323).

The realizations of two phase screens with $m_B^2 = 0.1$ are shown in Figure 12. The phase screen shown on the left corresponds to a medium characterized by the simple power law model (6), with $\beta = 11/3$ (Kolmogorov spectral index), $\ell_i = 0$, and $\ell_o = \infty$. The phase screen shown on the right corresponds to a medium characterized by the general power spectral density model (11), with $\beta = 11/3$, $\ell_i = 70$ cm, and $\ell_o = 300$ m. The wavelength is chosen to be 650 nm and the screen thickness is chosen to be 500 m. Due to the DFT being used to approximate the Fourier transform, the phase screen realizations are periodic. Therefore, analysis relying on simulation results obtained using the technique described in this section should be restricted to the middle portions of the realizations—for example, the central rectangular regions, one quarter of the spatial extent of the grid from the four edges of the realizations—to minimize the impact of the periodicity inherent in the realizations.

When simulating waves propagating through turbulent media using the recursion relation (307), the two-dimensional grid representing the plane perpendicular to the direction of propagation must be chosen with care. In particular, the spatial extent of the grid must be large enough and, at the same time, the spacing between the grid points must be small enough to capture all relevant length scales characterizing the propagation problem at hand. The length scales include the scattering disk size, $s_R = z\theta_s$; the Fresnel scale, r_F; and the field coherence length, s_0. The dependence on the inner and outer scales of turbulence is implicit in s_R and s_0 since s_R and s_0 are dependent on the inner and outer scales. The impact of the choice of the grid on simulation results is explored in more detail in [9]. A good choice for the spacing between the grid points in x and y directions is

$$\Delta x = \frac{r_F}{\sqrt{N_x}} \quad \text{and} \quad \Delta y = \frac{r_F}{\sqrt{N_y}}, \tag{331}$$

and a good choice for the spatial size of the two-dimensional grid is

$$L_x = r_F\sqrt{N_x} \quad \text{and} \quad L_y = r_F\sqrt{N_y}. \tag{332}$$

It follows that

$$\frac{L_x}{\Delta x} = N_x \quad \text{and} \quad \frac{L_y}{\Delta y} = N_y. \tag{333}$$

The input parameters for the numerical simulation are listed in Table 1.

The observed intensity fluctuations (diffraction patterns) for a plane wave propagating through an extended medium modeled with 20 phase screens for $m_B^2 = 0.1$, 0.7, 3, and 10 are shown in Figure 13. The simple power model (6) with $\beta = 11/3$ (Kolmogorov spectral index) is assumed for the turbulent medium.

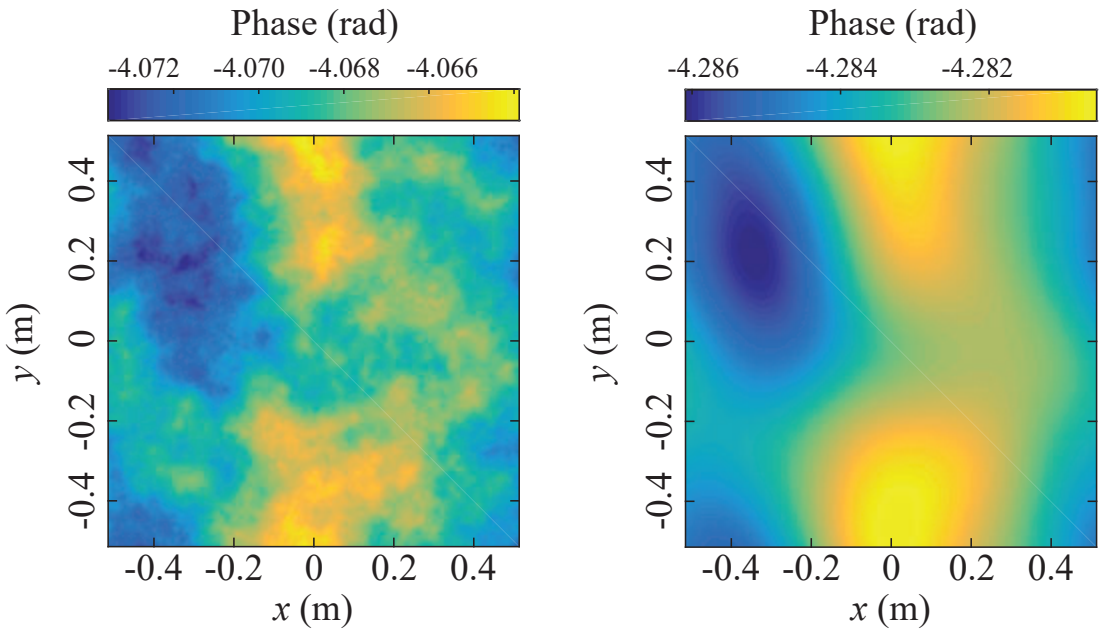

Figure 12: Phase screen realizations with $m_B^2 = 0.1$. The phase screen shown on the left corresponds to a medium characterized by the simple power law model (6), with $\beta = 11/3$ (Kolmogorov spectral index), $\ell_i = 0$, and $\ell_o = \infty$. The phase screen shown on the right corresponds to a medium characterized by the general power spectral model (11), with $\beta = 11/3$, $\ell_i = 70$ cm, and $\ell_o = 300$ m. The wavelength is chosen to be 650 nm and the screen thickness is chosen to be 500 m.

Table 1: SIMULATION PARAMETERS

PARAMETER	DESCRIPTION
N_x	Number of data points along the x-axis
N_y	Number of data points along the y-axis
N_z	Number of phase screens along the z-axis
z	Thickness of the extended medium
λ	Wavelength of the electromagnetic wave
m_B^2	Born variance (proportional to C_n^2)
β	Spectral index of turbulence
ℓ_i	Inner scale of turbulence
ℓ_o	Outer scale of turbulence

The wavelength is chosen to be 650 nm, and the extended medium is chosen to be 10 km thick, with the thickness of each phase screen being 500 m. Similar plots for the case of the extended medium modeled with the general power spectral density (11) with $\ell_i = 70$ cm and $\ell_0 = 300$ m are shown in Figure 14. The diffraction patterns (intensity fluctuations) associated with the plane wave existing each of the 20 phase screens for the general power model (11) with $m_B^2 = 0.8$ is shown in Figure 15. As in Figures 13 and 14, the wavelength is 650 nm, and the extended medium is 10 km thick, with the thickness of each phase screen being 500 m.

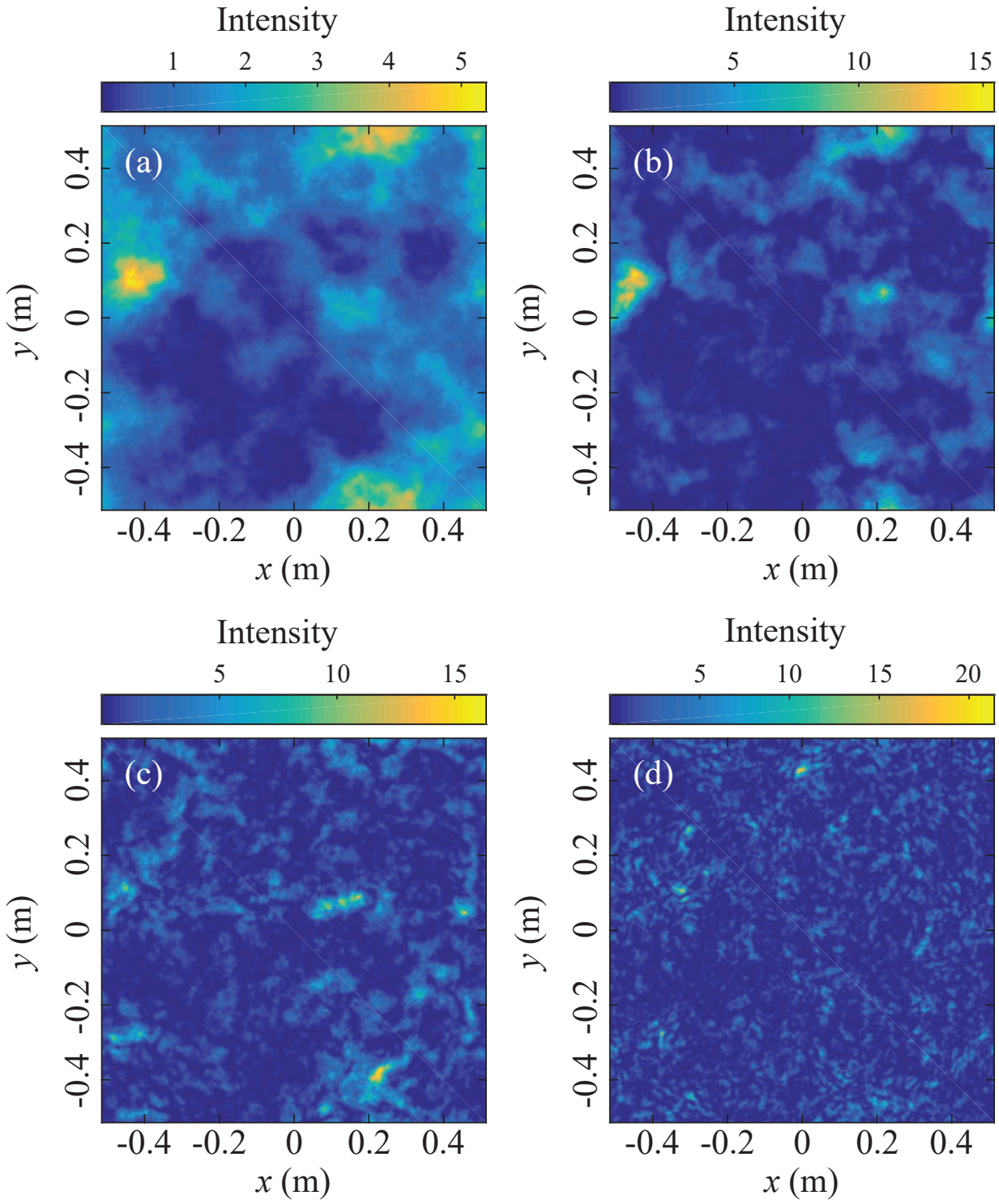

Figure 13: Observed diffraction patterns (intensity fluctuations) of the scattered waved field for (a) $m_B^2 = 0.1$, (b) $m_B^2 = 0.7$, (c) $m_B^2 = 3$, and (d) $m_B^2 = 10$. The simulation parameters are $N_x = 1024$, $N_y = 1024$, $N_z = 20$, $z = 10$ km, $\lambda = 650$ nm, $\beta = 11/3$ (Kolmogorov spectral index), $\ell_i = 0$, and $\ell_o = \infty$.

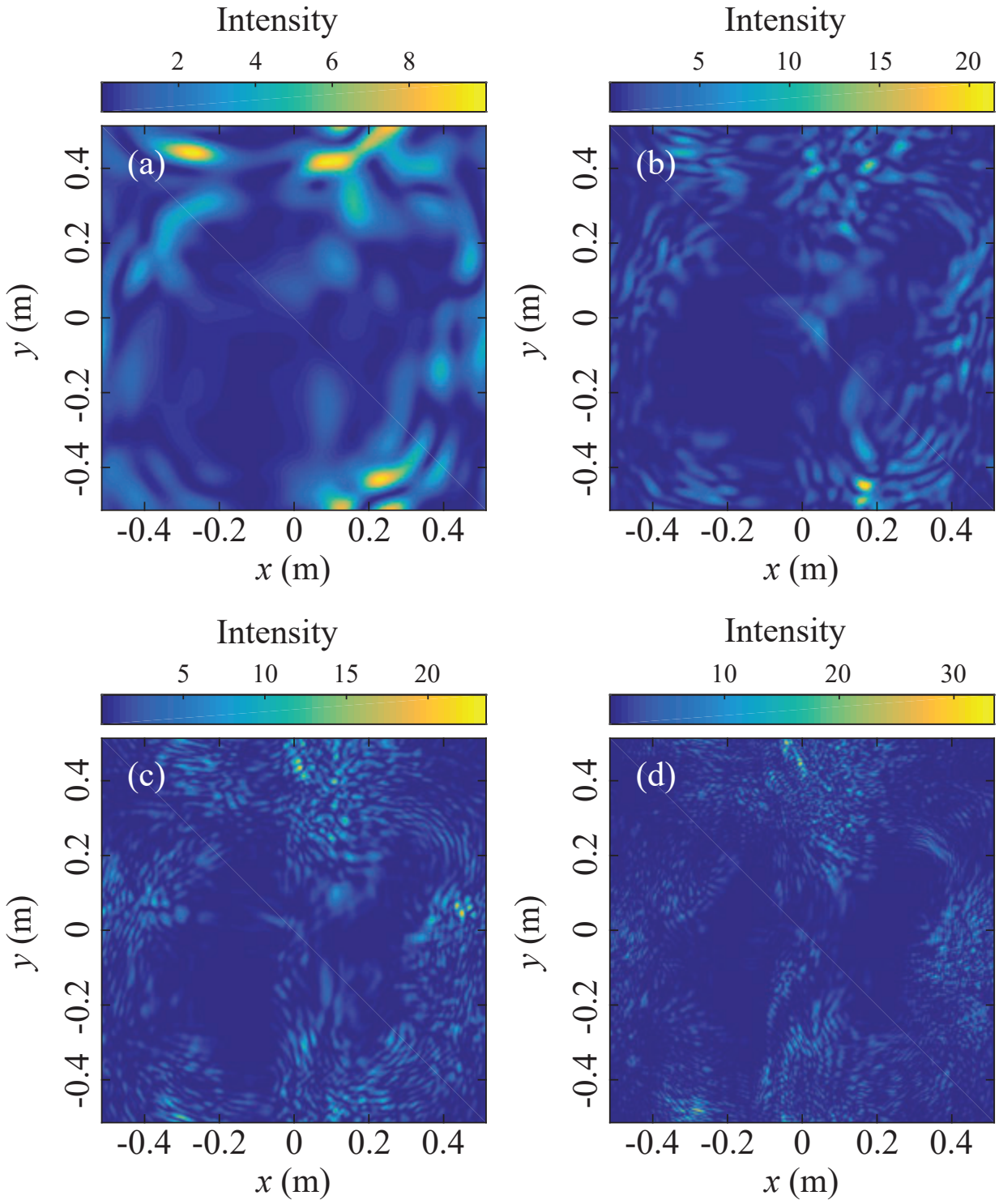

Figure 14: Observed diffraction patterns (intensity fluctuations) of the scattered wave field for (a) $m_B^2 = 0.1$, (b) $m_B^2 = 0.7$, (c) $m_B^2 = 3$, and (d) $m_B^2 = 10$. The simulation parameters are $N_x = 1024$, $N_y = 1024$, $N_z = 20$, $z = 10$ km, $\lambda = 650$ nm, $\beta = 11/3$ (Kolmogorov spectral index), $\ell_i = 70$ cm, and $\ell_o = 300$ m.

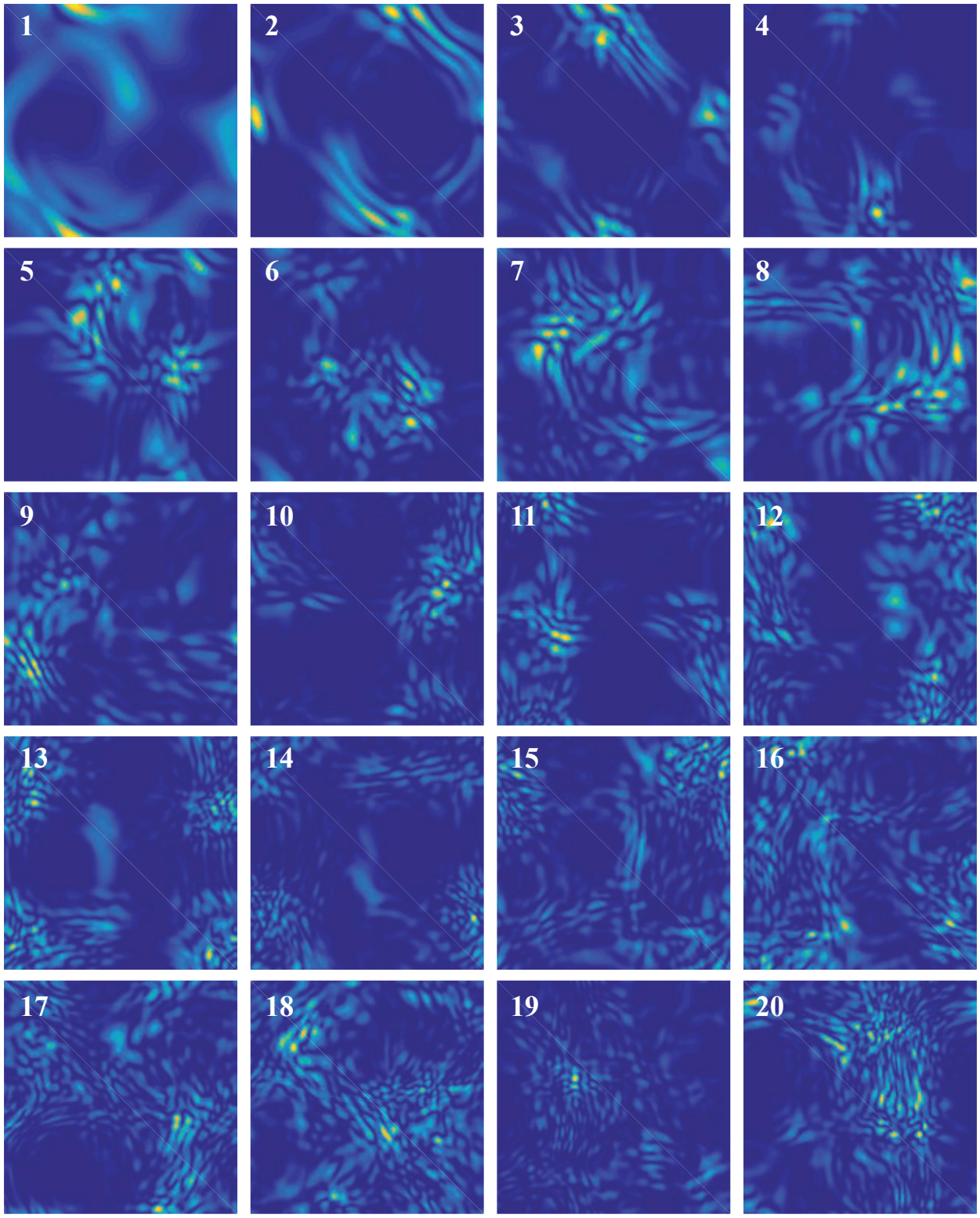

Figure 15: Diffraction patterns for a plane wave propagating through 20 phase screens, each with a thickness of 500 m. The simulation parameters are $N_x = 1024$, $N_y = 1024$, $N_z = 20$, $z = 10$ km, $\lambda = 650$ nm, $m_B^2 = 0.8$, $\beta = 11/3$ (Kolmogorov spectral index), $\ell_i = 70$ cm, and $\ell_o = 300$ m.

9 Summary

The index of refraction of the turbulent medium is the fundamental parameter affecting the propagation of electromagnetic waves. The general expression typically used for the power spectral density of the random fluctuations in the index of refraction of the air in the atmosphere is given by

$$P_n(q) = \frac{f(\beta) C_n^2}{\left(q^2 + \kappa_o^2\right)^\beta} \exp\left(-\frac{q^2}{\kappa_i^2}\right), \tag{334}$$

where $q = \|\mathbf{q}\| = \sqrt{q_x^2 + q_y^2 + q_z^2}$ is the magnitude of the three-dimensional wavenumber; C_n^2 is the turbulence structure constant; β is the spectral index; $\ell_i = 2\pi/\kappa_i$ is the inner scale of turbulence; and $\ell_o = 2\pi/\kappa_o$ is the outer scale of turbulence.

Wave propagation in random media was shown to be governed by the parabolic wave equation:

$$-2jk\frac{\partial \psi(\mathbf{s}, z)}{\partial z} + \nabla_\perp^2 \psi(\mathbf{s}, z) + 2k^2 n_1(\mathbf{s}, z)\psi(\mathbf{s}, z) = 0, \tag{335}$$

where $\psi(\mathbf{s}, z)$ is the scattered wave field; $\mathbf{s} = (x, y)$ is the component of the position vector perpendicular to the direction of propagation; z is the component of the position vector parallel to the direction of propagation; $\nabla_\perp^2$ is the Laplacian operator with respect to the transverse coordinates x and y; $n_1(\mathbf{s}, z)$ is the fluctuating component of the index of refraction; and $k = 2\pi/\lambda$ is the magnitude of the wave vector. The parabolic wave equation is valid when the fluctuations in the index of refraction are very small; the characteristic length scale of the index of refraction fluctuations is significantly greater than the wavelength of the wave; and the characteristic time scale of the index of refraction fluctuations is significantly greater than the inverse of the frequency of the wave. Under these assumptions, the scattering of waves is mainly in the forward direction and occurs at small angles. This fact is reflected through the presence of only the first partial derivative with respect to the component of the position vector in the propagation direction (z above) in the parabolic wave equation. A more detailed listing of assumptions used to derive the parabolic wave equation from the Maxwell equations is provided at the end of Section 3. An important consequence of these assumptions is that the Markov approximation can be applied, whereby the turbulent medium can be assumed to be uncorrelated along the direction of propagation.

The solution of the parabolic wave equation for the case of a wave propagating through a thin phase screen located at a distance z from the observer was shown to be given by

$$\psi(\mathbf{s}, z) = \frac{jk}{2\pi z} \int_{\mathbb{R}^2} \psi\left(\mathbf{s}', z\right) e^{-j\varphi(\mathbf{s}')} \exp\left(-\frac{jk}{2z}\left\|\mathbf{s}' - \mathbf{s}^2\right\|\right) d^2\mathbf{s}, \tag{336}$$

where the random phase fluctuations induced by the thin screen of thickness δz are given by

$$\varphi(\mathbf{s}) = k \int_0^{\delta z} n_1(\mathbf{s}, \zeta)\, d\zeta. \tag{337}$$

The power spectral density of the random phase fluctuations is related to the power spectral density of the random index of refraction fluctuations via the relation:

$$P_\varphi(\boldsymbol{\kappa}) = 2\pi k^2 \delta z P_n(\boldsymbol{\kappa}, 0). \tag{338}$$

The solution of the parabolic wave equation for the case of a wave propagating through an extended medium of thickness z was, in turn, shown to be given by the Feynman path integral:

$$\psi(\mathbf{s}, z) = \int \psi(\mathbf{s}(0), 0) \exp\left(-jk \int_0^z L(\mathbf{s}(\zeta), \zeta)\, d\zeta\right) D\mathbf{s}(z), \tag{339}$$

where

$$L(\mathbf{s}(\zeta), \zeta) = \frac{1}{2}\left\|\frac{d\mathbf{s}(\zeta)}{d\zeta}\right\|^2 + n_1(\mathbf{s}(\zeta), \zeta), \tag{340}$$

and $D\mathbf{s}(z)$ denotes a "functional differential" defined through

$$\int D\mathbf{s}(z) = \lim_{N\to\infty}\left[\left(\frac{jk}{2\pi\delta z}\right)^{N-1} \int_{\mathbb{R}^2}\cdots\int_{\mathbb{R}^2} d^2\mathbf{s}_{N-1}\cdots d^2\mathbf{s}_1\right]. \tag{341}$$

The statistical moments of the scattered wave field can be obtained directly from the above solutions of the parabolic wave equation. The second and fourth statistical moments are particularly useful. The second moment is defined as

$$\Gamma_2(\mathbf{s}_1, \mathbf{s}_2, z) = \langle \psi(\mathbf{s}_1, z)\psi^*(\mathbf{s}_2, z)\rangle\,, \tag{342}$$

and the fourth statistical moment is defined as

$$\Gamma_4(\mathbf{s}_1, \mathbf{s}_2, \mathbf{s}_3, \mathbf{s}_4, z) = \langle \psi(\mathbf{s}_1, z)\psi^*(\mathbf{s}_2, z)\psi(\mathbf{s}_3, z)\psi^*(\mathbf{s}_4, z)\rangle\,. \tag{343}$$

The second moment characterizes the mutual coherence function of the scattered wave field. Its Fourier transform corresponds to the brightness distribution function that determines the degree of angular scattering caused by the turbulent medium. The expression for the second statistical moment of a plane wave propagating through a thin phase screen was shown to be given by

$$\Gamma_2(\mathbf{s}) = \exp\left(-\frac{1}{2}D_\varphi(\mathbf{s})\right), \tag{344}$$

where $D_\varphi(\mathbf{s})$ is the phase structure function associated with the random phase fluctuations induced by the thin screen. The phase structure function was shown to be related to the power spectral density, $P_\varphi(\boldsymbol{\kappa})$, via the relation:

$$D_\varphi(\mathbf{s}) = 2\int_{\mathbb{R}^2} P_\varphi(\boldsymbol{\kappa})\left[1 - e^{-j\boldsymbol{\kappa}\cdot\mathbf{s}}\right] d^2\boldsymbol{\kappa}. \tag{345}$$

The field coherence length, s_0, is defined as the point where $D_\varphi(\mathbf{s}_0) = 1$. The characteristic scattering angle is, in turn, defined as $\theta_s = 1/(ks_0)$.

The fourth statistical moment can be used to obtain the correlation function of the observed intensity fluctuations. Two series expansions were derived to represent the intensity spectrum at low and high wavenumbers (or spatial frequencies). The intensity spectrum can be written as the sum of the two series expansions:

$$P_S(\boldsymbol{\kappa}, z) = \sum_{n=0}^{\infty} P_S^{\mathrm{LF}(n)}(\boldsymbol{\kappa}, z) + \sum_{n=0}^{\infty} P_S^{\mathrm{HF}(n)}(\boldsymbol{\kappa}, z). \tag{346}$$

In weak scintillation, when intensity fluctuations are small, it was shown that the intensity spectrum is given by the Born or Rytov approximation:

$$P_S^B(\boldsymbol{\kappa}, z) = 4P_\varphi(\boldsymbol{\kappa})\sin^2\left(\frac{r_F^2\,\|\boldsymbol{\kappa}\|^2}{2}\right), \tag{347}$$

where $r_F = \sqrt{z/k}$ is the *Fresnel scale* associated with the phase screen located at a distance z from the observation plane. In strong scintillation, it was shown that the intensity spectrum can be approximated with

$$P_S(\boldsymbol{\kappa}, z) \simeq P_S^{\text{LF}(0)}(\boldsymbol{\kappa}) + P_S^{\text{LF}(1)}(\boldsymbol{\kappa}, z) + P_S^{\text{HF}(0)}(\boldsymbol{\kappa}). \tag{348}$$

The first two terms of the low-wavenumber series expansion are given by

$$P_S^{\text{LF}(0)}(\boldsymbol{\kappa}) = \delta(\boldsymbol{\kappa}) \tag{349}$$

and

$$P_S^{\text{LF}(1)}(\boldsymbol{\kappa}, z) = 4P_\varphi(\boldsymbol{\kappa}) \exp\left(-D_\varphi\left(r_F^2 \boldsymbol{\kappa}'\right)\right) \sin^2\left(\frac{r_F^2 \left\|\boldsymbol{\kappa}\right\|^2}{2}\right). \tag{350}$$

The first term of the high-wavenumber series expansion is, in turn, given by

$$P_S^{\text{HF}(0)}(\boldsymbol{\kappa}) = \frac{1}{(2\pi)^2} \int_{\mathbb{R}^2} e^{-D_\varphi(\mathbf{s})} e^{j\boldsymbol{\kappa}\cdot\mathbf{s}}\, d^2\boldsymbol{\kappa}. \tag{351}$$

It was shown that in weak scintillation, the characteristic length scale of the intensity fluctuations is given by the Fresnel scale, r_F. In strong scintillation, it was shown that the intensity fluctuations are dominated by two distinct characteristic length scales. It was shown in Section 7 that in strong scintillation, rapid "diffractive" intensity variations are modulated by slow "refractive" intensity variations. The characteristic length scale of the diffractive variations is given by the field coherence length, s_0. The characteristic length scale of the refractive variations is, in turn, given by the scattering disk size, $s_r = z\theta_s$. The parameter $u = r_F/s_0$ was found to be useful for specifying the strength of scintillation. It was shown in Section 7 that in weak scintillation, $u \ll 1$, and in strong scintillation, $u \gg 1$. Furthermore, the scintillation index, m^2, characterizing the degree of intensity fluctuations was shown to increase with the strength of scintillation parameter u in weak scintillation and then saturate and approach unity in strong scintillation.

The discussion in Sections 5, 6, and 7 focused on asymptotic solutions for plane waves propagating through a thin phase screen with the power spectral density of the random phase fluctuations modeled as a simple power law. More general problems require resorting to numerical simulations. The recursive FFT split-step algorithm for propagating a wave through an extended turbulent medium characterized by an arbitrary power spectral density was presented in Section 8. Monte Carlo analyses based on numerical realizations of the scattered wave field yield insight into problems that are not analytically tractable, such as propagation problems that occur in the transition region from weak to strong scintillation.

A Fourier Transform Pairs

- n-dimensional spatial Fourier transform pair:

$$f(\mathbf{r}) = \int_{\mathbb{R}^n} F(\mathbf{q})\, e^{-j\mathbf{q}\cdot\mathbf{r}}\, d^n\mathbf{q}, \tag{352}$$

$$F(\mathbf{q}) = \frac{1}{(2\pi)^n} \int_{\mathbb{R}^n} f(\mathbf{r})\, e^{j\mathbf{q}\cdot\mathbf{r}}\, d^n\mathbf{r}, \tag{353}$$

  where $\mathbf{r} \in \mathbb{R}^n$ and $\mathbf{q} \in \mathbb{R}^n$.

- Three-dimensional spatial isotropic Fourier transform pair:

$$f(r) = \frac{4\pi}{r} \int_0^\infty F(q) \sin(qr)\, q\, dq, \tag{354}$$

$$F(q) = \frac{1}{(2\pi)^3} \frac{4\pi}{q} \int_0^\infty f(r) \sin(qr)\, r\, dr, \tag{355}$$

where $r = \|\mathbf{r}\| = \sqrt{x^2 + y^2 + z^2}$ and $q = \|\mathbf{q}\| = \sqrt{q_x^2 + q_y^2 + q_z^2}$.

- If $r = \mathbf{r}^{\mathrm{T}} A \mathbf{r}$ and $q = \mathbf{q}^{\mathrm{T}} A^{-1} \mathbf{q}$, where $\mathbf{r} \in \mathbb{R}^3$, $\mathbf{q} \in \mathbb{R}^3$, and A is a 3-by-3 positive definite matrix, then

$$f(r) = \frac{4\pi}{r} \sqrt{\det(A)} \int_0^\infty F(q) \sin(qr) q\, dq, \tag{356}$$

$$F(q) = \frac{1}{(2\pi)^3} \frac{4\pi}{q\sqrt{\det(A)}} \int_0^\infty f(r) \sin(qr)\, r\, dr. \tag{357}$$

- Two-dimensional spatial isotropic Fourier transform pair (Hankel transform pair):

$$f(s) = 2\pi \int_0^\infty F(\kappa) J_0(\kappa s)\, \kappa\, d\kappa, \tag{358}$$

$$F(\kappa) = \frac{1}{(2\pi)^2} 2\pi \int_0^\infty f(s) J_0(\kappa s)\, s\, ds, \tag{359}$$

where $s = \|\mathbf{s}\| = \sqrt{x^2 + y^2}$ and $\kappa = \|\boldsymbol{\kappa}\| = \sqrt{\kappa_x^2 + \kappa_y^2}$.

- If $\kappa = \boldsymbol{\kappa}^{\mathrm{T}} B^{-1} \boldsymbol{\kappa}$ and $s = \mathbf{s}^{\mathrm{T}} B \mathbf{s}$, where $\mathbf{s} \in \mathbb{R}^2$, $\boldsymbol{\kappa} \in \mathbb{R}^2$, and B is a 2-by-2 positive definite matrix, then

$$f(s) = 2\pi \sqrt{\det(B)} \int_0^\infty F(\kappa) J_0(\kappa s) \kappa\, d\kappa, \tag{360}$$

$$F(\kappa) = \frac{1}{(2\pi)^2} \frac{2\pi}{\sqrt{\det(B)}} \int_0^\infty f(s) J_0(\kappa s)\, s\, ds. \tag{361}$$

- Temporal Fourier transform pair:

$$f(t) = \int_{-\infty}^\infty F(\omega) e^{j\omega t}\, d\omega, \tag{362}$$

$$F(\omega) = \frac{1}{2\pi} \int_{-\infty}^\infty f(t) e^{-j\omega t}\, dt. \tag{363}$$

- n-dimensional Fourier transform of a constant:

$$\frac{1}{(2\pi)^n} \int_{\mathbb{R}^n} e^{\pm j(\mathbf{q}' - \mathbf{q}) \cdot (\mathbf{r}' - \mathbf{r})} d^n \mathbf{r}' = \delta(\mathbf{q}' - \mathbf{q}). \tag{364}$$

- Fourier transform of a one-dimensional Gaussian function:

$$\int_{-\infty}^\infty e^{-ax^2} e^{\pm j\kappa_x x}\, dx = \sqrt{\frac{\pi}{a}}\, \exp\left(-\frac{\kappa_x^2}{4a}\right). \tag{365}$$

References

[1] V. I. Tatarskii, *The Effects of the Turbulent Atmosphere on Wave Propagation*. Jerusalem, Israel: Israel Program for Scientific Translations, 1971.

[2] R. J. Sasiela, *Electromagnetic Wave Propagation in Turbulence*. Heidelberg, Germany: Springer-Verlag, 1994.

[3] T. E. VanZandt, J. L. Green, K. S. Gage, and W. L. Clark, "Vertical profiles of refractivity turbulence structure constant: Comparison of observations by the sunset radar with a new theoretical model," *Radio Science*, vol. 13, no. 5, pp. 819–829, 1978.

[4] F. D. Eaton and G. D. Nastrom, "Preliminary estimates of the vertical profiles of inner and outer scales from White Sands Missile Range New Mexico, VHF radar observations," *Radio Science*, vol. 33, no. 4, pp. 895–903, 1998.

[5] R. P. Feynman, "Space-time approach to non-relativistic quantum mechanics," *Reviews of Modern Physics*, vol. 20, no. 2, pp. 367–387, 1948.

[6] J. L. Codona, D. B. Creamer, S. M. Flatté, R. G. Frehlich, and F. S. Heyney, "Solution for the fourth moment of waves propagating in random media," *Radio Science*, vol. 21, no. 6, pp. 929–948, 1986.

[7] M. Abramowitz and I. A. Stegun, *Handbook of Mathematical Function*. New York: Dover Publications, 1972.

[8] I. S. Gradshteyn and I. M. Ryzhik, *Table of Integrals, Series, and Products*, 8th ed., D. Zwillinger, Ed. Academic Press, 2015.

[9] W. A. Coles, J. P. Filice, R. G. Frehlich, and M. Yadlowsky, "Simulation of wave propagation in three-dimensional random media," *Applied Optics*, vol. 34, no. 12, pp. 2089–2101, 1995.